

Old Dominion University

ODU Digital Commons

Electrical & Computer Engineering Theses & Dissertations

Electrical & Computer Engineering

Spring 2019

Design, Implementation, and Analysis of Electrical System Architecture for CubeSat to Ground Communications

Anthony G. Cappiello

Old Dominion University, dmarieca21@gmail.com

Follow this and additional works at: https://digitalcommons.odu.edu/ece_etds



Part of the [Electrical and Computer Engineering Commons](#)

Recommended Citation

Cappiello, Anthony G.. "Design, Implementation, and Analysis of Electrical System Architecture for CubeSat to Ground Communications" (2019). Master of Science (MS), Thesis, Electrical & Computer Engineering, Old Dominion University, DOI: 10.25777/w5cz-pa62
https://digitalcommons.odu.edu/ece_etds/161

This Thesis is brought to you for free and open access by the Electrical & Computer Engineering at ODU Digital Commons. It has been accepted for inclusion in Electrical & Computer Engineering Theses & Dissertations by an authorized administrator of ODU Digital Commons. For more information, please contact digitalcommons@odu.edu.

**DESIGN, IMPLEMENTATION, AND ANALYSIS OF
ELECTRICAL SYSTEM ARCHITECTURE FOR
CUBESAT TO GROUND COMMUNICATIONS**

by

Anthony G. Cappiello
B.S. August 2018, Old Dominion University

A Thesis Submitted to the Faculty of
Old Dominion University in Partial Fulfillment of the
Requirements for the Degree of

MASTER OF SCIENCE

ELECTRICAL AND COMPUTER ENGINEERING

OLD DOMINION UNIVERSITY
May 2019

Approved by:

Dimitrie C. Popescu (Director)

Robert L. Ash (Member)

Otilia Popescu (Member)

ABSTRACT

DESIGN, IMPLEMENTATION, AND ANALYSIS OF ELECTRICAL SYSTEM ARCHITECTURE FOR CUBESAT TO GROUND COMMUNICATIONS

Anthony G. Cappiello
Old Dominion University, 2019
Director: Dr. Dimitrie C. Popescu

CubeSats facilitate a low barrier to entry in University and Industrial space research. With the rapid, low-cost development of CubeSats, the need for a reliable and robust communications subsystem becomes evident to ensure mission accomplishment. With the advent of Software Defined Radio, Old Dominion University is compelled to upgrade the rigid Legacy Hardware systems in place with inexpensive and flexible Software Defined Radio Solutions. Currently, Old Dominion University is on the cusp of conducting its first space science mission as a member organization of the Virginia Space Grant Consortium Cubesat Constellation and is manifest for launch on April 17, 2019 NASA Wallops Flight Facility. To conduct this mission, the design and construction of a 1U Nano-Satellite and the upgrade to existing ground station architecture was necessary. To relay data in a point-to-point fashion as required by the Science Mission, Old Dominion University has developed custom ground station hardware and software to communicate with its own satellite and the satellites of others. This thesis presents the salient design aspects in implementing a complete electrical system architecture for a 1U spacecraft and the upgrades required in the Ground Station Architecture to support the required demodulation and decoding of a 9600 baud GMSK signal from a model of the deployed satellite necessary to conduct a true science research mission as part of a University Satellite Constellation. The demodulating signal processing steps are designed in GNU Radio Companion and deals with parts of the AX.25 data link layer protocol. Additionally, analysis shall be presented to highlight the design choices made for both the spacecraft and the ground station and will demonstrate various system parameters and characteristics of interest based on the Orbital Simulation results obtained from Systems Toolkit (STK). Finally, results of the architecture design shall be reported on the system by measuring Communications Link Performance benchmarks such as Bit-Error-Rates (BER) and Signal-To-Noise Ratios (SNR).

Copyright, 2019, by Anthony G. Cappiello, All Rights Reserved.

This Thesis is dedicated to my beautiful wife Diana. Without her, I wouldn't even be a remote version of who I am today. She is the driving force behind any success or accolades I may have achieved in my Military or Academic Career. Not only is she an extraordinary Person of Character, but she is an incredible mother and superb woman to live life beside. My life as it stands today is a direct result of her love, patience, and dedication to us as a couple and family. I am forever indebted to her in more ways than I could describe in words.

For God, Country, and Family. It's not a cliché, its the blueprint.

ACKNOWLEDGEMENTS

I would be remiss if I did not thank three faculty members at Old Dominion University. First, thank you to Dr. Lee Belfore for always teaching immensely challenging courses that always paid off huge in the end due to their practical nature for “Real-World” engineering. I also must thank Dr. Belfore for igniting a new passion I have for digital design and synthesis. It was your digital systems design course that I will always remember as one of the toughest yet most rewarding courses of my academic career. Thank you for always going beyond the theory and teaching us the “nuts and bolts” of Computer Engineering. Secondly, thank you to Dr. Bob Ash of the Mechanical and Aerospace Department here. Without his connections and insights, there would be no Old Dominion University CubeSat. Being that the CubeSat is the basis of my Thesis, there would be no Thesis if it weren’t for his influence. Thank you also for your sage advice and for supporting me on my physics and aerospace tangents that I thoroughly enjoyed going on under your guidance. Finally, thank you to Dr. Dimitrie C. Popescu. There is so much I could say but I fear I couldn’t do it justice, nonetheless I shall try. Going into my final year at ODU, I was beyond frustrated and disgruntled. Studying Engineering was not how I expected it was going to be and taking your elective courses were just going to be some checks in the box I needed to graduate. However, you proved me wrong and I am thankful I took your courses because you revived the passion and curiosity for formal mathematical study that I thought was lost in my first years of engineering education. Furthermore, you’ve proven a strong mentor both academically and professionally speaking. You’ve tasked me with monumental challenges in the theoretical and applied arenas of engineering and guided me with a light-hearted attitude that I needed to keep me sane along the way. You’ve helped me sharpen my critical thinking and analytical skills better than anyone and you’ve presented me with opportunities far beyond anything I thought I’d ever be capable of doing. Your confidence in me, mentorship, and friendly demeanor were exactly what I needed to get out what I needed out of an Engineering Education and for that I am forever indebted to you.

TABLE OF CONTENTS

	Page
LIST OF TABLES	viii
LIST OF FIGURES	xi
Chapter	
1. INTRODUCTION	1
1.1 THE MISSION AND MOTIVATION	2
1.2 BACKGROUND	3
1.3 LITERATURE REVIEW AND THEORETICAL FRAMEWORK ...	6
1.4 THESIS ORGANIZATION AND CONTRIBUTION	7
2. ORBITAL MECHANICS AND THE DEVELOPMENT OF A FORMAL SYSTEM SPECIFICATION	10
2.1 STK SIMULATION PARAMETERS	11
2.2 ORBITAL LIFETIME	21
2.3 POWER REQUIREMENTS	26
2.4 DATA LINK REQUIREMENTS	36
3. SPACECRAFT HARDWARE DESIGN	40
3.1 THE SPACE CRAFT RADIO FREQUENCY MODULE	40
3.2 THE MOTHERBOARD DESIGN	56
4. THE COMMUNICATIONS SYSTEM AND DATA LINK	64
4.1 GAUSSIAN MINIMUM SHIFT KEYING	64
4.2 AX.25 DIGITAL PROTOCOL	67
4.3 DIGITAL ENCODING, MODULATION AND GNU RADIO	70
4.4 DATA LINK BUDGET	71
5. EXPERIMENTAL RESULTS	76
5.1 RADIO LINK PERFORMANCE	76
6. CONCLUSION	83
6.1 FUTURE WORK	83
REFERENCES	88
APPENDICES	
A. MATLAB	89
B. COPYRIGHTS	94

C. PIN MAPPING	96
VITA.....	99

LIST OF TABLES

Table	Page
I Comparison of COTS to University Designed Hardware	5
II Alternate Orbital Elements and When to Use Them in Analysis	12
III Summary of STK Simulation Parameters	21
IV Aeternitas Orbital Lifetime Simulation Results 3 Initial Models	22
V VCC Orbital Lifetime Simulation Results for 2 Most Accurate Models ...	23
VI GOMSPACE P110u Specifications	28
VII Theoretical Power Consumption Table based on 1.46 hour orbit	32
VIII HPOP Power Generation for $P_{ave} = 1.69$ Watts	32
IX Two Body Power Generation for $P_{ave} = 1.69$ Watts	32
X Theoretical Power Budget Adjusted for Radio and EPS Heater Duty Cycles	34
XI SpaceCraft Data Link Intrinsic Constraints	37
XII Global Access Statistics for Aeternitas Mission	38
XIII Lithium II Radio Design Parameters	42
XIV Generic AX.25 Information Frame Structure	68
XV Information Frame Structure Specific to Aeternitas Payloads	68
XVI Aeternitas Link Budget with Full Analysis Performed with STK	75
XVII Matlab Simulated SNR to BER	81

LIST OF FIGURES

Figure	Page
1 ODU CubeSat Electrical Systems Architecture Required to Support a Telemetry and Communications Science Payload	2
2 Interdependance of Hierarchy of System Requirements Generated From Mission Objectives	8
3 Spacecraft Subsystems For Development of a University Scientific Payload	9
4 Visualization of the Four Dimensional Celestial Mechanics Simulation Using STK	11
5 Visual depiction of Semi-Major Axis	13
6 Orbital Depiction of Eccentricity	14
7 Simulated Eccentricity Plot over the course of the mission	15
8 Orbital inclination	16
9 RAAN Illustration	17
10 Argument of Perigee Illustration	18
11 Drag Brake Mock Up During Satellite Assembly Which Accounts for the extra 26 cm ² of Exposed Drag Area vs The Other Two VCC Satellites . . .	23
12 CubeSat CAD model with Solar Panel Characteristics and Drag Brake Area Added	24
13 Comparative VCC Orbital Simulation for Satellite Lifetimes	25
14 Aeternitas Orbital Eccentricity Characteristics using 2-Body Propagator Model	26
15 Aeternitas Orbital Eccentricity Characteristics using HPOP Model	27
16 Solar Irradiance For a One Year Solar Cycle	28
17 Power Harvesting Curves for Aeternitas HPOP Model	29
18 Power Harvesting Curves for Aeternitas 2-Body Model	30

19	Ground Station Antenna Direcionality as Aeternitas Arrives From Below the Horizon	39
20	Visualization of Antenna to Satellite Data Link	39
21	Picture of Lithium II Radio used for transmission of data	41
22	Dipole Radiation Pattern Described by Equations (17) and (18)	44
23	3D model of Cubesat Antenna in its deployed state	45
24	$\theta = 65^\circ$ Far Field effects of Aeternitas Antenna Assembly Cut to Resonate at 400MHz	47
25	$\phi = 35^\circ$ Far Field effects of Aeternitas Antenna Assembly Cut to Resonate at 400MHz	48
26	Far Field effects of Aeternitas Antenna Assembly Cut to Resonate at 400MHz	49
27	RF Characteristic Impedance using $\epsilon_r = 4.2$ and a substrate height $h = 1.74mm$	51
28	First Design Iteration for Spacecraft RF Module Hardware using IPC-2141 and Wadell Models for Impedance Matching	53
29	Balun Design Test Jig mounted on 1.74mm FR4 substrate used for design iteration in CubeSat RF module	54
30	Balun Design in LTSpice Prepared for Simulation	55
31	3D CAD Rendering of the Ground Station Switching Hardware to interface the existing Antennas to the USRP B200.	62
32	3D CAD Rendering of the Motherboard Design Used to Interface all On-board Satellite Hardware	63
33	GMSK System Block Diagram	66
34	Semilog Plot of Free Space Path Loss for Aeternitas across the satellite's range over the course of its lifetime.	72
35	Link Margin Worst and Best Case Scenarios for Satellite Access Distances Over the life of the Satellite.	73
36	Experimental Setup for AFSK 1200 and GMSK 9600.	77

37	RTL-SDR receiving "Hello World!" on 1200 AFSK	77
38	Matlab Binary Decode Clarity at 7 dB SNR.....	78
39	Matlab Binary Decode Clarity at 22 dB SNR.....	79
40	Transmit Chain for Experiment	80
41	Receive Chain for Experiment	81
42	Received Image Payload at 7 dB SNR	82
43	Received Image Payload at 22 dB SNR	82

CHAPTER 1

INTRODUCTION

CubeSats have attracted increased interest from the academic community in recent years due to their relative low cost and short development cycle. As is the case with all autonomous spacecraft, CubeSats rely on radio communications with ground stations to receive commands for performing scientific missions, and to transmit telemetry and measurement data back to Earth for processing.

Small Satellites are subdivided into many sub classes based on their mass. A 1U CubeSat generally falls under the class with masses between 1 and 50 kg. CubeSats are favored in industry and research for their modular design and low barrier to entry apropos cost and capability [1]. By definition, a 1U CubeSat is a 10 cm x 10 cm x 10 cm cube with a mass of around 1 kg [1, 2].

CubeSats are a class of small satellites that enable universities to design and perform low-cost space experiments by using commercial off-the-shelf (COTS) components and take advantage of affordable launches in orbit as secondary payloads in various missions such as International Space Station (ISS) re-supply missions [1]. An important aspect of a CubeSat mission design is the communication link, which enables the CubeSat to receive commands and to transmit telemetry and scientific data to ground stations [3]. From the author's perspective, it can be said that other than power, there is no more important Electrical Subsystem than the Communications Module. Without power and communications capabilities, launching a satellite into Low Earth Orbit (LEO) is an expensive and futile endeavor.

While the main objective of this thesis was to implement a robust communications subsystem for a basic 1U CubeSat, that subsystem cannot be isolated from the specific orbits required for the mission. The scope of the Old Dominion University (ODU) *Aeternitas* Space project and its research objectives expands far beyond the critical Radio Communications Link.

The system depicted in Figure 1 is a Cartoon Schematic illustrating the principal communications systems objective of this thesis within the scope of a Virginia-Wide, University CubeSat Constellation Research Mission. It is important to note that the scope of this Thesis could not be limited to only communications, but required

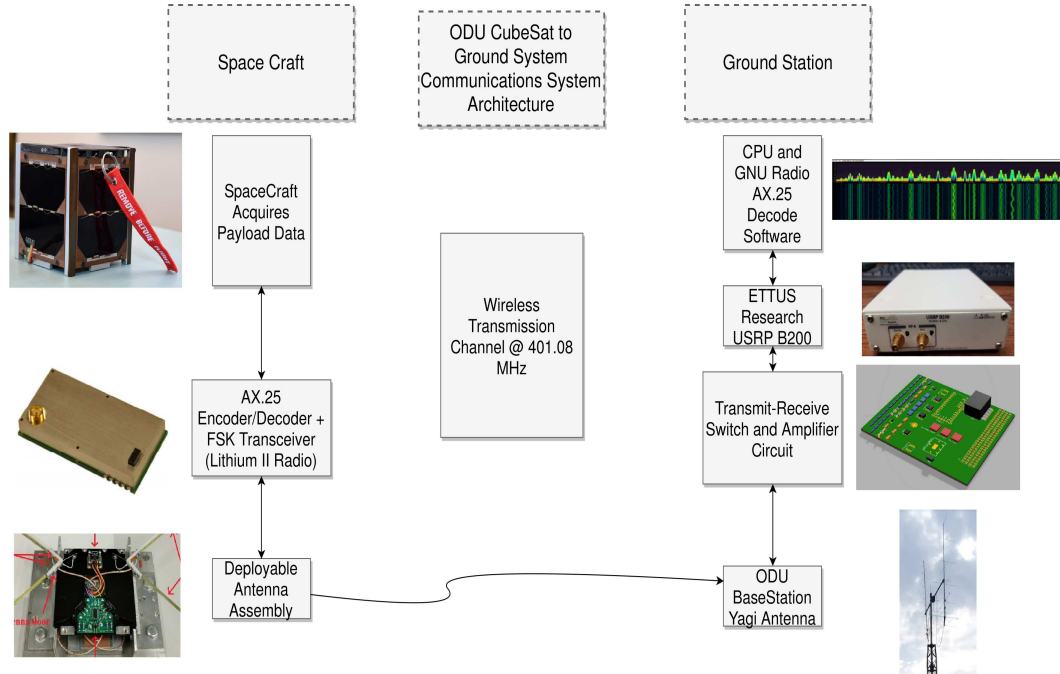


Fig. 1: ODU CubeSat Electrical Systems Architecture Required to Support a Telemetry and Communications Science Payload

knowledge of the entire electrical architecture required for the spacecraft and the ODU ground station supporting the Communications Link. Considerations of Power, Data Link Budgeting, Software Development, Hardware Design Choices, Attitude Control, and interoperability of each of these facets must be given for both the Spacecraft and the supporting Ground Station[4].

1.1 THE MISSION AND MOTIVATION

The Virginia Space Grant Consortium (VSGC), supported by the National Aeronautics and Space Administration (NASA) through its *University Science Instrument Program* (USIP) selected to deliver three 1U CubeSats to be deployed from orbits similar to the *International Space Station* (ISS), and intended to obtain space weather data. Originally, Old Dominion University, the University of Virginia and Virginia Tech were to deliver their separately designed and fabricated space-qualified CubeSats to NASA Johnson Space Center (JSC) in September 2018. Undergraduate atmospheric science students from Hampton University were the science leads, (responsible for interpreting the space weather output.)

Due to the unprecedented complexity of the project and delays in delivering the final CubeSat design, resulting primarily from the lack of actual project experience by undergraduate engineering students, the CubeSat electrical system architecture required extreme and rapid engineering solutions. Only then would it be possible to achieve the scientific objectives and associated deadlines. The fundamental scientific objective was to provide drag-based, local density data that could contribute to our understanding of how variations in solar activity, along with day-night changes in thermospheric density influence orbital decay. These data can improve our understanding of the Sun's influence on Lower Earth Orbit (LEO) weather, thereby improving our ability to predict entry trajectories of space debris.

The constellation was manifest originally for a November 2018 delivery to International Space Station. The constellation was to be inserted into orbit from ISS at a later date. Unfortunately, the ISS resupply flight schedule was disrupted due to unexpected problems with ISS components and Soyuz delivery vehicles, delaying the constellation delivery schedule, and subsequent orbit insertion. Presently, the VSGC constellation is manifest on the April 17, 2019 *Northrop Grumman Cygnus* ISS delivery flight from the Mid Atlantic Regional Spaceflight facility, Wallops Island, VA. The overall mission goals of the Virginia CubeSat Constellation (VCC) were to provide actual hands-on spacecraft design project experience for undergraduate Science, Technology, Engineering and Mathematics (STEM) students and to obtain data that could improve orbital decay forecasts based on the aerodynamic behavior of three nanosatellites inserted initially in nominally identical LEO orbits. Additional ODU CubeSat-specific goals, specific to the ODU CubeSat, included design and implementation of a three-axis magnetorquer-based attitude control system and a novel deployable drag brake system, intended to accelerate deorbit.

1.2 BACKGROUND

Because of the variability in the level of project complexity, time, and the experience level of undergraduate engineering teams, first-time CubeSat Designers had a critical design choice to make from the very beginning with regard to how to accomplish their mission [4]. More specifically, “To what extent should Commercial-Off-The-Shelf (COTS) parts be utilized in the ODU CubeSat?”

To one extreme, it is possible to purchase a fully off-the-shelf CubeSat unit consisting of an entire CubeSat chassis with integrated solar electric power, data acquisition

and communications systems, lacking only mission-specific scientific instrumentation. At most, the only engineering taking place is in the development of the software to be deployed on the spacecraft.

At the other extreme, ambitious (and sometimes overzealous) design teams elect to minimize COTS parts and instead design and fabricate most of the hardware, while designing and implementing most of the electronics and software. A near-maximum level of engineering occurs on this type of project and therefore maximizes the learning involved for those dedicated enough to see the project through to completion.

With these two extremes in mind, ODU considered the Mission Objectives dictated by our customer (VSGC) and decided to bias the ODU CubeSat toward the ambitious end of the spectrum [5].

Primary Mission Objectives :

- Provide a hands-on, student-led flight project experience for undergraduate students by designing, developing, integrating, testing and flying an orbital constellation of three 1U CubeSats
- Obtain measurements of the orbital behavior of a constellation of satellites to develop a database of atmospheric drag and the associated variability of atmospheric properties

Secondary Mission Objectives :

- Develop teams of students from Old Dominion University, Virginia Tech, University of Virginia, and Hampton University to work effectively under the umbrella of the Virginia Space Grant Consortium (VSGC)
- Test Ultem 9085 as a CubeSat structural material

With the increasing growth of commercial spacecraft deployers like *NanoRacks LLC* and parts suppliers like *Gomspace*, *Pumpkin*, and *ClydeSpace*, engineers have a stable of established small satellite component suppliers companies from to choose in order to best-meet their mission objectives and design requirements. To meet our needs, the only COTS parts purchased from vendors for the ODU CubeSat design

were a *Gomspace P31u* (P31u Power Module and its four associated P110 Solar Panels), a *SkyFox Labs* Pi-Nav GPS Module, and an *Astrodev LLC* Lithium II Radio Module. All other components were designed, tested, and verified primarily by ODU engineering students. Their design product included: the spacecraft chassis, the deployable antenna assembly, the deployable, four-petal drag brake mechanism, and all PCBs to support the off-the-shelf components. In total, six PCBs were designed by the ODU Electrical and Computer Engineering Team and were subsequently custom-manufactured. The present author was solely responsible for designing the motherboard that interfaces all six PCBs with their drivers, as well as housing the spacecraft software.

TABLE I: Comparison of COTS to University Designed Hardware

COTS Components	Designed Components
Pi-Nav GPS	Motherboard PCB
Lithium II Radio	RF PCB
GOMSPACE EPS P31u	GPS PCB
GOMSPACE Solar Panels P110UA	Telemetry and Sensing PCB
	Debug Port PCB
	Deployable Antenna
	Deployable Drag Brake
	CubeSat Chassis

As for communication with the ODU Ground Station, Amateur Radio equipment was selected as the communications link between the VSGC spacecraft constellation and the ODU ground station [6]. The ODU Satellite Ground Station was initially implemented using an ICOM-910 multi-mode transceiver. While it was adequate at the time, the initial design was rigid and inflexible, constraining communications research to only the 434 and 144 MHz Bands [7].

Commercially available Software Defined Radio systems are substantially more versatile and flexible solutions at reasonable costs. Since ODU is now flying an actual orbital space mission, the long overdue Clarion call for upgrading the existing ground station to communicate with launched satellites on our mission has come. Employing the upgraded architecture, ODU will not only be able to communicate with Spacecraft specific to the VCC, but will also have the capability to communicate with other satellites to support research, regardless of frequencies used or modulation schemes employed. One Software Defined Radio can replace thousands of dollars worth of analog equipment much like the one used at ODU for so many years and thus is the obvious choice for the centerpiece in implementing the Ground Station Communications Architecture.

1.3 LITERATURE REVIEW AND THEORETICAL FRAMEWORK

Perhaps the greatest contribution of this manuscript, even more so than the Communications Systems Results, will be the heuristic foundation it shall lay out for the next University Research Team undertaking its first ever Spacecraft Design.

After careful review and study of the present state of University CubeSat Research, it became apparent the compressed time line and scope of design for a project of this nature has never been documented if accomplished and hasn't been documented beyond a conference paper level treatment for any single subsystem. A clear research need from both a macro systems level approach as well as the micro level, design engineering approach presented itself.

As far as complete spacecraft design, there have been publications found in review that present a rudimentary overview of their spacecraft designs or continued research in model based approaches in systems literature [8, 9].

As for specific system design, there are innumerable papers treating multiple subsystems on a case by case basis such as antenna design, communications links and their performance, digital architectures for processing, signal processing, attitude

control, power analysis, and many others [10, 11, 12, 13, 14, 15]. Given the current state of the literature, the need and opportunity have arisen for such a treatise as this on complete spacecraft electrical systems architecture design and implementation.

1.4 THESIS ORGANIZATION AND CONTRIBUTION

With the apparent need for a complete "How To" for Spacecraft and Ground Station System Design, this thesis shall lay out the heuristic model for future University Space Systems development for supporting future science missions. The author made heavy use of Systems Engineering Approaches in order to keep design and testing on schedule as much as was possible with the given time constraints. Two major aspects played a particular role in the formulation of a plan of attack for the Mission Systems Design.

First, the objectives of the mission give birth to the mission requirements [4]. The goals outlined in section 1.2 of this manuscript give a clear and definitive science mission which may be summarized as "Obtain Orbital Decay Data to better model the LEO Thermospheric Density." Figure 2 illustrates the interdependence of generating subsystem specifications from Mission Objectives. Part of the difficulty in ODU's design was how best to balance the assessments of each design tradeoffs related to each block in Figure 2. In particular, Spacecraft Subsystem requirements and Ground Segment Requirements were the most thoroughly addressed.

This hierarchy of System Requirements leads to the second major aspect in designing a plan of attack for ODU's Electrical Systems Architecture and that is further reduction of mission objectives and its natural system requirements into subsystems [4]. Of particular note in the development of an electrical systems architecture to support the VCC's Mission Requirements, the Spacecraft Subsystem Requirements and the Ground Station Segment Requirements are of the utmost importance. Figure 3 shows an overall system architecture for the development of a scientific space payload. Most careful attention was given to the Power, Data Handling, and Telemetry and Command segments and thus dictates the general structure of this thesis.

The single most important design constraints perhaps are related to the altitude and time of year of launch that occurs with the mission [4].

Chapter 2 shall show the required analysis of orbital mechanics for generating the technical specifications requirement for the spacecraft. A simulation in Systems Toolkit (STK) shall be provided to confirm analytic results and those results shall

serve as the basis for the generation of specific design specifications such as power budgeting, link budgeting, and spacecraft lifetime estimates. These simulations shall serve as a basis for the development of the complete system architecture.

Chapter 3 will provide a discourse for the salient design aspects for implementing a 1U Spacecraft Electrical System Architecture to include PCB impedance matching, PCB design for Electromagnetic Interference and Compatibility (EMI/EMC), Impedance Transformation Networks for RF applications, Motherboard Design for interfacing multiple PCBs using a PC/104 Form Factor and multiple sensor communication protocols, and example driver software used for future software development.

Chapter 4 will give specifics on the Data Link and the AX.25 Digital Radio Protocol. An analysis of the system's Performance metrics and experimental results shall follow the presentation of GNU Radio Flow Graphs and a proper introduction to the AX.25 protocol. Measured results will be conducted considering all other design specifications and constraints derived from the orbital mechanics analysis of Chapter 2.

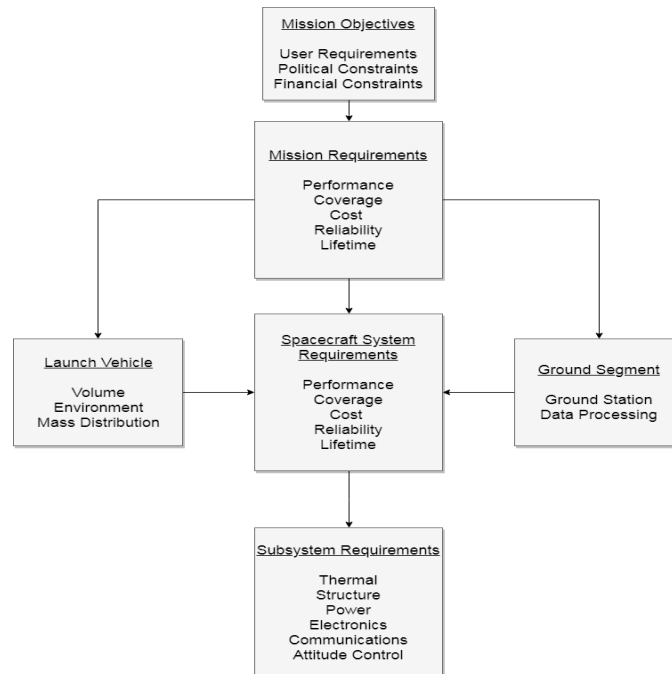


Fig. 2: Interdependance of Hierarchy of System Requirements Generated From Mission Objectives

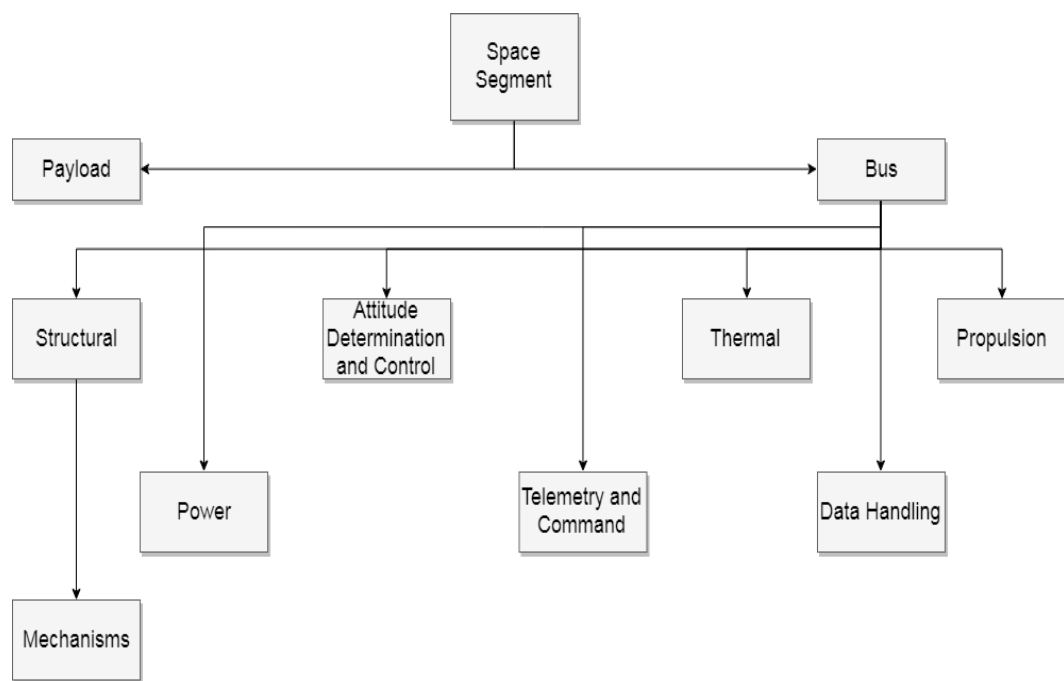


Fig. 3: Spacecraft Subsystems For Development of a University Scientific Payload

CHAPTER 2

ORBITAL MECHANICS AND THE DEVELOPMENT OF A FORMAL SYSTEM SPECIFICATION

“The theory of celestial mechanics underlies all the dynamical aspects of the orbital motion of spacecraft” [4]. The Aeternitas Spacecraft trajectory around Earth is governed by the mutual gravitational force of attraction described by the well-known “Two-Body Problem” from Physics. From this physical-mathematical understanding, we can better visualize the orbits of celestial bodies not only relative to the stars, but “over-the-ground” relative to Earth. *Analytical Graphics, Inc.* (AGI) Systems Toolkit(STK) has been employed for enhanced orbital trajectory simulations. STK is described as “The premiere software for providing four-dimensional modeling, simulation, and analysis of objects from land, sea, air, and space in order to evaluate system performance in real or simulated-time” [16].

Access to this software under an educational license agreement, enables ODU students to utilize STK for spacecraft orbital simulations over a range of scenarios. It was necessary to utilize STK for the system performance assessments required to develop reliable system specifications and guide the hardware selection germane to Power Systems, RF and Communications Subsystems, along with Ground Station Scheduling (Orbit-specific scheduling intervals when the ODU Ground Station will have radio access to the satellite).

From this analysis and the simulations on which they are predicated, it has been possible to evolve formal system performance specifications and select hardware based on those results. In that way, it was possible to proceed with the actual system design. Reliable orbital performance specifications were critical since they set the groundwork for all system and subsystem designs with respect to available power, data links, and spacecraft lifetime. Figure 4 represents a simple STK orbital trajectory simulation which includes the expected orbital mechanics of the Aeternitas Spacecraft relative to “Place1” which was later simulated as Kaufman Hall - The location of ODU’s Ground Station.

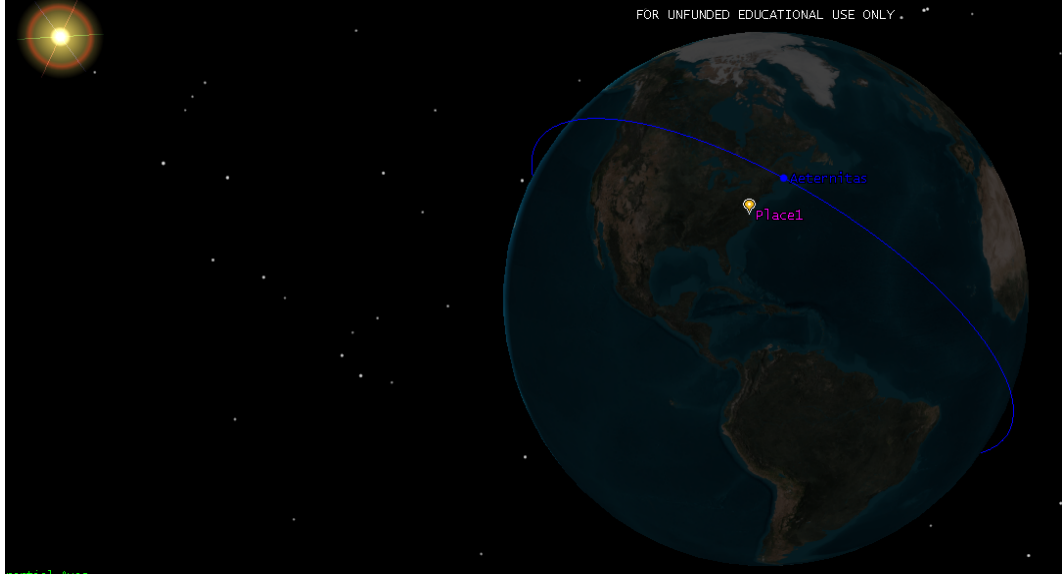


Fig. 4: Visualization of the Four Dimensional Celestial Mechanics Simulation Using STK

2.1 STK SIMULATION PARAMETERS

In order to use STK simulations and interpret the results, an understanding of the input parameters required for each simulation is critical for obtaining realistic and repeatable results.

Johannes Kepler is credited with discovering the elliptical nature of the orbits of planets around our sun as is Newton with mathematically formulating the conical section model for satellites [17]. The Keplerian Elements as they are called, provide us with the foundation to visualize satellite orbit size, shape, and orientation, along with its instantaneous position relative to the specific bodies in question.

In total, six parameters are required to perform an analysis utilizing Keplerian Elements or Classical Orbital Elements (COEs). The first two COEs, Semi-Major Axis, and Eccentricity give the size and shape of the orbit. The following three, Inclination, Right Ascension of the Ascending Node (Ω), or RAAN, and Argument of Perigee (ω) define to the inertial orientation of the satellite orbit. The final COE, True Anomaly (v), shows the satellite's location in the particular orbit at one instant in time.

Alternative parameters to the COEs can be employed when some of the COEs

TABLE II: Alternate Orbital Elements and When to Use Them in Analysis

Element	Name	Description	Range of Values	When to Use
u	Argument of Latitude	Angle from ascending node to Spacecraft Position	$0 \leq u \leq 360^\circ$	No perigee ($e = 0$)
Π	Longitude of Perigee	Angle from the principle direction to perigee	$0 \leq \Pi \leq 360^\circ$	Use when equatorial ($i = 0$ or 180°) no ascending node
l	True Longitude	Angle from the principal direction to the spacecraft's position	$0 \leq l \leq 360^\circ$	No perigee and ascending node ($e = 0$ and $l = 0$ or 180°)

are undefined [17]. These special variables are defined in Table II.

For purposes of this analysis, only COEs will be employed. STK accounts fully for the cases when the Alternate Orbital Elements are required, producing consistent results.

2.1.1 SEMI-MAJOR AXIS

The semi-major axis, a , is equivalent to the average radius of an elliptic orbit, measured between its nearest approach (to the Earth in this case) and the farthest distance, along a straight line. This parameter represents the size of the satellite orbit and for the Aeternitas mission a can be approximated as the radius of the Earth plus the nominal circular altitude above Earth. Since the Earth is not a perfect sphere the circular radius beneath the orbit has been taken to be 6371 km; the nominal altitude of the ISS, from which the CubeSat will be deployed, is 400 km. Thus the parameter (a) for our simulation shall be 6771 km.

2.1.2 ECCENTRICITY

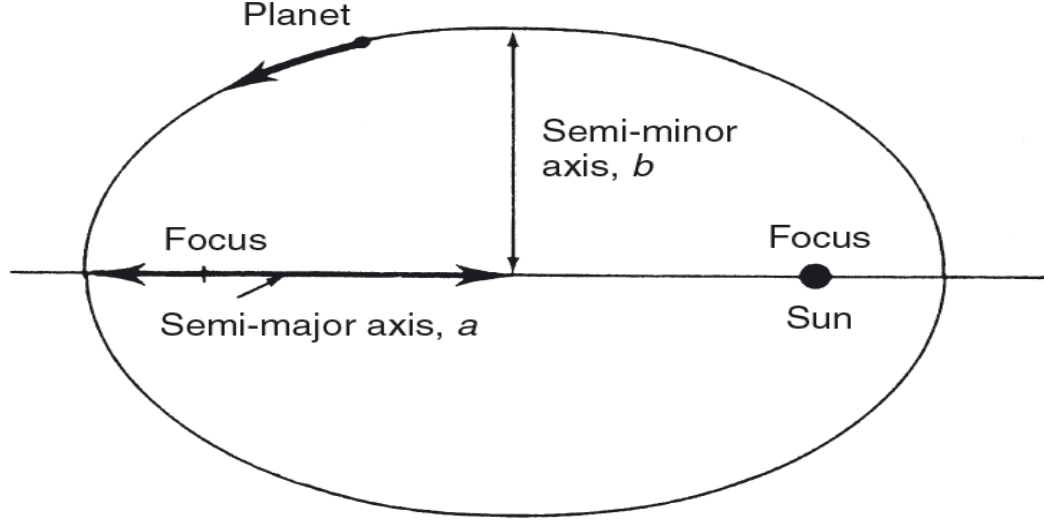


Fig. 5: Visual depiction of Semi-Major Axis

With the size of the satellite orbit specified, the other required orbital shape parameter required for the simulation is the eccentricity, e . From Geometry we know that the eccentricity is a measure of out of roundness of a conic section. Simply put, the eccentricity is the ratio of the distance between two foci and the length of the major axis. Referring to Figure 6, we have equation 1. Borrowing nomenclature from NASA we have the quantities below.

$$e = \frac{2c}{2a} = \frac{c}{a} \quad (1)$$

A more useful eccentricity equation can be defined as the square root of the difference between a circular orbit, i.e. where $b/a = 1$, and the ratio of the squares of the semi-minor and semi-major axes of a satellites orbit.

$$e = \sqrt{1 - \frac{b^2}{a^2}} \quad (2)$$

The semi-minor axis distance, b , is the sum of the radius of the Earth (6371km) and the minimum satellite orbit altitude. The semi-major axis, a , is the sum of the radius of the Earth and the average of the maximum and minimum satellite orbital altitudes, as stated. Using a mean ISS eccentricity we can validate our results and use $e = .0003864$ for a height of 406 km above the Earth which correlates with a nearly circular orbit - the assumption we made from the beginning. With the shape

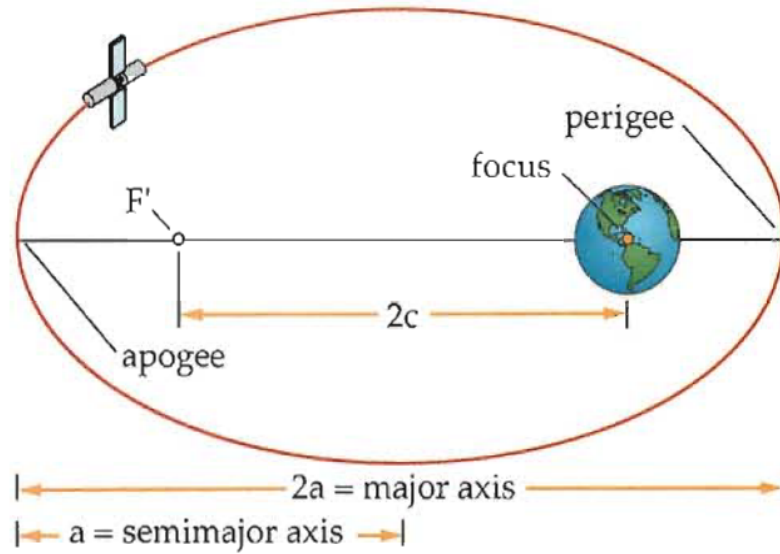


Fig. 6: Orbital Depiction of Eccentricity

and size of the Aeternitas Spacecraft orbit, we are ready to proceed with defining the orientation of the spacecraft relative to a geocentric equatorial coordinate system [17]. Figure 7 is a qualitative depiction of oscillations in eccentricity over the expected life of Aeternitas (in blue) compared to the height of apogee and perigee (yellow and red respectively) over the course of the mission. It is important to observe how the perigee history relates to expected re-entry.

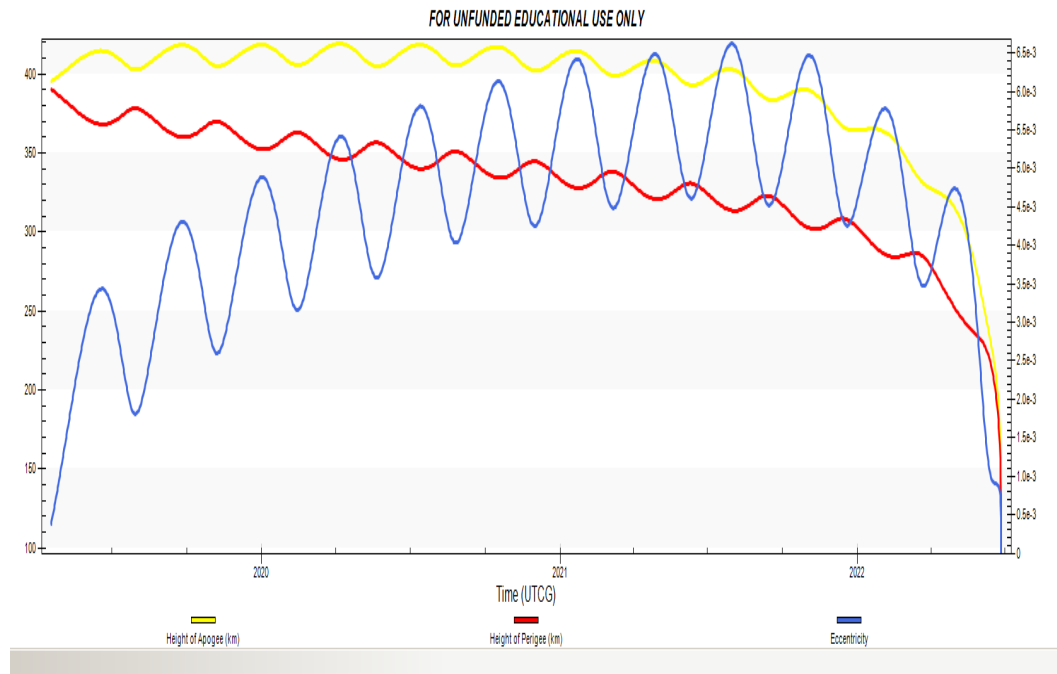


Fig. 7: Simulated Eccentricity Plot over the course of the mission

2.1.3 INCLINATION

For Earth orbits, the fundamental plane is the equatorial plane and the orbital inclination defines the tilt of the particular orbital plane relative to our equatorial plane, providing a sense of the spacecraft motion with respect to the equator[17]. For reference, a satellite that orbits directly above the equator has zero inclination. The opposite of this would be a satellite orbiting from the geographic north pole to the south pole, which would have a 90° inclination. Conversely, a satellite with an orbit of 180° orbits above the equator in the opposite (retrograde) direction to the Earth's rotation. Borrowing from the same NASA reference sources, an ISS orbital inclination of $i = 51.64^\circ$ has been employed in these simulations.

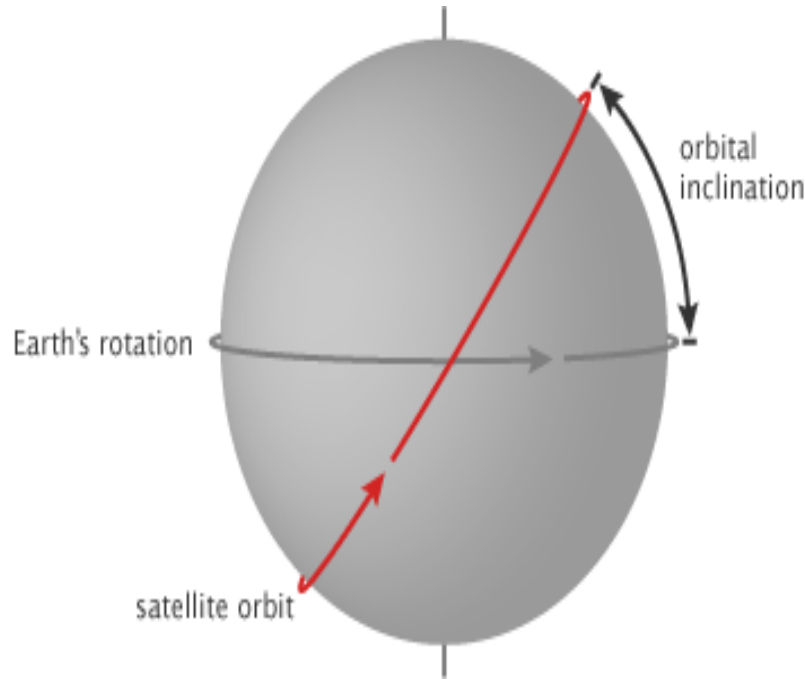


Fig. 8: Orbital inclination

2.1.4 RAAN

The fourth COE is the RAAN. For Earth orbits, a satellite that is not in an Equatorial Orbit pierces the Equatorial plane at two points in a each orbit. The (Right) Ascending Node is where the satellite passes through the Equatorial plane from south to north [17]. The term right ascension is similar to longitude but uses the vernal (Spring) equinox as the inertial-reference x-coordinate, passing between the centers of the Earth and Sun and therefore that coordinate direction does not rotate with Earth.

The Ascending Node terminology comes from the fact that the intersection of the orbital plane and the fundamental plane forms a line of nodes. The two points at which the orbit crosses the equatorial plane are the nodes of interest [4, 17]. When the spacecraft traverses from below the equator to above it is the ascending node. Conversely, if the spacecraft were in such an orbit that it crossed into the southern hemisphere from the north of Earth, that would be the descending node.

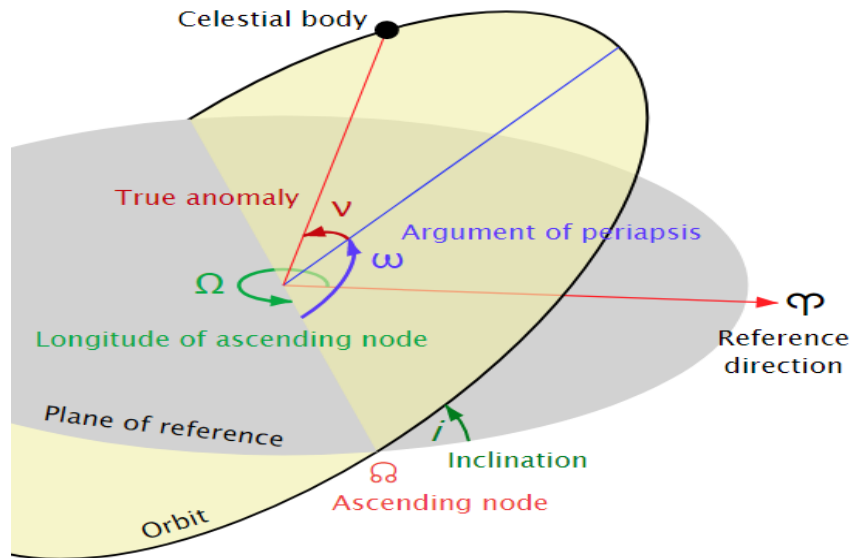


Fig. 9: RAAN Illustration

2.1.5 ARGUMENT OF PERIGEE

On an elliptical orbit around Earth, the point closest to Earth is the perigee while the farthest from Earth is the apogee. The Argument of Perigee measure of the angle in the orbital plane, between the Ascending Node and the Perigee. Note, there is no value for the Argument of Perigee if the satellite is in the equatorial plane, or in a perfectly circular orbit [17]. Based on the ISS data, $\Omega = 324.944^\circ$ has been assumed in STK.

For the given parameters used previously from ISS data, we use 324.944° as the input parameter to STK.

Location: Argument of Perigee (ω)

We locate perigee relative to the ascending node (in the orbit plane)

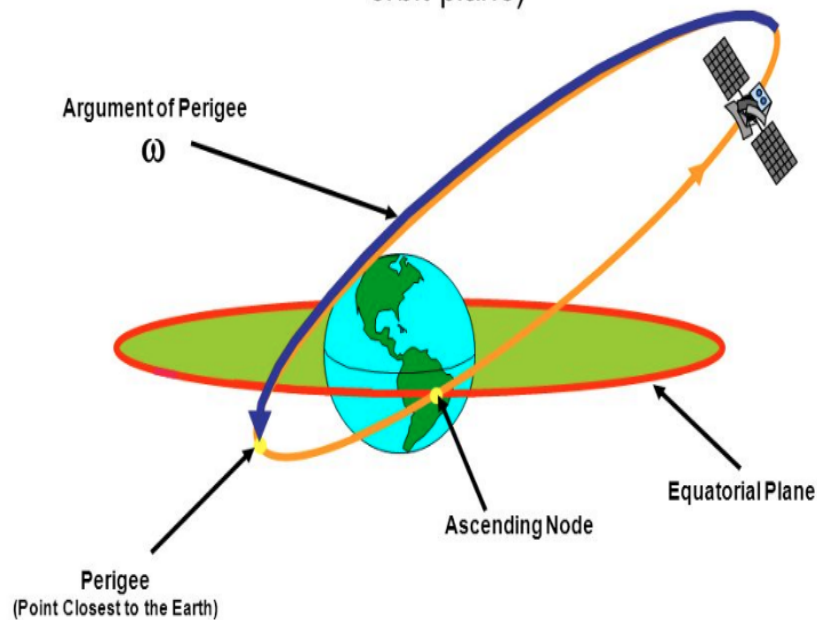


Fig. 10: Argument of Perigee Illustration

2.1.6 TRUE ANOMALY

Finally, after the size and shape of the orbit, along with the spacecraft orbital orientation, have been specified, the true anomaly, locating the satellite on that orbit at a specific time, is required for the simulations. True Anomaly gives the location of the satellite within the orbit and since the satellite is constantly moving, True Anomaly constantly changes and thus we leave the calculation to STK. True Anomaly measures the angle between Perigee and the satellite location, measured in the direction of the Spacecraft motion.

2.1.7 SPACECRAFT TUMBLING AND THE INERTIA TENSOR MATRIX

Up to this point, our STK software has been provided with the input parameters required to simulate the motion of a “point on the particular orbit. That enables it to predict the motion of the center of gravity (center of mass in space), but STK cannot determine the orientation with respect to whether the sun is shining on the solar cells or whether the radio antennae are pointing toward a ground station. A full STK simulation requires data related to spacecraft moments of inertia. The Moment of Inertia Matrix, is considered to be a second order input; however leaving the default values in STK leads to drastically different simulation results.

A simplification must first be made as we model the CubeSat in STK. This simplification is to first model the cubesat as a cube of solid mass M and a side a rotating about a corner. Since this mass is evenly distributed in our simplified model, the upper left element becomes:

$$\mathbf{I}_{xx} = \int_0^a dx \int_0^a dy \int_0^a dz \tilde{\rho}(y^2 + z^2) \quad (3)$$

where $\tilde{\rho} = M/a^3$ denotes mass density. 9 such integrals exist to denote each combination along the xyz axes, however by symmetry we see that $\mathbf{I}_{xx} = \mathbf{I}_{yy} = \mathbf{I}_{zz}$. The same applies to the off-diagonal elements as well. Completing the integral we have:

$$\mathbf{I}_{xx} = \tilde{\rho} \left(\int_0^a dx \int_0^a y^2 dy \int_0^a z^2 dz \right) = \frac{2}{3} \tilde{\rho} a^5 = \frac{2}{3} M a^2 \quad (4)$$

The off-diagonal elements are of the form:

$$\mathbf{I}_{xy} = -\tilde{\rho} \int_0^a x dx \int_0^a y^2 dy \int_0^a z^2 dz = -\frac{1}{4} \tilde{\rho} a^5 = -\frac{1}{4} M a^2 \quad (5)$$

Thus the moment of inertia tensor about a corner is: $\mathbf{I} = \begin{bmatrix} \frac{2}{3}Ma^2 & -\frac{1}{4}Ma^2 & -\frac{1}{4}Ma^2 \\ -\frac{1}{4}Ma^2 & \frac{2}{3}Ma^2 & -\frac{1}{4}Ma^2 \\ -\frac{1}{4}Ma^2 & -\frac{1}{4}Ma^2 & \frac{2}{3}Ma^2 \end{bmatrix}$

More concisely: $\mathbf{I} = -\frac{Ma^2}{12} \begin{bmatrix} 8 & -3 & -3 \\ -3 & 8 & -3 \\ -3 & -3 & 8 \end{bmatrix}$

If we shift the origin of the coordinate system in equations 4 and 5 to the center of the cube, the diagonal element integrals become:

$$\mathbf{I}_{xx} = \tilde{\rho} \left(\int_{-a/2}^{a/2} dx \int_{-a/2}^{a/2} y^2 dy \int_{-a/2}^{a/2} z^2 dz \right) = 2 \frac{2}{3} \tilde{\rho} a^2 (a/2)^3 = \frac{1}{6} Ma^2 \quad (6)$$

For the off-diagonals we have all odd functions thus:

$$\mathbf{I}_{xy} = -\tilde{\rho} \int_0^a dx \int_0^a y dy \int_0^a dz = -\frac{1}{4} \tilde{\rho} a^5 = 0 \quad (7)$$

Therefore, we have the Inertia Tensor Matrix:

$$\mathbf{I} = \frac{Ma^2}{6} \begin{bmatrix} 1 & 0 & 0 \\ 0 & 1 & 0 \\ 0 & 0 & 1 \end{bmatrix} \quad (8)$$

In order to use equation 8, we must determine next the acceleration due to gravity at the altitude of the cubesat. We know that the acceleration due to gravity is governed by the equation:

$$g = \frac{GM}{R^2} \quad (9)$$

Rewriting in terms of gravity due to the height above the Earth's Surface we have:

$$g_h = g \frac{GM}{(R+h)^2} \frac{R^2}{GM}$$

Proceeding with cancellations we arrive at Equation 10:

$$g_h = g \frac{1}{(1+h/R)^2} \quad (10)$$

Where g_h is the well-known acceleration due to gravity at Earth's Surface, h is the height above the Earth's Surface (in the case of the Cubesat we use 400 km for LEO), and R is the radius of the Earth - roughly 6371 km. Proceeding with our parameters we ascertain that the acceleration at the beginning of the mission is approximately

$8.676m/s^2$. Using this result, we use Equation 8 to complete the Inertia Tensor Matrix Calculation with an intrinsic spacecraft mass of 1.169 kg, yielding a result of $14.6667kg/m^2$.

2.1.8 SUMMARY OF STK INPUT PARAMETERS

Given the analysis and assumptions of the preceding section, we are ready to simulate our mission. A table of the relevant parameters is shown to summarize the STK inputs.

TABLE III: Summary of STK Simulation Parameters

STK Parameter	Input
Orbit Propagator	Two Body
Semi-Major Axis	6771 km
Eccentricity	0.000386
Inclination	51.64°
Argument of Perigee	324.944°
RAAN	1.0083°
True Anomaly (STK Calculated)	3.43E-10°
Mass	1.169 kg
Inertia Matrix input	14.667 kg m^2
Earth Albedo	0.34
Material Emissivity	0.77
Material Absorptivity	0.14
Cross Sectional-Area	36 cm^2
Shape Model	Cubesat + Plate

Emissivity and Absorptivity were cited from datasheet specifications for Anodized Aluminum for the Aeternitas Chassis.

2.2 ORBITAL LIFETIME

From the inputs summarized in section 2.1.8 we are now confident in the simulation data to provide accurate results for our specification requirements [4]. STK simulates the orbital lifetime of the Aeternitas Satellite to be estimated at 3.0 to

3.2 years using the High-Precision Orbit Propagator (HPOP) and the Two Body Propagator respectively. An additional model of the satellite as a crude plate was also used as a measure of how much better the HPOP and two-body propagators improve the analysis over a rough approximation. The most crude model used, modeling the cube as a plate of mass 1.169 kg, yields a total orbital lifetime of about 3.9 years. Given the calculations were done correctly and the assumptions we made were reasonable, we ascertain that the orbital lifetime for Aeternitas is nearly a full year shorter than the other two satellites in the VCC constellation. The other satellites launched by Virginia Tech and University of Virginia, both do not have the deployable drag brake mechanism that Aeternitas has and thus our approximation of the orbital lifetimes makes sense when compared to the data of the other two spacecraft. The output data from each of the three simulations is given in tables.

The three orbital models used were the High-Precision Orbit Propagator (HPOP), a simple two-body propagator, and the crudest model, a plate. Using the same input parameters for Aeternitas and only leaving the total drag area as the variable of concern, we are able to show a comparative analysis for Aeternitas vs the other VCC Satellites Lifetimes based on the exposed drag area based on the mechanical design. The total area added to the Aeternitas design versus the VCC constellation is 36 cm^2 vs 10 cm^2 as each of the four drag break petals at maximum adds an additional 6.5 cm^2 per petal plus the maximum exposed area of the cubesat of 10 cm^2 .

“HPOP uses numerical integration of the differential equations of motions to generate ephemeris” as well as other modeling effects such as a full gravitational field model (based upon spherical harmonics), third-body gravity, atmospheric drag and solar radiation pressure [16]. As such, of the three models used in our simulation results, the HPOP is considered to be the most accurate.

TABLE IV: Aeternitas Orbital Lifetime Simulation Results 3 Initial Models

Model	Orbits	Years Lifetime	Mission End Date
HPOP	17201	3	4/13/2022 0:22
2-Body	18352	3.2	6/26/2022 17:32
Plate	22366	3.9	2/5/2023 8:02

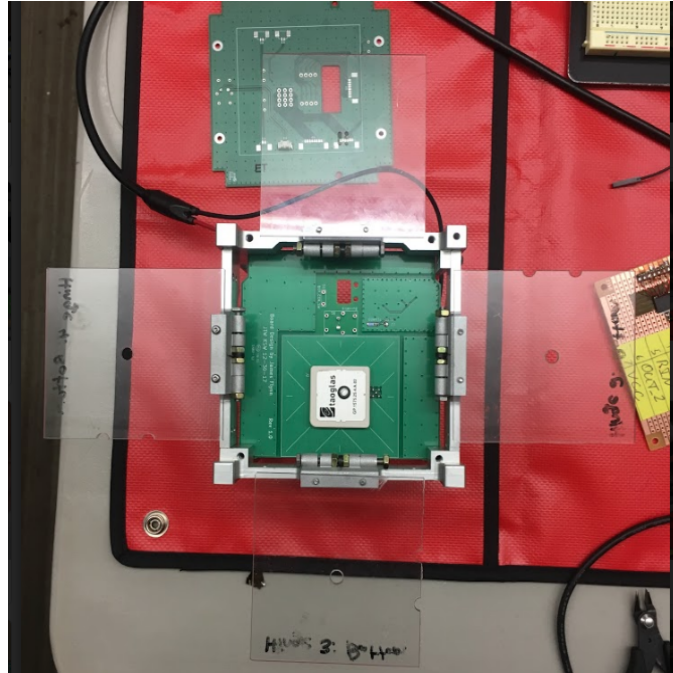


Fig. 11: Drag Brake Mock Up During Satellite Assembly Which Accounts for the extra 26 cm² of Exposed Drag Area vs The Other Two VCC Satellites

TABLE V: VCC Orbital Lifetime Simulation Results for 2 Most Accurate Models

Model	Orbits	Years Lifetime	Mission End Date
HPOP	31780	5.5	10/25/2024 1:28
2-Body	33930	5.9	3/13/2025 18:26

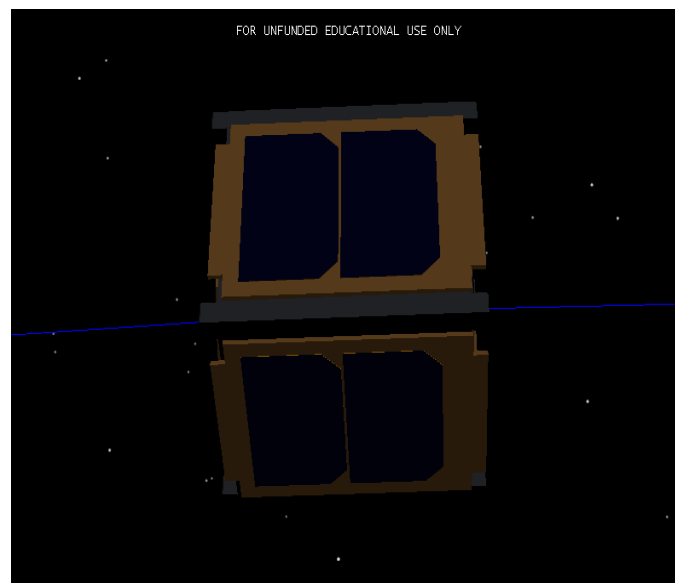


Fig. 12: CubeSat CAD model with Solar Panel Characteristics and Drag Brake Area Added

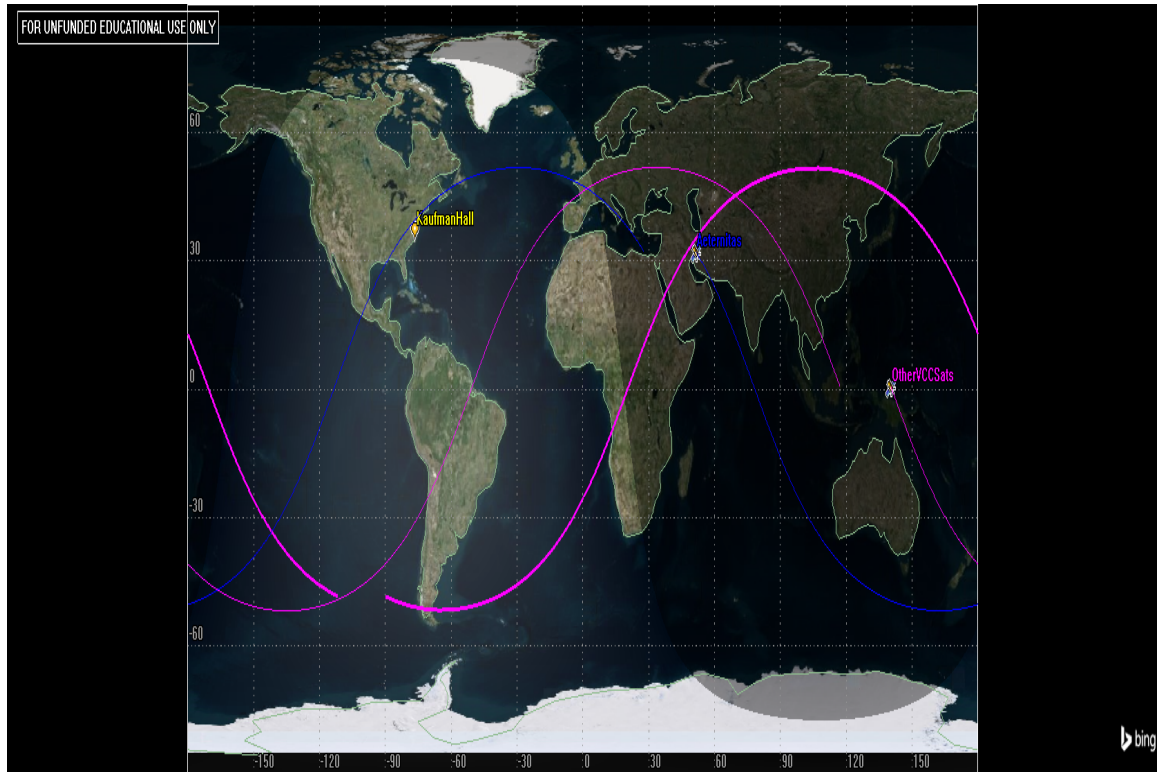


Fig. 13: Comparative VCC Orbital Simulation for Satellite Lifetimes

One can observe also, the Eccentricity, Height of Apogee, and Height of Perogee in Figures 13 and 14 over the lifetime of the Satellite for the Two-Body and HPOP models respectively.

Given these initial Mission Simulation Results and the validation they provide apropos the mission lifetime based on the intrinsic characteristics of the satellite, we are now able to move forward with the specifying the system hardware based on further analyses made by hand and validating these results with a “Day in the Life” Concept of Operations (CONOPS) model in STK.

With validated analysis via STK simulation results in hand, we proceed now with further analysis and validation for the two most important electrical subsystems on any University CubeSat, Power, and Communications. In addition to these two crucible subsystems the design of a Telemetry Acquisition and Command Interface for this Spacecraft Hardware which complement the COTS parts summarized in the table below shall be explored as well.

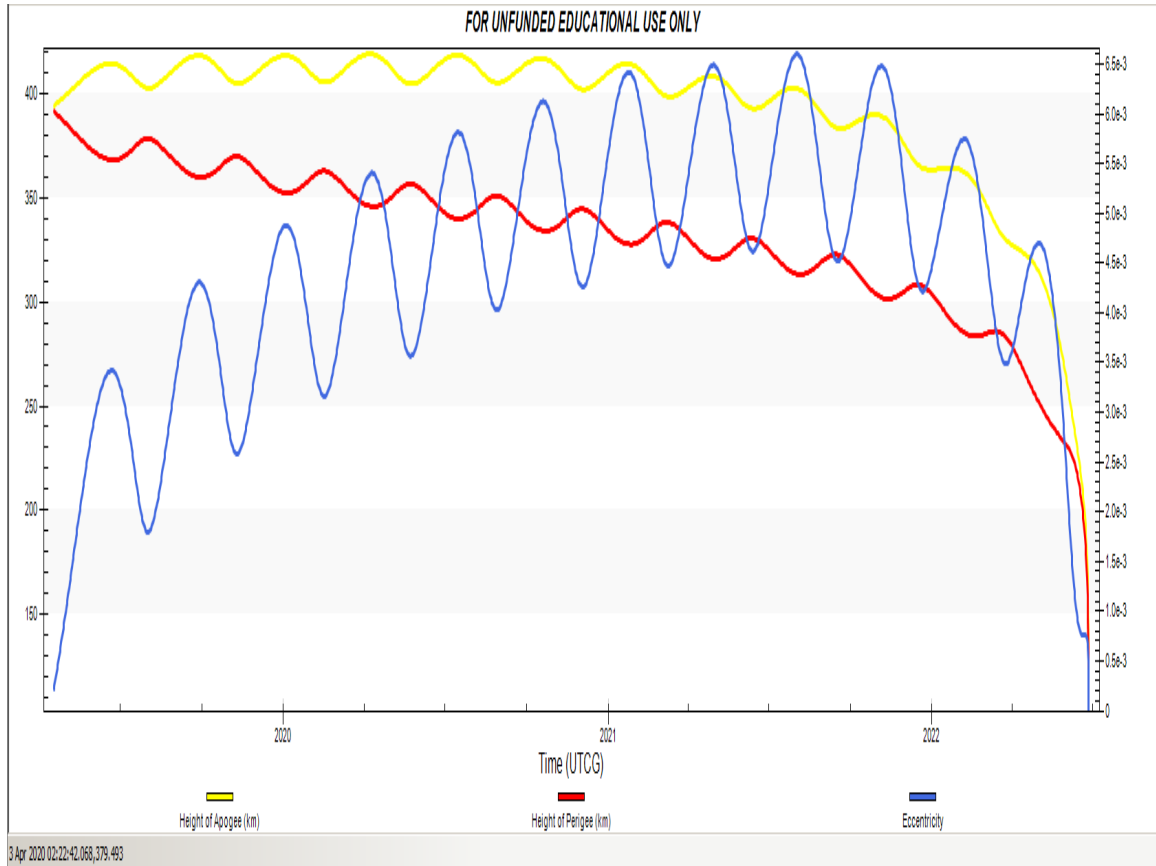


Fig. 14: Aternitas Orbital Eccentricity Characteristics using 2-Body Propagator Model

2.3 POWER REQUIREMENTS

The provision of power for space vehicles is called “The most fundamental requirement for the satellite payload” in basically any space systems literature or textbook one might review [4, 8, 17].

With the reasonable baseline for our mission lifetime established in Chapter 2, we can begin to ask questions about Power Harvesting and Solar Cycles. This is by far the biggest question in assessing the power needs and capability of Aternitas, as it will be limited by the maximum power that can be harvested during which times the satellite is not blocked by celestial bodies, namely the Earth. The goal of the Power simulations was to determine the worst case power scenario by performing a “Day in the Life” Orbital Simulation down to one second resolution.

In the Aternitas Simulation, the CubeSat is modeled using each of the Power

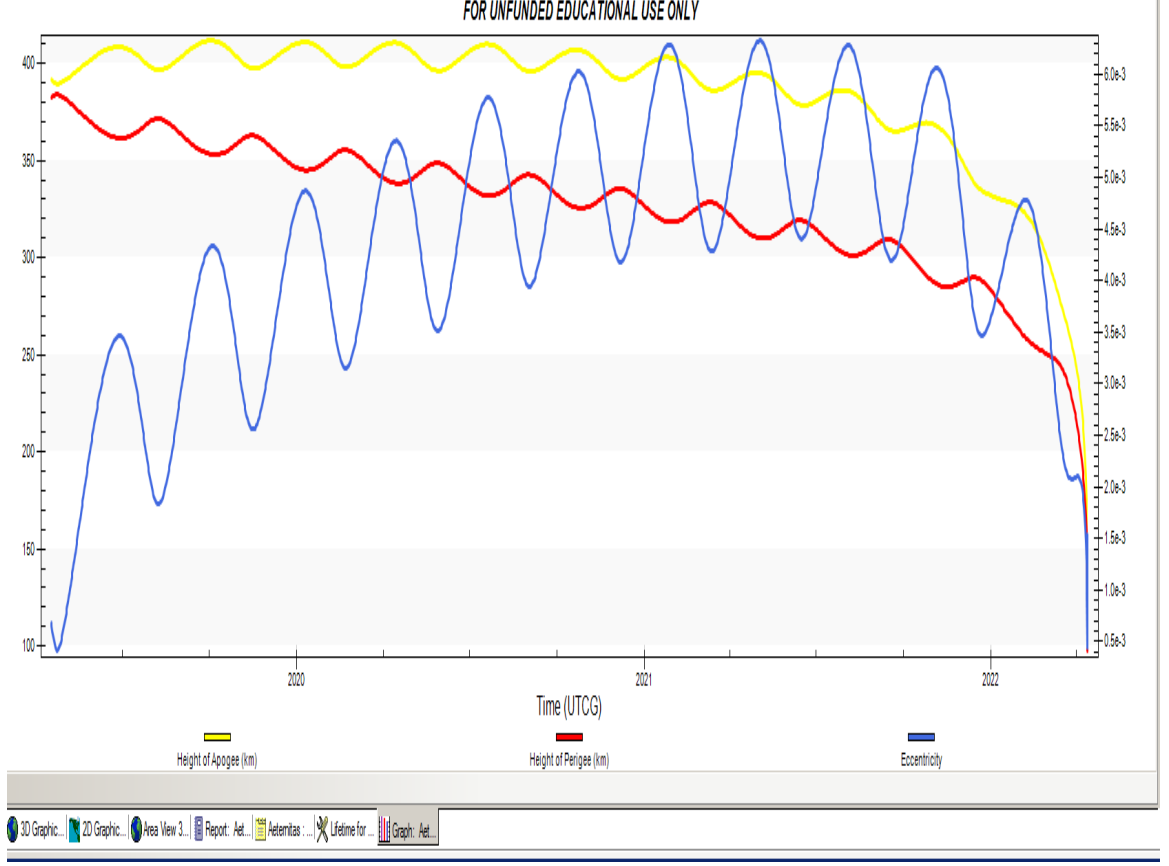


Fig. 15: Aeternitas Orbital Eccentricity Characteristics using HPOP Model

Panels by taking an ideal case and a worst case scenario we can find again, reasonable baselines to specify our power system capabilities.

The solar panel hardware selected for simulation analysis was the *GOMSPACE* P110UA Solar Panel and has the following specifications: In order to calculate a power harvesting budget, we must know the intrinsic parameter of efficiency and effective area for our hardware, and the variables which change based on the orbital characteristics of the spacecraft, Solar Intensity and Solar Irradiance (I_0). From this we use Equation (11) to calculate harvested power in [W].

$$P_{Harvested} = \eta_{Panel} \cdot A_{Panel} \cdot SI \cdot I_0 \quad (11)$$

Where SI is the Solar Irradiance in [Wm^{-2}] and I_0 is given in [W/m^2]. These two parameters are highly variable and are thankfully accounted for by STK based on the input simulation parameters we feed in. However, a simple model for I_0 exists and is given by equation (12) where I_0 is extraterrestrial irradiance on a plane orthogonal

TABLE VI: GOMSPACE P110u Specifications

Parameter	Condition	Min	Typ	Max	Unit
Voltage	Optimal Voltage	4.64		4.84	V
Current	Current at Optimal Voltage	490		508	mA
Power	Maximum Power Rating	2270		2400	mW
Efficiency		29.8	30	30.2	%

to the Sun's Rays given in $[\text{W}/\text{m}^2]$, I_{SC} is the solar constant ($1367 [\text{W}/\text{m}^2]$) and n is given as the day of the year such that for January 1st $n = 1$.

$$I_0 = I_{SC} \left[1 + 0.0034 \cos \frac{2\pi n}{365.25} \right] \quad (12)$$

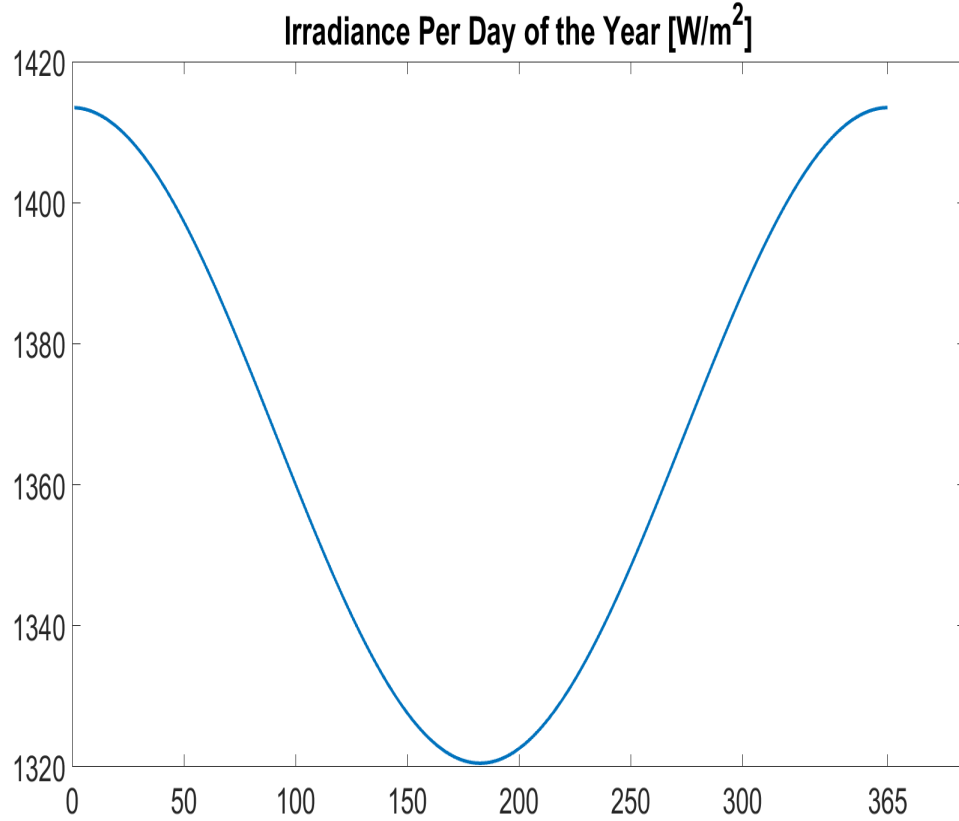


Fig. 16: Solar Irradiance For a One Year Solar Cycle

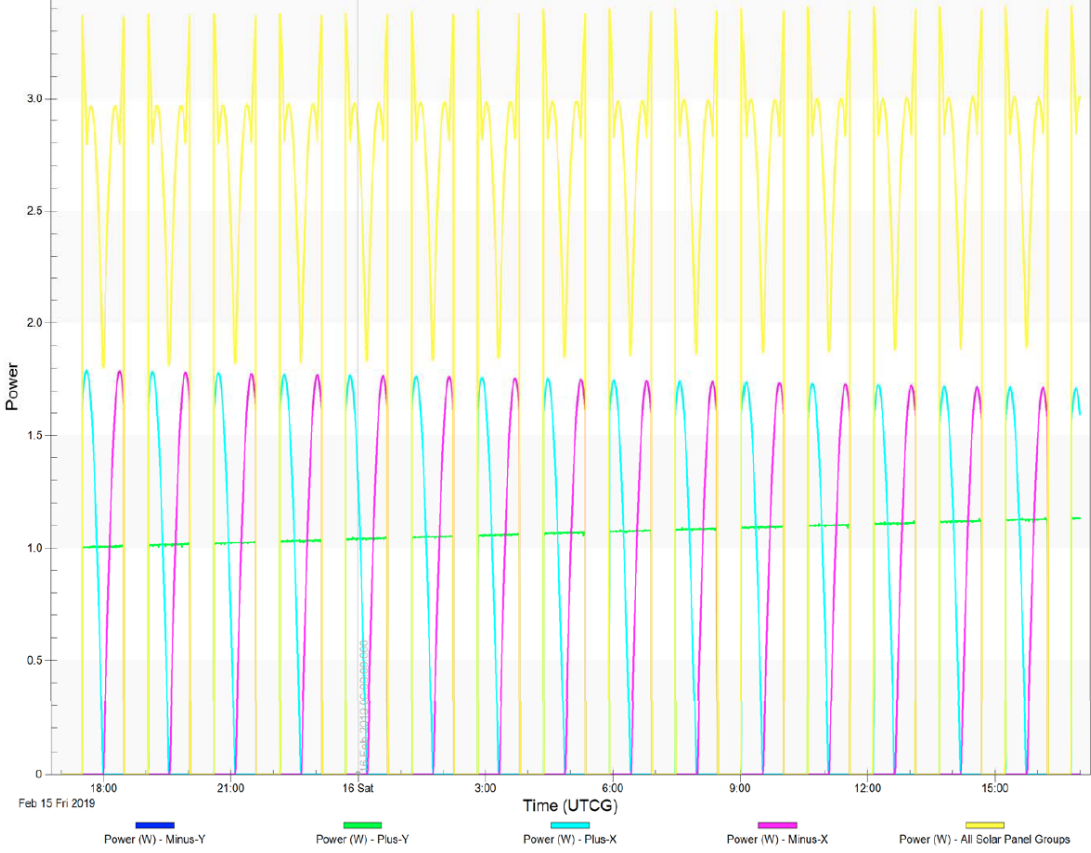


Fig. 17: Power Harvesting Curves for Aeternitas HPOP Model

Plotting Equation 12 gives good sense to how Solar Irradiance Varies as the Year goes on for a given location.

Figures 15 and 16 above display the Power Harvesting Capabilities for the Cubesat given the dynamic nature of the HPOP and 2 Body Propagation Models discussed in Chapter 2. With the typical system parameters from the *GOMSPACE* P110u Solar Panels and accounting for the damaged solar panel on the assembled prototype, we can make accurate assessments with regard to the spacecraft power budget.

Power Budgets are typically broken down into three instances: Power Consumption, Power Generation, and Power Storage. As with balancing basic circuit models, we also balance power budget calculations to perform.

Power Consumption is first estimated based on the high power elements of Aeternitas in each of the satellites main modes of operation, Sleep, Sensor Acquisition, and Transmission mode.

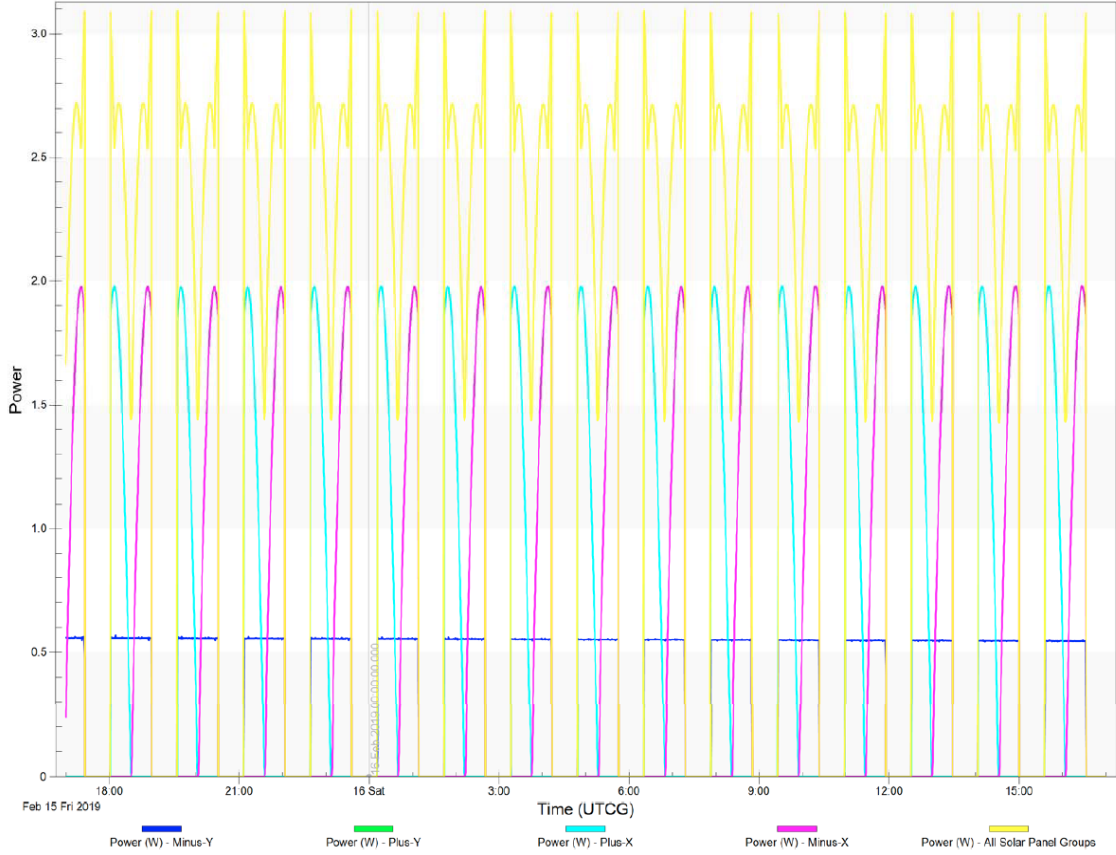


Fig. 18: Power Harvesting Curves for Aeternitas 2-Body Model

2.3.1 POWER CONSUMPTION

The first power component calculated for power consumption was the PiNAV-L1 GPS. From the datasheet we see that typical power consumption is 125 mW under normal operating conditions. An overestimation of 44% was used arbitrarily to account for any excess power leakage and parasitics from the module.

The first *major* power consumption component in the satellite is the Lithium II Radio. Though the Lithium II is rated at up to 28W, the license for ODU is only authorized up to 2W maximum and thus the hard theoretical limit is treated as such during transmission [18]. In addition to this hard upper limit, this does not take into account the efficiency of the team-designed antenna and the fact that the Radio is powered from the EPS Boost Converters. Therefore, we take the rated power of the Radio and multiply this by the rated efficiency of the Buck Converter Efficiency

advertised by *GOMSPACE* which varies from 96-78%. For our theoretical calculations we assume worst case scenarios for power consumption and efficiency, therefore we use 78% for all EPS efficiency conversion circuitry. Theoretically then with 2W power consumption, the radio operating at 5V will consume 400 mA current (which gives 2W). Then, we multiply by best and worst case efficiencies to get minimum and maximum Wh for the device.

The next power consumer to be calculated was the processor in its two extreme states, full capacity, and sleep mode. The processor runs on 3.3V, but is also linearly regulated from the EPS power conversion circuitry and is also susceptible to the power dissipated as heat in the EPS. The battery voltage of the EPS also varies as the charge of the battery varies. With the Processor and all of its peripherals running on the ODU designed motherboard, an overestimate of the processor was approximated to be 100mA and with a nominal P31u Voltage of 7.4V we have .74W for the processor running at full capacity.

The processor running in sleep mode draws a mere 20 mA in sleep mode and with a nominal voltage of 7.4V this equates to a sleep mode draw of .148 W. Again because these components run from the EPS conversion circuitry, they are subject to losses due to heat and such, the best and worst case scenarios are again found using the 96 and 78% efficiency ratings found in the EPS datasheet.

Table VII summarizes the theoretical Power Consumption Budget for the Aeternitas Spacecraft. This table accounts for the absolute maximum, worst-case scenario for power consumption of the space craft. These numbers are derived considering full-time operation of the spacecraft components 24/7 at maximum operating capacity.

At the bottom of Table VII, a full-time ON, max power calculation per orbit around Earth is calculated using an average orbit length of 88 minutes or 1.46 hours.

TABLE VII: Theoretical Power Consumption Table based on 1.46 hour orbit

Power Component	Voltage	Normal Power(Wh)	Min Power(Wh)	Max Power(Wh)
piNAV-L1 GPS	3.3v	0.18		0.18
Lithium-2 Radio	5v	0.3	1.56	1.92
EPS Heater	Built into EPS	0.66		0.9
EPS Operation	Onboard Processing	0.160		0.48
Magnetorquer (per)	3.3v	0	0	0.5
Power Consumed		1.898	0	3.98

2.3.2 POWER GENERATION SIMULATION RESULTS

Aeternitas Solar Cells are estimated to provide a time average of 0.619W in the worst case scenario and 1.69W for the best case scenario over the lifetime of the mission. Given the two accurate models we accepted from our analysis in Chapter 2, tables VIII and IX are given to summarize the power generation capabilities of the four solar cells for the duration of the mission.

TABLE VIII: HPOP Power Generation for $P_{ave} = 1.69$ Watts

Generated Power		
4 Solar Cells (with 1 damaged)	Power (W)	Energy (Wh)
Worst Case	0.619	16200
Best Case	1.69	44400

TABLE IX: Two Body Power Generation for $P_{ave} = 1.69$ Watts

Generated Power		
4 Solar Cells (with 1 damaged)	Power (W)	Energy (Wh)
Worst Case	0.619	17300
Best Case	1.69	47400

After observing these tables, the approximations are initially seen as a problem. For the Full Power ON 100% of the time assumption we made in the beginning of our power consumption calculations, we have a power burden of 104,500 Wh over the course of 1095 days constrained to the HPOP model. Given our best and worst case scenarios from table VIII, we have at best given the “Full ON” an unacceptable deficit of 60 kWh for the lifetime of the mission.

However this is not the end of the story for the power consumption of the satellite. An “Always ON” at full power approach is not practical in our original assumptions as one must consider the duty cycle of the equipment. Referencing Table VII, we see the two major culprits of the Aeternitas power consumption. This supports the evidence presented by Woellert and colleagues and their statements that in general, “communications systems, when transmitting, consumer approximately 50% or more of the total power demand in satellites” [19]. Theoretically, with the radio operating at full power continuously for the life of the mission, it would absorb over 52 kWh for the lifetime of the mission. This is not practical from both a standpoint of operations and engineering. The satellite simply could not acquire data and transfer it quickly enough to transmit new information all the time, and no engineer worth hiring would ever engineer a system to pollute the RF spectrum 100% of the time during operations especially if the data communications payloads don’t require it.

By adjusting only the two primary power consuming components, the radio and the EPS heater, we are able to achieve energy balance within a reasonable tolerance. Considering a reasonable duty cycle of 5% for the radio, we achieve an overall power savings of over 49 kWh for the life of the mission [20].

One additional communications system note related to power is that the energy per bit transmitted is dependent on the transceiver design as well as the operation and management of the transceiver. In other words, the energy requirement for communications is proportional to the number of bits processed and transmitted in a given period of time. With this information, prior to the final design phase of the student-designed hardware, the amount of satellite access is vitally important.

As with the radio, the EPS heater would never be on for a 100% duty cycle as the batteries would overheat and be rendered useless as a result. A reasonable maximum assumption to make is 50%. With a 50% duty cycle, we assume the EPS heater is on during eclipse conditions and off for sun exposed time periods. Any further assumption beyond this would not be responsible without experimental validation or

TABLE X: Theoretical Power Budget Adjusted for Radio and EPS Heater Duty Cycles

Worst Case Scenario	[Wh]
EPS Heater	23600
Radio	52000
All others	28900
Total Power Absorbed [W]	104500
Total Deficit	60100
Resolved Radio and EPS Duty Cycle	
EPS Heater	11800
Radio	2600
Savings	61200
Net Power	1100

using models to further analyze the EPS heater, but a 50% duty cycle is conservative. With 50% duty cycle, we obtain a power savings of nearly 12 kW over the lifetime of the mission. From this we have our surplus denoted by the negative power (Passive Sign Convention for Power Delivered):

With the adjusted duty cycles of the radio and EPS we estimate that the effective average Aeternitas Load is responsible for is approximately 1.706 W over the mission lifetime. The results from table X illustrate the large power demands that the communications system of any satellite place on the system as a whole. With a net positive result with our chosen power hardware and COTS components, we can now move ahead with the rest of the hardware specification and design as we've come to a net positive result in raising power for the satellite.

2.3.3 POWER STORAGE CAPABILITY

In Aeternitas and other satellites like it, the power system is divided into several sub elements, two of which pertain to energy sources, the primary and secondary sources [4]. In the case of the ODU spacecraft, the primary energy source is the harvesting system comprised of its four solar panels. It is the spacecraft mechanism

and circuitry which converts solar fuel into usable energy but does not contain a fuel cell to store that energy. This energy can be directly drawn upon by components in operation, or if the solar array is accompanied by a storage circuit, the unused charge may be delivered to the storage circuit.

However the secondary energy source is the COTS EPS battery system. This energy source is the energy storage hub of the satellite and also the source from which power is drawn to operate all other circuitry on board. Additionally, the main purpose of this circuitry aside from storage is to operate the satellite during conditions of eclipse. It is customary for satellite missions flown in LEO to have an eclipse period of approximately 40% of the orbital cycle and 5000-6000 shallow-depth charge/discharge cycles per year based on the inclination of the satellite [4]. Given this fact, the engineer must size the storage cells of their satellite appropriately and also consider the battery chemistry given the knowledge that the batteries will be going through several thousand charge/discharge cycles.

In the case of ODU, the flight hardware selected came with the EPS PCB and contains two Li-Ion 18650 cells capable of delivering nearly 2,000 charge discharge cycles with a depth of discharge of 25%. Because the P31u is sized to deliver power to payloads of up to 30W and considering the maximum use of Aeternitas will be up to 4 W, the maximum depth of discharge Aeternitas will experience is 13%. Furthermore, the 4 W parameter is peak power, thus the average power consumption of the satellite is much less than this. Finally, the spacecraft will not be completely drawing from the batteries

From the given data in the battery datasheet, we are able to derive a model for the Charge/Discharge Cycles of the batteries to deduce how many charge/discharge cycles of which the batteries are capable of achieving.

By interpolating the data we arrive with a model with an R value of 99.95% therefore, we can have considerable confidence in the model assuming the datasheet is correct.

$$Cycles = 3508.1 * e^{-.021*depth} \quad (13)$$

What this model tells us is that for a given battery under the load conditions of Aeternitas at maximum power yields a Cycle Lifetime for each battery of 2669 cycles. When we use two batteries of this type we effectively half their loads and double our cycle lifetime and achieve 5400 cycles. Again, accounting for the duty cycles of our

Radio and EPS heater, we surmise that the maximum average load for the Spacecraft is only 1.706 W and thus the depth from equation 13 is considered to be only $1.706/30$ or approximately 5%. Given this final assertion, we obtain a single battery life of 3503 cycles totaling 7007 cycles for Aeternita's two batteries.

2.4 DATA LINK REQUIREMENTS

From our simulation data obtained through the system specific simulations in STK, we are now able to assess the Communications Link between Spacecraft and Ground Station.

The first order of business is to ascertain when the satellite will be accessible from the ground station and vice versa. STK additionally allows for imposing constraints on the simulation to the hardware specifications used in the design to assess what is truly valid access.

An access is defined by and computed for two objects - a primary object and an associated object. In the VCC mission, Aeternitas and Kaufman Hall are the two objects of interest and must be modeled accurately to assess the data link. The key interests in the design of the satellite and its RF subsystem is a direct result of how many access will the satellite and ground station have, and for how long. From this knowledge the designer can proceed with calculating a rough link budget to accomplish the mission. Also, in this preliminary stage, the designer gets an idea of how much data can be fit into a telemetry or science payload and derive a theoretical amount of information that can be relayed given the COTS component specifications and the mission requirements.

First, Aeternitas has several design constraints right from the start. Geometry and space, the radio and its modulation scheme and digital encoding, power, and the point from which the satellite will be placed into orbit. The table below summarizes the principal constraints that go into modeling the system for data link access and coverage.

From Table XI we are now ready to model our satellite access capabilities and determine the important mission parameters of when and for how long are we able to communicate with the satellite.

2.4.1 ACCESS AND SATELLITE COVERAGE

When simulating an access and AER report for Aeternitas for the lifetime of the

TABLE XI: SpaceCraft Data Link Intrinsic Constraints

Hardware	Constraint
Radio	20KHz Bandwidth
	401.08 MHz
	9600 baud
	2W transmit Power
	AX.25 Digital Encoding
Antenna	FSK/GMSK
	0 dBi
	200 Ohm Impedance
Initial Orbit	Refer to table III

mission, we obtain global statistics only for the two body propagator model as it is the longest lasting scenario and least computationally costly to perform. From the analysis of the satellite orbit and the location of the ground station, we obtain a minimum contact time of 9.896 seconds on 20 June 2020 and a maximum contact time of 636.555 seconds or 10.6 minutes on 10 July 2021. Additionally, this contact occurs at ranges of a minimum of 307.56 km and a maximum of 2024.87 km and mean range of occurrence over the life of the mission at a range of 1523.31 km.

It is apparent from these statistics that not all of the 7867 accesses of the mission are going to be usable. The time needed to transmit a message of Length L and at a rate of R is simply given as L/R. The Lithium II Radio operates at 9600 baud and digitally encodes its 256 byte payload data into AX.25 Packets and therefore dictates a payload size of 52 bytes (416 bits) [21]. The time needed to transmit an N bit message is N/9600 and with a science payload of 256 bytes the round trip latency for the 9600 baud transmission is at maximum 50% multiplied by the propagation delays for the radio waves. Understanding this, we can approximate the effective round trip propagation time T_{Eff} for the entire channel transmitting a Payload in bytes with a baud rate of 9600 bps over a distance R as:

$$T_{Eff} = 2 \cdot \left(\frac{Bytes}{Rate} + \frac{R}{c} \right) \quad (14)$$

Using equation (14) and the data generated in our orbital simulations we know

the operational extremes within which Aeternitas must operate. At maximum value, Aeternitas has an effective maximum roundtrip signal propagation time of 100.16 ms and a minimum of 88.72 ms with a mission average of 96.82 ms. Later in the required analysis for a link budget, effective packet throughput can be approximated using this data.

Table XII summarizes the Access Requirements set forth for the Aeternitas mission and shall be used later in the link budget analysis.

TABLE XII: Global Access Statistics for Aeternitas Mission

Global Statistics	Access Number	Date	Time (s)
Min Duration	3097	6/20/2020 11:25	9.89
Max Duration	5877	7/10/2021 19:20	636.5
Mean Duration			527.2
Total Duration			4148000
Total Accesses			7800

With the completed Power and Access Requirements Specified for the COTS components used in building Aeternitas, we are now ready to proceed with the salient aspects of the custom hardware design.

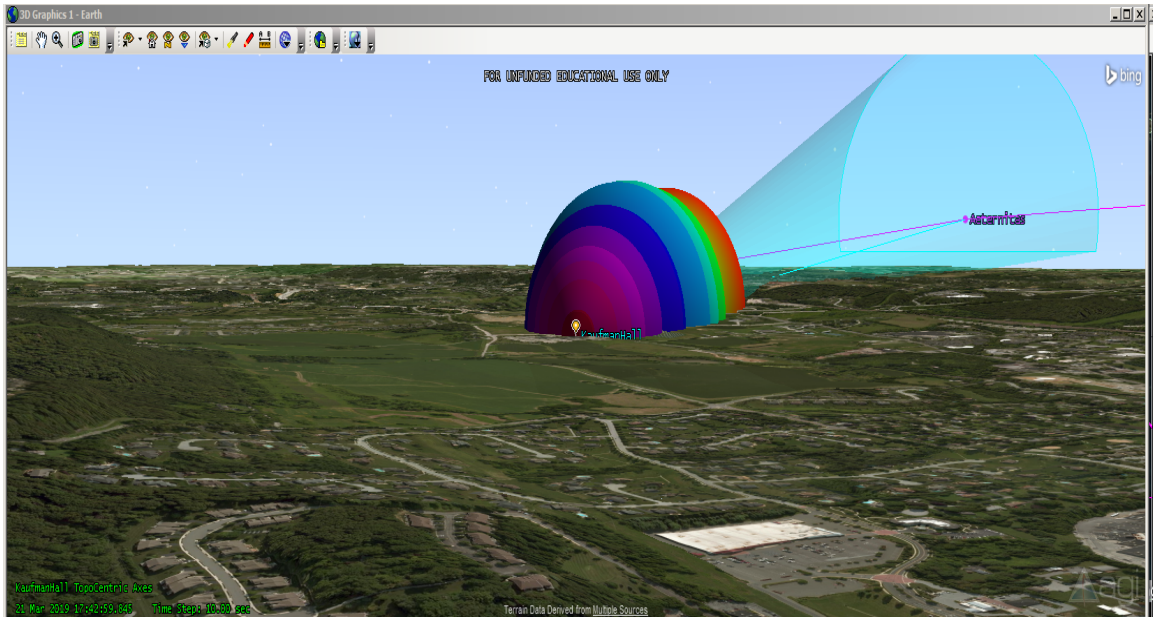


Fig. 19: Ground Station Antenna Directionality as Aeternitas Arrives From Below the Horizon

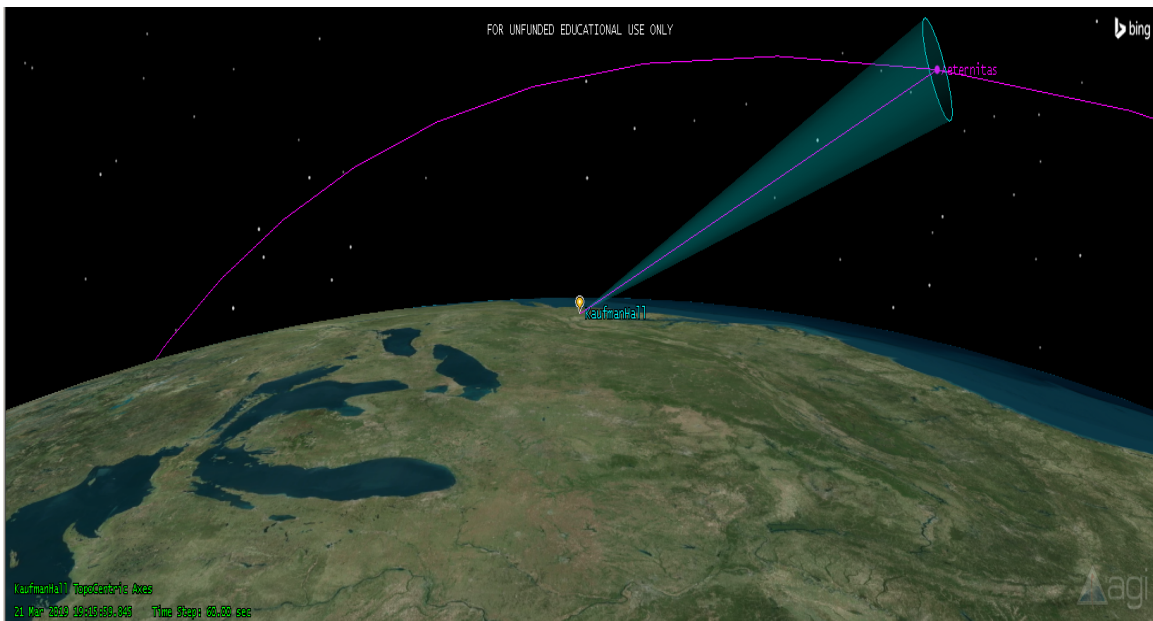


Fig. 20: Visualization of Antenna to Satellite Data Link

CHAPTER 3

SPACECRAFT HARDWARE DESIGN

3.1 THE SPACE CRAFT RADIO FREQUENCY MODULE

The System implemented by Old Dominion University is designed to operate at 401.08 MHz with a maximum bandwidth of 20 KHz. The overall system architecture is outlined in Figure 1.

At present, the ground station is capable of receiving all frequencies from 70MHz to 1GHz with the combination of its Yagi and omnidirectional antennas stationed atop the University Engineering Hall. Using an Ettus Research USRP B200 and custom designed switching hardware, the half duplex nature of the B200 will be overcome by using an integrated power detect circuit with a Transmit Receive IC integrated with a microcontroller to control the direction of communication within the system.

The space craft is designed to send data at the nominal rate of 9600 Kb/s using a special form of Frequency Shift Keying (FSK), Gaussian Minimum Shift Keying [18]. The AX.25 Protocol dictates that the telemetry and sensor data must fit within a bitstream or buffer no greater than 256 bytes in length [21]. Space Systems Engineering dictates that satellite communications designers must consider three categories of system constraints [4]. The customer requirements, technical requirements, and the international regulations all must be carefully considered [4] when designing a spacecraft communications subsystem.

Our requirements first dictated the need to apply for special licensing. From this application process, ODU obtained an experimental license from the FCC at the 401.08 MHz band with an authorized transmit power of 2 Watts and a bandwidth of $\pm 0.00025\%$. This led to the selection of a space certified radio from Astronautical Development LLC [18].

After selection of the radio module a PCB and custom design Balanced-Unbalanced (Balun) PCB were implemented to accommodate the Lithium II radio's 50Ω input Impedance and provide matching from the antenna to the PCB traces required to

interface the radio with the rest of the RF circuitry in the board. Figure 2 shows the CAD model outputs for the board implemented to accommodate the Radio and Balun Circuitry and Figure 3 shows the Characteristic Impedance Curve used to select PCB Trace Widths during the design process.

The Radio Frequency (RF) module containing the Balun and Radio Support Circuitry is designed as a two way communications pathway for the radio to receive “Dump” commands from the ODU Ground Station. For instance, upon receiving the RF signal to “Dump” Telemetry and Housekeeping Data, a GPIO pin onboard the radio toggles its logic state to interface the motherboard. This logic initiates a sequence with the motherboard to retrieve and feed a serial information buffer to the radio from the Spacecraft’s data storage hardware using a 9600 baud, Universal Asynchronous Receiver/Transmitter (UART) interface. A summary of the pertinent radio hardware characteristics is summarized in Table XIII.

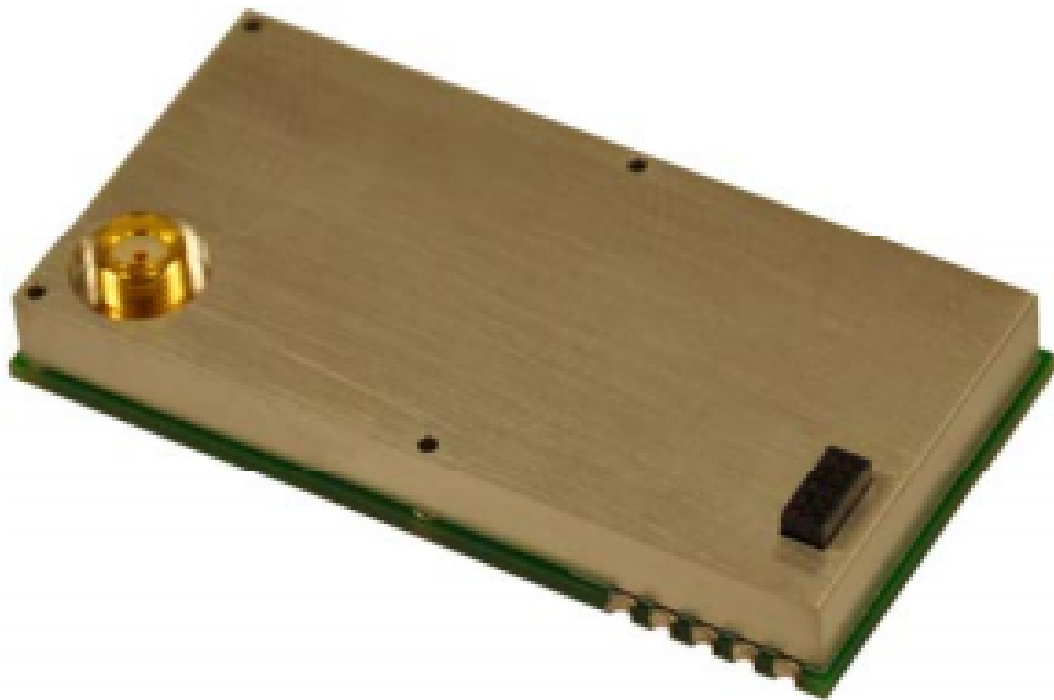


Fig. 21: Picture of Lithium II Radio used for transmission of data

TABLE XIII: Lithium II Radio Design Parameters

Radio Parameter	Value
Frequency	401.08
Bandwidth	Up to 20KHz
Power Output	Up to 2W
Power Usage RX	≤ 200 mW
Power Usage TX	≤ 2 W as per license
Footprint	33 mm x 65 mm x 10 mm (W x H x D)

3.1.1 ANTENNA DESIGN

To use the Lithium II Radio aboard Aeternitas, an antenna was designed in house by the ODU team. Prior to the physical manufacture, analysis must be done to ensure the system feasibility.

The antenna designed is integrated into the spacecraft hull and deploys using a student-designed, spring loaded, antenna deployment mechanism. A 3D generated model using *Altair's* CADFEKO simulation software is depicted in Fig. 22.

All antennas are conductors that take Radio Frequency current from a transmitter, fed by a feedline into the feed-point, and radiate electromagnetic waves into the surrounding free space. The physical shape and electrical characteristics of the antenna conductor, as well as conductors in the surrounding environment (the reactive near field and radiating near field) determines the characteristics of the antenna [22]. Fundamentally speaking, the radiation pattern and the feed-point impedance are determined by these electrical characteristics.

The wavelength λ of the RF an antenna must radiate is the most basic design criteria. For a conductor to radiate electromagnetic waves, its dimensions must approach the size of the RF wavelength it carries.

$$\lambda = \frac{c}{f_c} \quad (15)$$

Given the parameters of the license a wavelength of .747 meters was obtained, a modified half wavelength dipole antenna was designed and cut to match an electrical length of 186.75 mm.

3.1.2 UNDERSTANDING THE FEKO ELEMENTS

With the antenna designed as a half-wavelength dipole (comprised of two quarter length elements inserted into its feed-point) we model the Electric and magnetic fields of the antenna assembly with the classical equations for the half-wavelength dipole.

Far-field electric fields are proportional to the magnetic vector potential \mathbf{A} :

$$\mathbf{E} = -j\omega\mathbf{A}$$

and the magnetic field is from:

$$|\mathbf{E}| = \eta|\mathbf{H}|$$

Realizing the cross product of the electric field with the magnetic field points in the direction of power flow, the Poynting Vector. Thus, we derive the magnetic vector potential from a retarded volume integral over the current density \mathbf{J} :

$$\mathbf{A} = \mu \iiint_V \frac{\mathbf{J}(\mathbf{r}')e^{-jk|\mathbf{r}-\mathbf{r}'|}}{4\pi|\mathbf{r}-\mathbf{r}'|}dV' \quad (16)$$

Given a point on the antenna \mathbf{r}' , the phase difference is $k\mathbf{r}' \cdot \hat{\mathbf{r}}$ and substituting into equation (16) we have the magnetic vector potential \mathbf{A} :

$$\mathbf{A} = \frac{e^{-jkr}}{4\pi r} \mu \iiint_V \mathbf{J}' e^{j\mathbf{k}\mathbf{r}' \cdot \hat{\mathbf{r}}} dV' \quad (17)$$

We determine the magnitude of the Electric Vector Potential \mathbf{F} with magnetic currents. The far-field magnetic field is proportional to the electric vector potential:

$$\mathbf{H} = -j\omega\mathbf{F}$$

Where μ is given as the permeability of free space. We determine the magnitude of the electric field by remembering it is perpendicular to \mathbf{H} . The electric vector potential is found from a retarded volume integral over the magnetic current density \mathbf{M} . Applying radiation approximation we find:

$$\mathbf{F} = \frac{e^{-jkr}}{4\pi r} \epsilon \iiint_V \mathbf{M}' e^{j\mathbf{k}\mathbf{r}' \cdot \hat{\mathbf{r}}} dV' \quad (18)$$

Where ϵ is given as the permittivity of free space.

Integrating Equations (17) and (18) and using the fundamental constitutive relations described above, we compute the far fields for dipole radiators centered on the

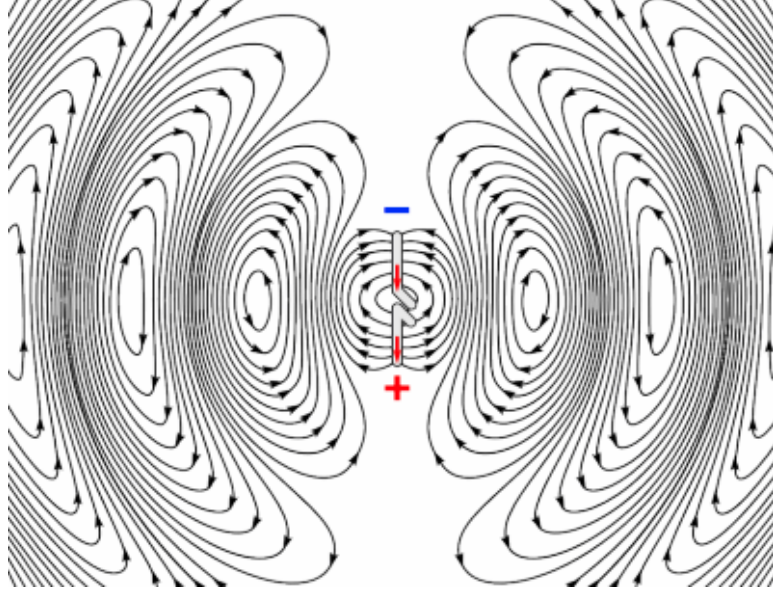


Fig. 22: Dipole Radiation Pattern Described by Equations (17) and (18)

z-axis, (19) and (20). Fig. 22 shows the radiation pattern described by integrating these two equations. For the Aeternitas Spacecraft, a slice down the middle of the figure is the plane in which the Dipole Antenna Structure sits. In the FEKO simulation, one may observe the radiation pattern emanate from this plane (The X,Y plane) into the Z direction in Fig. 26.

$$\mathbf{E}_\theta \approx j\eta \frac{\mathbf{I}_0 e^{-jkr}}{2\pi r} \left[\frac{\cos(\pi/2)\cos(\theta)}{\sin(\theta)} \right] \quad (19)$$

$$\mathbf{H}_\phi \approx j \frac{\mathbf{I}_0 e^{-jkr}}{2\pi r} \left[\frac{\cos(\pi/2)\cos(\theta)}{\sin(\theta)} \right] \quad (20)$$

The far-field power densities, are the Poynting Vectors given by: $S_r = \frac{|E_\theta|^2}{\eta}$ for the dipole antenna. When these Poynting Vectors are integrated over the radiation sphere containing the dipole apparatus to compute radiated power, the result contains $|I_0|^2$ and yield equation (21), the classical equation for Radiation Resistance of a Dipole.

$$R_r = \frac{2P_{rad}}{|\mathbf{I}_0|} = \frac{P_{rad}}{|\mathbf{I}_0|^2} \approx 73\Omega \quad (21)$$

These equations are the fundamental basis for how FEKO generates the far-field mesh effects of the Aeternitas Antenna Assembly where η is the impedance of free space (376.7Ω).

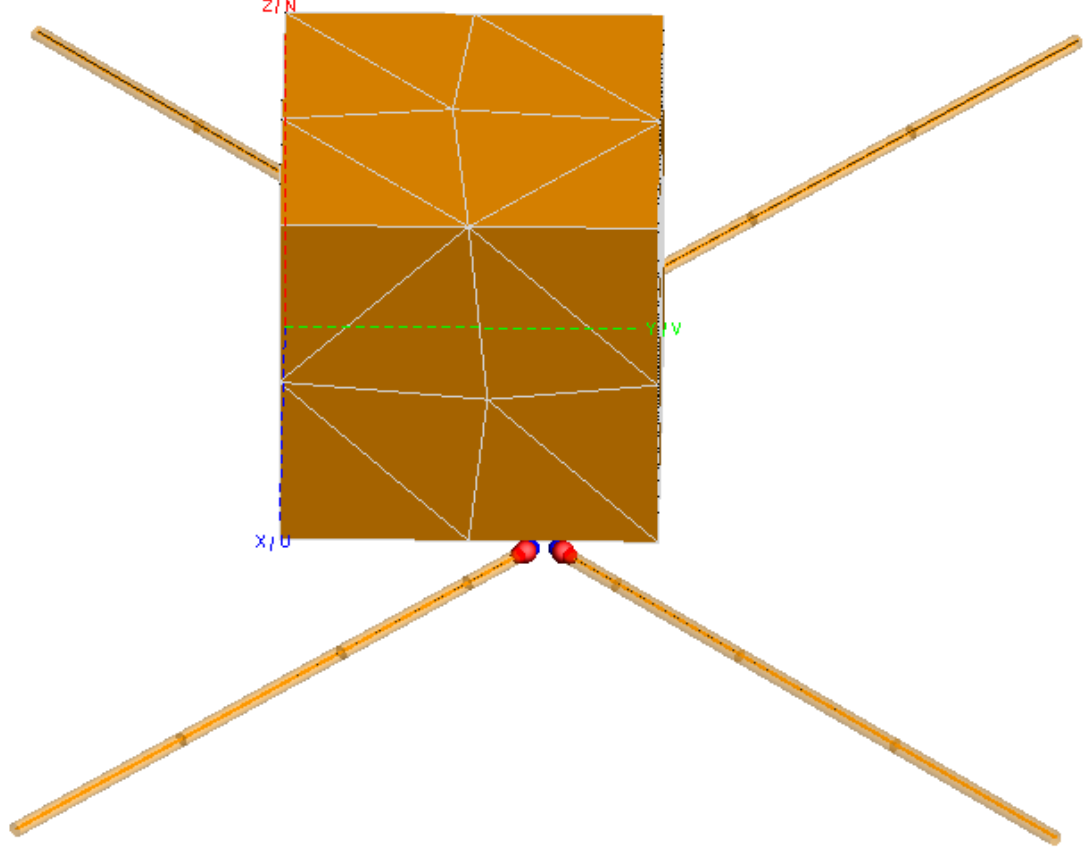


Fig. 23: 3D model of Cubesat Antenna in its deployed state

Note the final input impedance for a $\lambda/2$ dipole is $73 + j42.5\Omega$. Physically speaking, to rid this efficient radiator of the imaginary portion of its input impedance, we cut the dipole to an electrical length suitable to find a total input impedance comprised of a 100% real Z_0 .

From equations (19) and (20), we surmise that the input impedance of a half-wavelength dipole is given as:

$$Z_{input} = 73 + j42.5\Omega \quad (22)$$

With this information we refer to engineering handbooks to find a generalized formula for cutting antenna lengths appropriately to resonate at the Center Frequency of the designed system, optimized for realizing a purely resistive input impedance [22].

$$Length = 0.48\lambda - diameter \quad (23)$$

For the center frequency of 401.08 MHz, we have an antenna segment length of 172 mm. This agrees with the above analysis of estimating the electrical length of a dipole from equation (15) as 186.995 mm. By this analysis, the antenna was cut to have an idealized input impedance $\approx 200\Omega$ with a total electrical length of 172 mm, which virtually eliminates the complex impedance seen in the antenna.

From this analysis, the antenna now may be modeled in CADFEKO to determine far-field effects and the directivity of the antenna.

As constructed in Fig. 22, the antenna has a θ of 65° and ϕ of 35° by virtue of the physical construction of the structure. We can now pass this information into FEKO as the input parameters for the mesh generation based on the analysis and derivation of equations (15-20). FEKO does the analysis numerically to produce the Far Field Antenna Model for the Aeternitas Spacecraft depicted in Fig. 23 and Fig. 24.

Also, in Fig. 25 we have a visualization not only the 3dB gain of the antenna but also its near field-intensities and directionality as well.

This information contained within the FEKO simulations becomes vital in the future development of an accurate link budget as we now have the antenna gain and far-field influence of the antenna for link budget analysis.

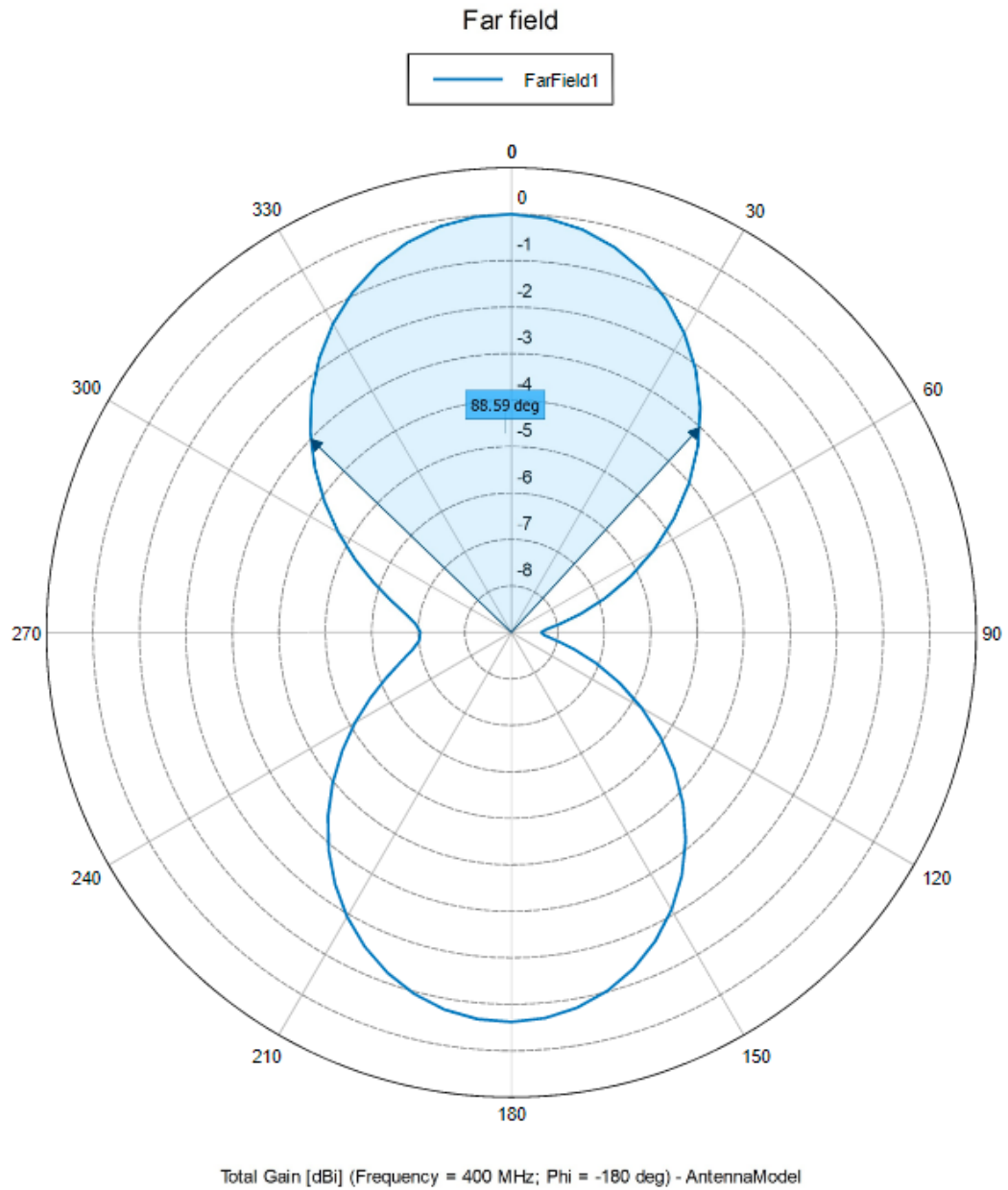


Fig. 24: $\theta = 65^\circ$ Far Field effects of Aeternitas Antenna Assembly Cut to Resonate at 400MHz

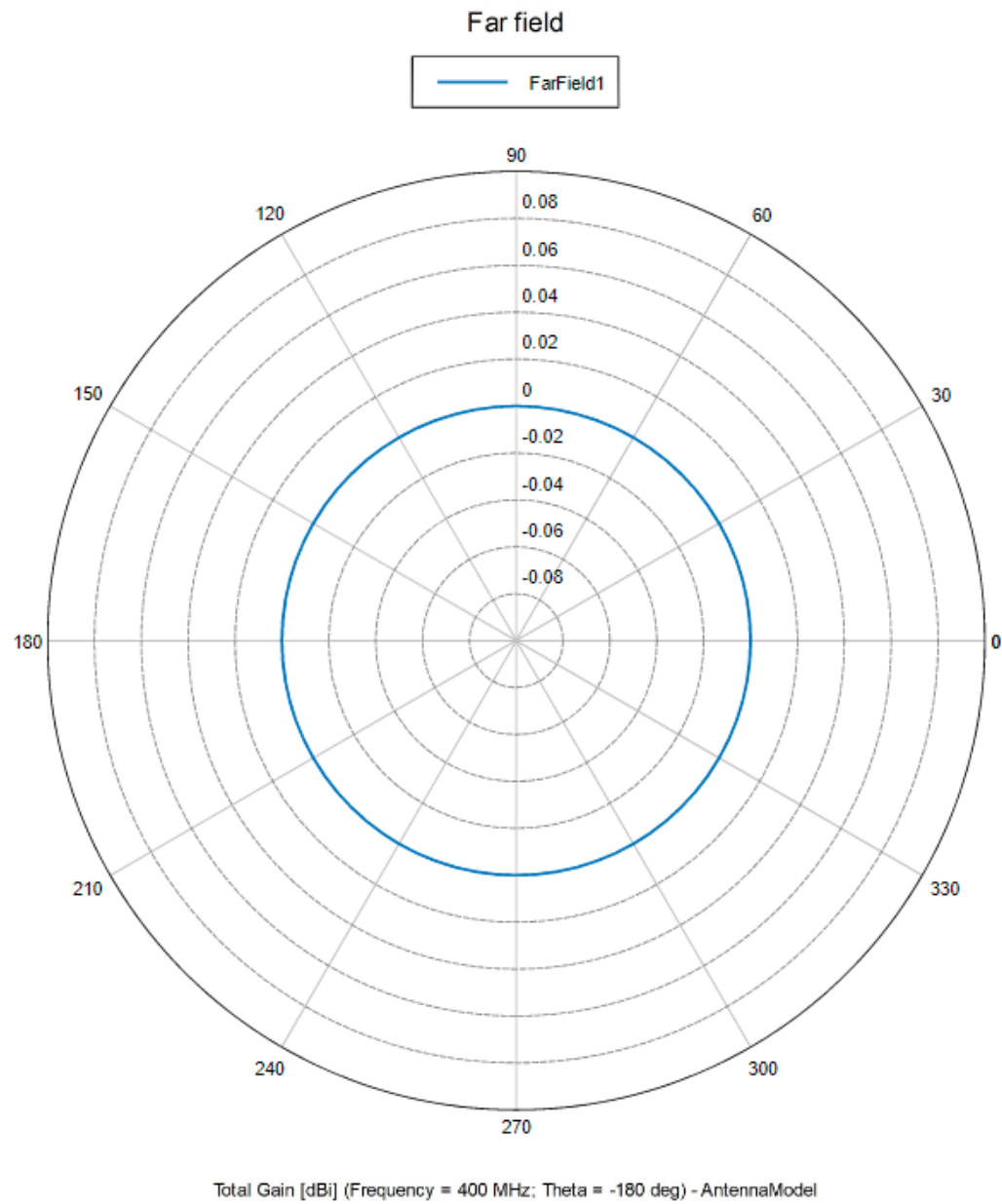


Fig. 25: $\phi = 35^\circ$ Far Field effects of Aeternitas Antenna Assembly Cut to Resonate at 400MHz

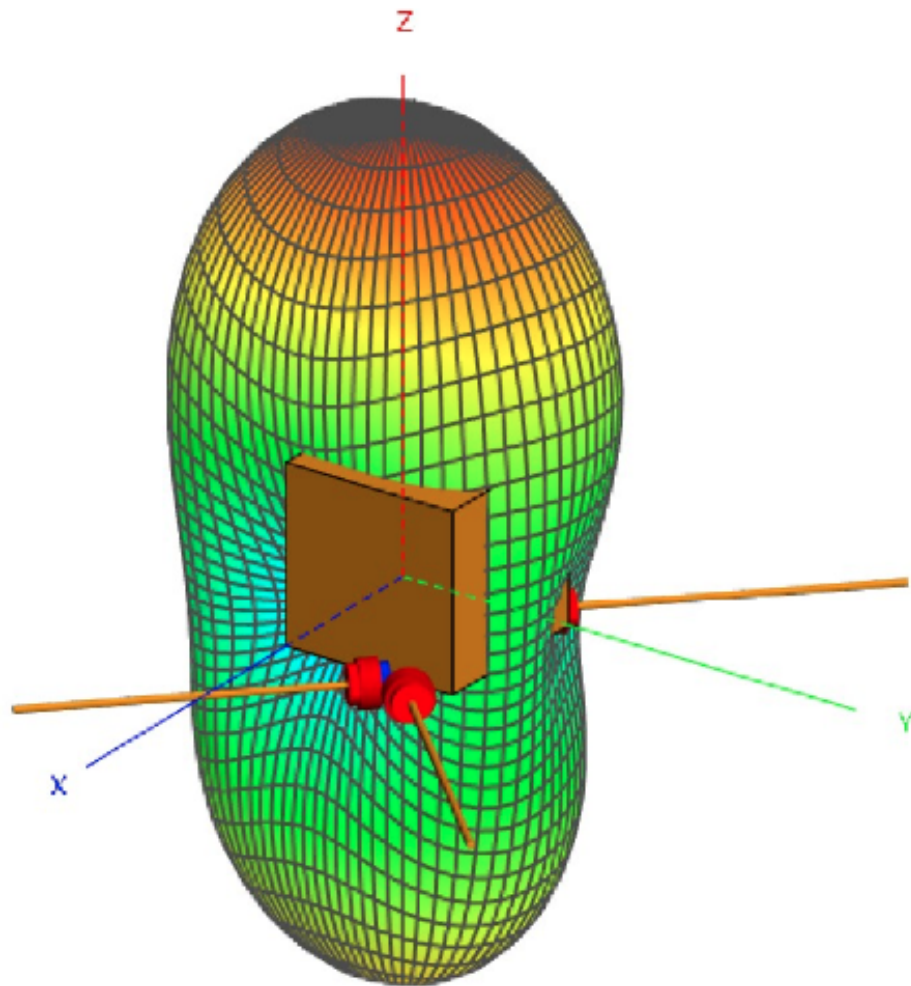


Fig. 26: Far Field effects of Aeternitas Antenna Assembly Cut to Resonate at 400MHz

3.1.3 IMPEDANCE MATCHING FOR RF TRACES

With the antenna cut to length and a foundational understanding of its field-effects as it relates to the propagation of the RF energy for packet transmission, we can proceed now with implementing the remainder of the RF circuitry aboard the RF subsystem.

The design of any RF circuit requires careful attention to Impedance Matching to prevent Reflection Losses and maintain proper signal integrity [23, 24]. With ODU's Dipole Antenna Structure designed with a 200Ω Input Impedance and FR4 PCB Substrate with $\epsilon_r \approx 4.2$ at 401.08MHz, careful implementation of the trace widths for the RF module were selected for impedance matching [25].

In Engineering Standards and in Literature, two widely accepted models based on Wheeler's Equations for inductance and impedance matching and Schneider's Formula for Effective Dielectrics are regularly applied to Engineering the proper parameters into impedance-matched RF circuitry [23, 24].

$$Z_0 = \frac{87.0}{\sqrt{\epsilon_r + 1.41}} \ln \left(\frac{5.98h}{0.8w + t} \right) \quad (24)$$

Generally, this model presented in Equation (24) is well accepted as a good starting point for design, however a more accurate model for all ranges of ϵ_r and w given $\eta_0 = 376.7\Omega$ or $\approx 120\pi$ for Free-Space Impedance is available from Wadell[24].

$$Z_0 = \frac{\eta_0}{2.0\sqrt{2.0\pi}\sqrt{(\epsilon_r + 1)}} \ln \left(1.0 + \frac{4.0h}{w'} \sqrt{A + B} \right) \quad (25)$$

where

$$A = \frac{14.0 + 8.0/\epsilon_r}{11.0} \cdot \frac{4.0h}{w'} \quad (26)$$

and

$$B = \sqrt{\left(A^2 + \frac{1.0 + 1.0/\epsilon_r}{2.0} \cdot \sqrt{\pi} \right)} \quad (27)$$

with

$$w' = w + \Delta w' \quad (28)$$

such that

$$\Delta w = \frac{t}{\pi} \ln \left(\frac{4e}{\sqrt{(t/h)^2 + \left(\frac{1/\pi}{w/t + 1.1} \right)^2}} \right) \quad (29)$$

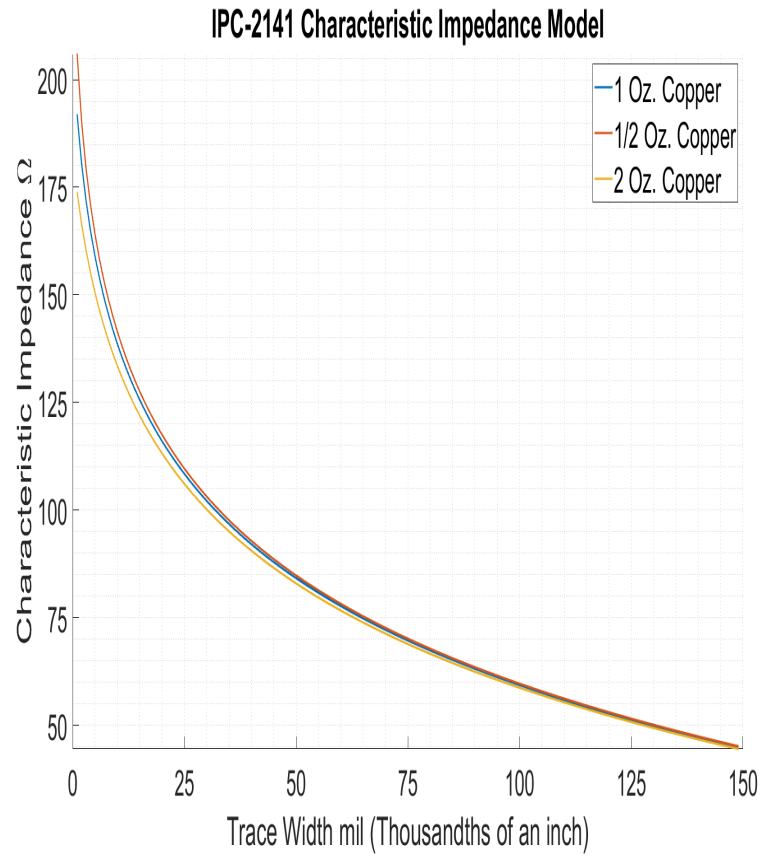


Fig. 27: RF Characteristic Impedance using $\epsilon_r = 4.2$ and a substrate height $h = 1.74mm$

and

$$\Delta w' = \Delta w \frac{1.0 + 1.0/\epsilon_r}{2.0} \quad (30)$$

From the model presented in Fig. 26 using Equation (24) we surmise that the trace width to optimize a 401.08 MHz signal propagating through the RF circuitry is 125 mils. Given the size of the Surface Mount Technology (SMT) ordered by previous teams, it will be necessary to run these traces from the larger 125 mil traces and stub them down to a trace width of less than 20 mils to provide the Lithium II Radio with the necessary 50Ω input impedance it requires to operate properly [18].

Prior to discussing the Balun Circuitry to match the 200Ω antenna with the 50Ω impedance of the Lithium II Radio, a discussion of why the Transformation network is required is warranted.

First, bring attention to Fig. 26. In any circuit network, to deliver maximum power across the terminals of a load, the Thevenin Equivalent Resistance, R_{Th} must match that of the load place across its terminals.

In the case of an RF system, we must also account for reflection losses in the circuitry due to impedance mismatches.

In a circuit, DC or AC, the curve depicted in Fig. 28 serves as the scale of the impedance versus power curve. The centerpoint, where the curve is at maximum represents the point where the impedance of the load is perfectly matched to the impedance of the source.

Practically speaking, we can imagine, as load impedance increases toward infinity, the power tends to zero because the circuitry becomes a virtual open and therefore cannot deliver any current to the load. Conversely, if impedance tends toward 0, the circuitry represents a virtual short, and therefore the source cannot develop a voltage across the terminals of the load because current is infinite and therefore, resistance is 0.

The point at which maximum is found for the load matching is derivative of the Maximum Power transfer theorem. For Fig. 27, the power delivered to a load across the Thevenin Equivalent Circuit representing our radio board is given as:

$$P_L = V_L I_L = R_L I_L^2 = R_L \left(\frac{v_s}{R_L + R_{Th}} \right)^2 = v_s^2 \frac{R_L}{(R_L + R_{Th})^2} \quad (31)$$

Following the standard calculus procedure for finding relative maxima/minima, we compute the derivative of P_L with respect to R_L , set to zero, and solve for R_L .

$$\frac{dP_L}{dR_L} = \frac{d}{dR_L} \left(v_s^2 \frac{R_L}{(R_L + R_{Th})^2} \right) = v_s^2 \frac{R_{Th} - R_L}{(R_L + R_{Th})^3} = 0 \quad (32)$$

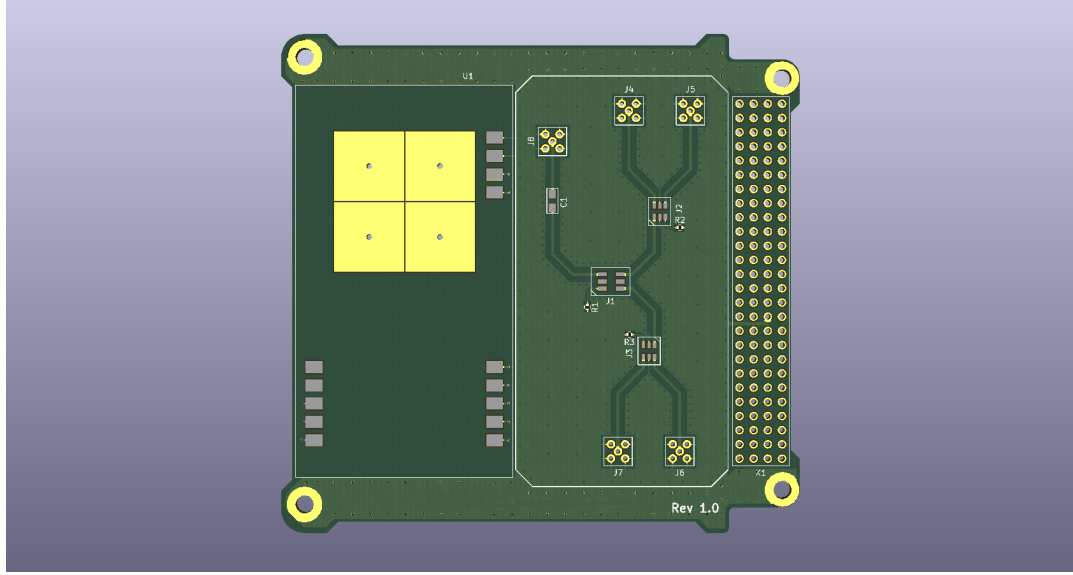


Fig. 28: First Design Iteration for Spacecraft RF Module Hardware using IPC-2141 and Wadell Models for Impedance Matching

From which we see $R_L = R_{Th}$ in order to satisfy Equation (32). Substituting $R_L = R_{Th}$ into the result of Equation (31), we see that:

$$P_{max} = v_s^2 \frac{R_{Th}}{(R_{Th} + R_{Th})^2} = \frac{v_s^2}{4R_{Th}} \quad (33)$$

Therefore, we see by way of Equation (33) we must match the load to the source in order to achieve maximum power transfer. This holds true for sinusoidally varying sources as in our RF submodule design. As such, reflection losses are minimized and maximum power transmission is achieved through the impedance matched circuitry.

3.1.4 THE BALUN CIRCUITRY

With the custom-designed, dipole antenna made by ODU's team of Engineers, and a reported dipole antenna feed impedance of $\approx 200\Omega$, a Balun Transformer Ratio of 4:1 to match the 50Ω input impedance of the RF PCB in order to satisfy the maximum power transfer theorem. In other words, the dipole antenna design initially used represents a Differential 2-Port Network of input impedance 200Ω s. The RF module traces and Lithium II Radio represent a single-ended input impedance of 50Ω s and thus requires the conversion of 4:1 [26].

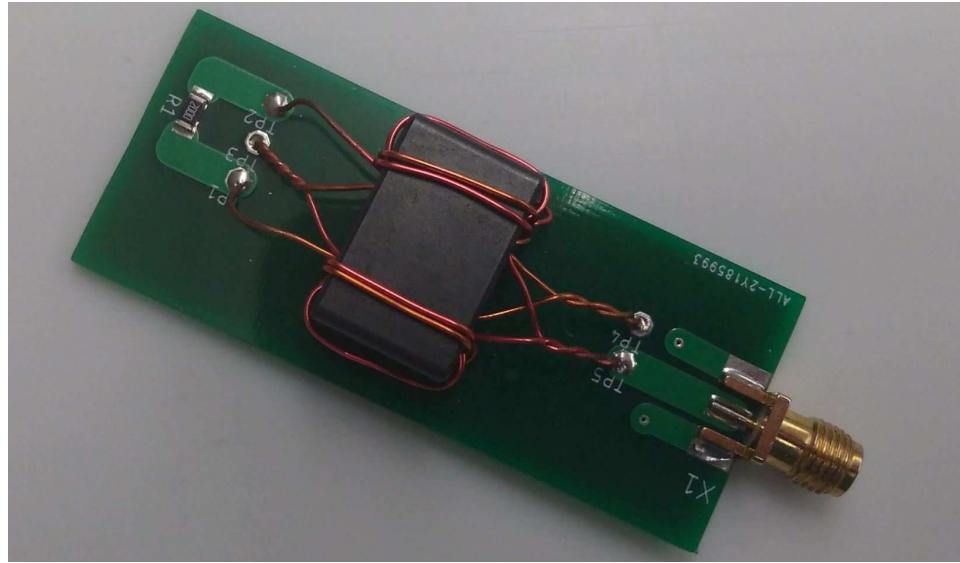


Fig. 29: Balun Design Test Jig mounted on 1.74mm FR4 substrate used for design iteration in CubeSat RF module

The design comes from the implementation proposed by Parker and simulation results were achieved in LTSpice to show the 4:1 conversion in voltage and thus impedance [26]. The LTSpice model was stimulated by a 1V peak-to-peak sinusoidal source with a frequency of 401.08 MHz to model our current Spacecraft configuration. Fig. 31 shows the schematic representing the 50Ω impedance of the radio and the balun circuitry stepping down a 200Ω s antenna “generator.” Fig. 32 displays the idealized model waveform achieved from simulating the antenna apparatus at a center frequency of 401.08 MHz.

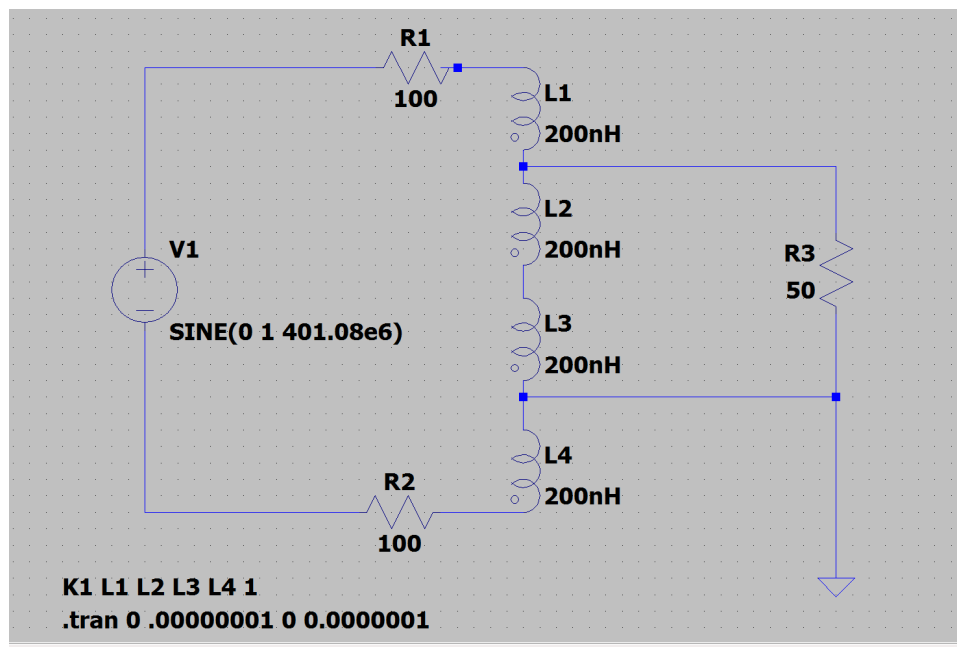


Fig. 30: Balun Design in LTSpice Prepared for Simulation

3.2 THE MOTHERBOARD DESIGN

We the power modules, and RF Subsystems designed, and other COTS component support circuitry laid out in accordance with their specification set forth in their respective data sheets, the final phase of hardware design for the spacecraft can be performed. The motherboard which is responsible for interfacing all PCBs and Telemetry instruments to effectively support mission operations can now be designed [4].

Due to poor transitions between semesters, the graduation of team members, and a cyclic team membership by club members, a great portion of the motherboard hardware design required a working design on short notice. With less than six months from the delivery date remaining, there was no working schematic of the proposed system, no PCB layout, and little to no deployable software development completed. Thus, time was the single most limiting factor in the design constraints. Considering this, the greatest tradeoffs with respect to saving time were in the complexity and robustness of the PCB controller design, and the incurred cost for expedited delivery and population of the RF and Controller PCBs.

The most significant decision which rested upon the time constraints in this design was to use a microcontroller to implement the distributed system vice a single board computer with its own onboard processor.

3.2.1 NON-TECHNICAL CONSTRAINTS OF THE MOTHERBOARD DESIGN

The stakes for the project were extremely high being that ODU has invested nearly a hundred thousand dollars, countless hours, and has received some high profile exposure in the local media on this project. Even considering the time constraint, it would be ethical to deliver only the best and operable product as part of the team. Additionally, the compliance of the RF module of the system was contingent on the license obtained to operate above the FCC Part 15 requirements [18].

Upon the undertaking of the project, less than \$6,000 dollars were left for any further development or design of the electrical hardware systems. With two boards to complete and the motherboard being a four-layer design, money was a definite constraint. The final costs of the 4-layer, mixed-signal design motherboard from Advanced Circuits in Aurora, CO was roughly \$1,500 dollars and thus was successful

in the final costing for the hardware.

The sustainability of the design depends much on the environmental factors affecting the design. Because of the demands of space flight, the durability of parts selected played a key role in the design. Also, a power budget was necessary to ensure that the amount of computation and control required of the project could be sustained during periods of darkness behind the Earth on a solar cycle charge and thus plays an important role in the power analysis done previously in this manuscript.

The manufacturability of the design was also a crucial consideration during the PCB design and layout. The prospective manufacturer to be used claims tolerances of up to 3 mil for trace width and clearance. Because the Controller Board PCB contained two BGA components, extreme caution was exercised to ensure relatively small signal traces had sufficient trace clearances between them and the balls comprising their respective arrays.

3.2.2 MOTHERBOARD HARDWARE SELECTION CRITERIA

The current design will be deployed into the LEO at about 400 km orbital radius. Bearing in mind the altitude, the satellite could potentially face temperatures of down to -100°C , and temperatures up to 148°C . Also, the satellite will experience the full vibration, acceleration, and electromagnetic interference involved in the launch and orbit from and around Earth. Taking into account the harsh conditions of Space and the brute force it requires to get there, selected parts came only from MIL-Spec and ruggedized automotive grade components. Additionally, the CubeSat is a 1U design (10cm cubed) and must be stacked. Due to the form factor of the project, the PC/104 industry design standard was closely followed in order to ensure that all parts placed onto the board were in compliance with the stack configuration for the PC/104 standard.

Had there been sufficient time in the design proposal process, personal recommendations would have been made for the Controller Board would have been to implement a single board computer design similar to a Raspberry Pi or BeagleBone as the basis for the motherboard for their increased computational power and robust operating systems.

In the present design, a Microchip SAM3X8E Arm Cortex-M3 Microcontroller is implemented with an 84MHz Crystal Oscillator, 512 KB of Flash Memory, 96KB or SRAM, which features a 32-bit core allowing operations on 4 byte wide data within a

single clock cycle. With the prospect of possibly doing onboard processing and filtering of the data acquired by the satellite, an alternative design would have been better supported not just by a microcontroller but a full-scale single board computer with a dedicated processor. One main advantage of doing this vice only a microcontroller design is the capability to run multiple threads on the CPU core and therefore avoiding the need for programming microcontroller interrupts and gaining the capability to do processing and filtering while simultaneously continuing to run data acquisition and transmission operations. Additionally, an embedded Linux Distribution could have been installed onto the CPU which would allow for embedded system development from a master computer in the ODU Space Systems Laboratory. By using a single board computer design such as a 1GHz AM335x ARM Cortex-A8 processor, the system robustness for computation and multiple simultaneous task performance would increase by a full order of magnitude. Below, the two simple equations show the comparison of computational capacity for each 32-bit RISC architecture Core of the alternative design vs the current design. $1GHz \cdot (4bytes)/cycle = 4$ billion instructions per clock cycle and $84MHz \cdot (4bytes)/cycle = 336$ thousand instructions per clock cycle.

It is apparent from the above analysis that choosing to model a single board computer system with a dedicated processor is advantageous over a simple microcontroller design. Speed however, is not the only parameter to be optimized in this case. With the selection of a microcontroller design versus a full CPU design, the software development for the project becomes relatively easy to complete. With the current selection the microcontroller design, simply burning firmware onto the microcontroller and uploading a program in C is all that is required to begin using the system and its peripherals. In the case of a full CPU design, Operating System and communication protocol agreement between peripherals and other PCBs in the design becomes more complex and would require much greater manpower in the development of software and Operating System handling. Thus, due to time constraints and the difficulty in implementing a full CPU design with an onboard operating system such as Linux, the second microcontroller option was chosen for ease of PCB design and software implementation over system robustness and computational capacity.

3.2.3 PHYSICAL TOLERANCES

As discussed previously, the chassis and structural design dictated the dimensions of the Controller and RF modules. Following the PC/104 industry form factor, the controller board is designed to fit dimensions of 92.90mm by 89.30mm with a vertical clearance of just under 17 mm to leave room within the stack for the relatively large capacitors mounted on the P31u EPS. Careful attention was paid to the placement of each micro JST connector onto the controller board and the mechanical design team was instrumental in the collaboration effort to place the connections physically as close to the point of connection with other boards in the stack as possible.

Using Autodesk Eagle PCB design software, a 4 layer board with a 3.3V and ground plane set within the specified dimensions was first laid schematically and the circuit nets were named appropriately to ensure ease of readability by all team members. Each piece of hardware was researched and the footprints were entered into the software to ensure accurate dimensional relation among parts on the board. The PC/104 headers were placed to match the location of the existing EPS module manufactured by *GOMSPACE*.

Using Autodesk Eagle, the controller was laid out onto a 92.90mm by 89.30mm PCB. The design rules used in creating the PCB stem from IEEE 1394 EMI Board Design and Layout Guidelines.

3.2.4 NOISE REDUCTION TECHNIQUES IN THE MOTHERBOARD

Extrinsic noise is induced from an external source and can cause unsatisfactory operation of a circuit (interference) [27, 28]. The source of noise may be from another circuit on the same circuit board (often referred to as cross talk), or it may be external to the equipment. For interference to occur, there needs to be a source of noise and a means of coupling it into the circuit. The external source may come from conduction, capacitive coupling, magnetic coupling, or radiation. To reduce the effects of interference, the interference can be suppressed at the source, the source can be isolated by shielding or filtering, the coupling path can be reduced, or the receiving circuit can be made less sensitive to noise [27, 28].

To ensure minimal electromagnetic interference, this standard and references by Ott proposes several basic rules for circuit designers:

- Consider the source of Energy and its capability to pollute the system with noise
- Consider the Receptor of this energy and its susceptibility to noise
- Consider the Coupling paths between the Source and Receptor
- Consider the Analog and Digital Components of the design as needing to be mutually separate from one another

Given these generalized requirements the rules for this design were set out as follows:

- Separate the Analog and Digital Regions of the PCB with a separate Source and Ground Plane
- Keep the critical paths on filters and Data Lines as short and direct as possible
- When laying traces, ensure that the clearance between them are the same size wherever possible
- When laying traces, ensure that the clearance between them are the same size wherever possible

3.2.5 MAPPING HARDWARE LOGIC FOR SOFTWARE DEVELOPMENT

In the design the first consideration was “which pieces of hardware were we to control and acquire data from?” First a pin map was generated by hand and a table was generated using Microsoft Excel and can be found in Appendix C.

The pin map served as an aid to the software developers as a programming tool, whereas the hardware team used the table to double check the validity of the connections made to the Microcontroller and to also keep in mind the protocols and pin directions to be set. Careful attention was paid to the communication and clock lines in mapping the microcontroller as the protocols dictate how the signals are

interpreted and synchronized. For communication with the EPS, I2C is the protocol used and for communications with the Lithium 2 Radio from *AstroDev*, SPI is the interface. For programming and debugging JTAG is used. The JTAG connections for the microcontroller are traced to a micro JST connector in order to be jumped to the opening at the top of the satellite upon completion. This allows for testing and debugging the CubeSat after final construction via the only opening connected to the top board in the Satellite.

To store the data acquired by the satellites sensing suite, a 64 GB eMMC memory Ball Grid Array (BGA) was thrown out for an easier way to implement 64 GB SD card. BGAs have extreme pin pitch and considerably increase the manufacturing costs of the PCB [28]. Being that the memory chip came with no installed software/firmware to facilitate ease of data transfer, a solution to the problem was made by tracing 8 digital GPIO pins to the data lines of the memory chip to produce a platform for bit-banging the data into memory. Bit banging is a “technique for serial communications using software instead of dedicated hardware. Software directly sets and samples the states of pins on the microcontroller, and is responsible for all parameters of the signal: timing, levels, synchronization, etc. [6]. By implementing this setup, the software engineers have maximum flexibility in how to manage the data acquired by the sensor suite using their own user defined functions in C.

For the Magnetorquers onboard responsible for attitude determination and control, Pulse Width Modulation was a necessity in order to give the control system designers maximum flexibility in attitude control.

Micro JST connectors were used around the edge of the Controller Board to make jumper connections between devices on other hardware boards in the satellite design. For instance, the four NanoPower P110 Solar panels from *GOMSpace* are connected to the EPS with Micro JST connectors, but the sun sensors and temperature sensors are separately jumped using these connectors to the Controller Board designed by the team. Additionally, the extra Magnetorquer used to control the Z-Axis orientation is also jumped using these connectors.

Finally, 1.8V, 3.3V, and 5V rails were added to power all the peripheral devices on the controller board. Several pins on the microcontroller were provided for switching power to devices such as burn-wires which will act as the mechanism for releasing the spring loaded drag brake structure. Additionally, some pins were set to monitor the operation of some devices such as the switch closure sense module which monitors

the successful deployment of the drag brake and antenna deployers. A Trace width of 12 mil was selected for the voltage rails as these traces are current carrying. Using the largest trace width possible is advisable for such traces to allow the maximum current carrying potential in the line to support demands made by devices on the board.

The physical dimensions for the board outline, drill hole dimensions, and via placements are indicated in Fig. 34 and Fig. 33 shows the overall physical constraints that each designed and manufactured PCB must fit within. In Fig. 34, gray components and traces are on the top layer (analog and RF) of the board whereas the blue components and traces are on the bottom side of the board (High Speed Digital Interfaces).

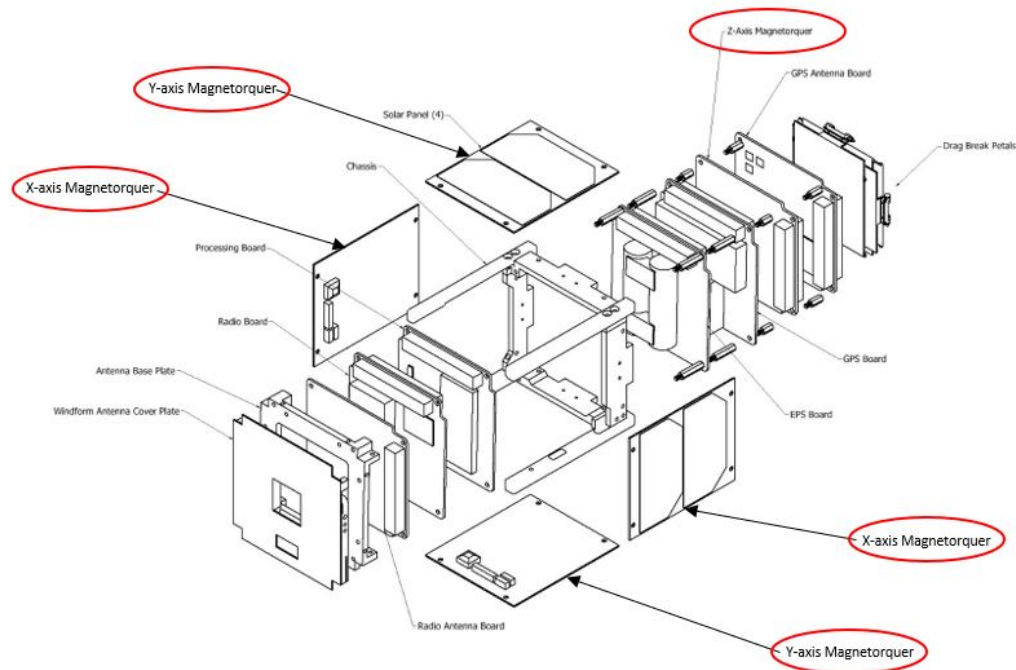


Fig. 31: 3D CAD Rendering of the Ground Station Switching Hardware to interface the existing Antennas to the USRP B200.

Fig. 32: 3D CAD Rendering of the Motherboard Design Used to Interface all Onboard Satellite Hardware

CHAPTER 4

THE COMMUNICATIONS SYSTEM AND DATA LINK

Within the context of any spacecraft and ground station network, the Communications Subsystem ranks among the highest in terms of system importance and mission accomplishment. The satellite and ground system is rendered useless without the capability to relay onboard sensing and telemetry data from the spacecraft to ground, thus the importance of a reliable and robust communications subsystem cannot be overstated.

Given the importance of such systems, the use of a well established protocol is necessary to reduce the time to develop them. AX.25 is the predominant choice for implementing communications in University small satellite research since it is well documented and supported by the amateur radio community [29].

Unlike most University CubeSats [10], the spacecraft developed at Old Dominion University was not designed to make use of frequencies allocated to amateurs. Instead, the engineering team applied for and was granted an experimental license on the 401.08 MHz band by the Federal Communications Commission (FCC) under the call sign WJ2XOH granted under file number 0255-EX-CN-2018.

4.1 GAUSSIAN MINIMUM SHIFT KEYING

The radio hardware onboard Aeternitas has a Lithium II radio which utilizes a 9600 baud, GMSK modulated RF front end [18]. GMSK is a special form of Continuous Phase Frequency Shift Keying (CPFSK) and thus requires a formal discussion.

Minimum shift keying (MSK) is a special type of continuous phase-frequency shift keying (CPFSK) with modulation index = 0.5. A modulation index of 0.5 corresponds to the minimum frequency spacing that allows two FSK signals to be coherently orthogonal, and the name minimum shift keying implies the minimum frequency separation that allows orthogonal detection [30, 31].

FSK can be thought of as the digital equivalent of analog frequency modulation (FM) [32]. With a modulation index = 0.5, MSK yields the minimum frequency separation for orthogonal signaling over a signaling interval of length T [33, 31]. MSK in

general, is popular in wireless communications because of its desirable characteristics such as minimizing the spectral sidelobes of the information bearing signal, bandwidth efficiency, and provides the choice for a trade-off between power efficiency and bandwidth efficiency due to the narrow filter used which increases the intersymbol interference and reduces the signal power. [30, 31]. For these reasons,

MSK with a Gaussian filter is termed as GMSK. GMSK is a simple binary modulation scheme which may be viewed as a derivative of MSK. In GMSK, the sidelobe levels of the spectrum are further reduced and provides much faster power-spectrum roll-off characteristics due to the lower time-bandwidth products.

To make the MSK output power spectrum more compact, the pre modulation LPF should be of narrow bandwidth and sharp cut off to suppress high frequency components, small overshoot impulse response to prevent excess deviation of the instantaneous frequency, and preservation of an integrated filter output pulse capable of accommodating a 90 degree phase shift to ensure coherent demodulation [31]. A pre modulation Gaussian LPF satisfying the above requirements is adopted for Gaussian Minimum Shift Keying (GMSK) modulation, where the data sequence (i.e., an information pulse train) is passed through a Gaussian LPF filter, and the output of the filter is MSK modulated [31]. The width of the Gaussian filter is determined by the bandwidth-time product BT (e.g., $BT = 0.3$ for GSM and $BT = 0.5$ for CDPD). The trade-off of having a more compact spectrum is that a pre modulation filter spreads the signal pulse and, thus, introduces inter-symbol interference (ISI) in the transmitted signal. The Gaussian pre modulation filtering spreads the pulse over an interval greater than T (the bit duration, equivalent to the inverse of the bit rate R), making GMSK a partial response signal (in a full response signal, the pulse is confined to the interval T). Differentially encoded rectangular data stream is filtered using a Gaussian low pass filter of 3-dB band width [31].

In GMSK, the digital, Non-Return to zero (NRZI) signal is first passed through an integrator premodulation Gaussian pulse shaping filter and the filter generates a signal which is used to shift the carrier phase. This is what yields the effects of considerably reducing the sidelobes levels in the transmitted spectrum. Premodulation Gaussian filter converts the full response message signal into a partial response scheme where each transmitted symbol spans several bit periods. GMSK is most attractive for its excellent power efficiency and its excellent spectral efficiency [30].

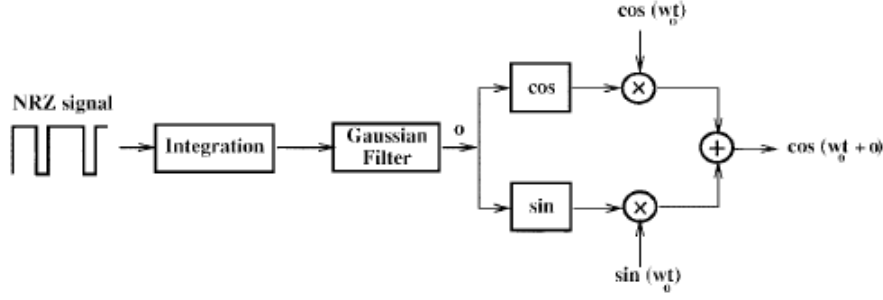


Fig. 33: GMSK System Block Diagram

First, the Gaussian Filter Impulse Response is given by:

$$h_g(t) = \frac{\sqrt{\pi}}{\alpha} e^{-\frac{\pi^2}{\alpha^2} t^2} \quad (34)$$

with the Transfer Function:

$$H_g(f) = e^{-\alpha f^2} \quad (35)$$

The parameter α is related to B, the 3dB baseband bandwidth of $H_g(f)$ by:

$$\alpha = \frac{\sqrt{\ln(2)}}{\sqrt{2}B} \quad (36)$$

The GMSK Filter is described in its entirety by the time-bandwidth product BT, where B is the bandwidth and T is the symbol duration.

The bit error rate for GMSK was first found in for AWGN channels, and was shown to offer performance within 1 dB of optimum MSK when $BT = 0.3$ (This is partly why the GSM standard adopted $BT = 0.3$). The bit error probability is a function of BT, since the pulse shaping impacts ISI [34].

The bit error probability for GMSK is:

$$P_e = Q\left(\sqrt{\frac{2\alpha E_b}{N_0}}\right) \quad (37)$$

Where α is a constant related to BT by $\alpha = 0.68$ for GMSK with $BT = 0.3$, E_b is the energy in one bit, N_0 is the Noise Power Spectral Density, and $Q(t)$ is the well-known Q function:

$$Q(t) = \frac{1}{\sqrt{2\pi}} \int_t^\infty e^{-\frac{\alpha^2}{2}} d\alpha \quad (38)$$

For GMSK, the BERs of coherent and non coherent demodulation will be degraded from these optimum values because of the ISI introduced by the pre modulation Gaussian filtering [35]. The GMSK modulation is a certain kind of binary digital modulation, its BER performance bound in the high SNR condition [30, 35].

The bit error rate or bit error ratio (BER) is the number of bit errors divided by the total number of transferred bits during a studied time interval. BER is a unitless performance measure, often expressed as a percentage. In a communication system, the receiver side BER may be affected by transmission channel noise, interference, distortion, bit synchronization, problems, attenuation, wireless multipath fading, etc.

The BER may be improved by choosing a strong signal strength (unless this causes cross-talk and more bit errors), by choosing a slow and robust modulation scheme. The bit error probability P_e is the expectation value of the BER. The BER can be considered as an approximate estimate of the bit error probability. The bit error probability is $\propto E_b/N_0$ (SNR). The energy per bit is the ratio of carrier power to bit rate and has the unit Joules. N_0 is given as the power in Joules/s per Hertz.

Finally, for Aeternitas a desirable benchmark for BER in the Data Link is 10^{-5} . Given equation (37) at a data rate of 9,600 baud and a transmit power of 2W at maximum for the Aeternitas Spacecraft, and a time bandwidth product of 0.3 for a GSM characteristic GMSK modulated signal, an approximate desired SNR is roughly 10.25 to 13 dB.

4.2 AX.25 DIGITAL PROTOCOL

The AX.25 Digital Communication Standard is used in Amateur Packet Radio on the Network and Data Link Layers of the Open Systems Interconnection (OSI) Model. Its purpose is to "ensure link-layer compatibility between stations" while still conforming to International Standards Organization (ISO) Information Standards (IS) 7809 High-level Data Link Control (HDLC) [21].

In general, the AX.25 protocol supports three different types of frames [21] including information, supervisory, and unnumbered frames. The Old Dominion University CubeSat Project almost exclusively uses Information frames for the purpose of its mission.

AX.25 is a link layer protocol for transmitting digital information using amateur radio systems, which originates from the X.25 protocol that was widely used in packet switched wide area networks during the 1980s and early 1990s [21]. AX 25 is

responsible for establishing link-layer connections between amateur radio terminals, transferring data in frames, and detecting transmission errors [21].

We note that, while the AX 25 protocol supports routing and may be used to send packets between two terminals (source and destination) through one or multiple relay nodes, it has most frequently been used to establish direct, point-to-point links between terminals, in which case the presence of additional network layers is not necessary. This feature, which implies low network overhead, makes the AX 25 suitable for use in radio links where the two terminals are a CubeSat in low Earth orbit and a ground station, and they have a limited time to establish a radio link to complete the data transmission. The AX.25 protocol supports three different types of frames: information, supervisory, and unnumbered frames [21]. However, only information frames are used in the radio link design for the ODU CubeSat and its corresponding ground station. The use of information frames only is sufficient to accomplish the CubeSat mission, which consists of transmitting GPS coordinates recorded during one orbital pass at 30 s intervals to the ground station.

Following AX.25, the data that is recorded by the CubeSat and should be transmitted to the ground station must fit within a 256-byte information frame (or packet) that is divided into seven sections as shown in Table XIV: Flag(s), Address, Control, Protocol Identifier (PID), Information (Info) data, and Frame Check Sequence (FCS). Each field in the information frame consists of one or multiple bytes that are formatted to serve specific functions:

TABLE XIV: Generic AX.25 Information Frame Structure

Flag	Address	Control	PID	Info	FCS	Flag
01111110	112/224 Bits	8/16 Bits	8 Bits	N*8 Bits	16 Bits	01111110

TABLE XV: Information Frame Structure Specific to Aeternitas Payloads

Flag	Address	Control	PID	Info	FCS	Flag
01111110	112/224 Bits	8/16 Bits	8 Bits	256*8 Bits	16 Bits	01111110

- The first byte, which is referred to as a flag byte, is used to delimit frames. It consists of the bit sequence 01111110, which occurs at both the beginning and end of each frame and cannot appear anywhere else in the frame.
- The address field for all frames consists of the source and destination call signs, along with a secondary station identifier (SSID). The call sign assigned by the FCC to the ODU CubeSat and ground station radios is WJ2XOH (6 bytes) and the SSID is 0 (one byte).
- The control field identifies the type of frame being sent and ensures that proper link control is maintained.
- The PID field is one byte long and identifies the Layer 3 protocol used. In our case it has the value 11110000 indicating that no Layer 3 protocol is used.
- The Info field contains the actual information to be transmitted and consists of 256 bytes by the operation of the Lithium-2 radio.
- The FCS is a two-byte number calculated by both the transmitter and the receiver and it is used to insure that the frame was not corrupted by the channel, in which case it is discarded.

Each field in an Information Frame is comprised of octets of bits and is specially formatted to serve its own specific functions [21]. The purpose of the flag is to delimit frames and always consists of 01111110 or 7E in Hex. The address field of all frames consists of a destination, and a source at minimum. Each subfield consists of a callsign and a Secondary Station Identifier (SSID). The callsign is made up of upper-case alpha and numeric ASCII characters only. The HDLC address field is extended beyond one octet by assigning the least-significant bit of each octet to be an extension bit. The extension bit of each octet is set to 0 to indicate the next octet contains more address information, or to 1, to indicate that this is the last octet of the HDLC address field. To make room for this extension bit, the amateur radio call-sign information is shifted one bit left [21]. The control field identifies the type of frame being sent and are modeled after the ISO HDLC balanced operation control fields [21]. The Protocol Identifier (PID) field appears in information frames (I and

UI) only. It identifies which kind of Layer 3 protocol, if any, is in use (in ODU's case no layer 3 protocol is in use). The info field is in particular to ODU, a 256 byte buffer no more than 6 windows deep at any given time as this is constrained by the operation of the Lithium II radio [18]. The FCS is a frame check sequence of 16 bits. If an invalid frame is received, or a frame is received with an FCS error, the frame is discarded [21].

Analytical Equations have been derived for effective AX.25 Throughput for both Full Duplex and Half Duplex Systems[36]. In the case of ODU, the half-duplex model was implemented for analysis and simulation to provide insights into the effective throughput of the data link. Equation 39 shows the transmission time for a half duplex radio link implementing AX.25,

$$T_f = \left\lceil \frac{L}{N_1} \right\rceil \left(\frac{64 \cdot 8N_1}{63R_{wl}} \right) + \left\lceil \frac{L}{N_1 k} \right\rceil \left(T_2 + 2T_{103} + (1+k) \frac{64 \cdot 160}{63R_{wl}} \right) \quad (39)$$

where the user data is L bytes long and the radio link operates at R_{wl} bps. Observe that for ODU, the effective throughput for a full 6 window deep buffer in the Lithium II Radio allows for just under 5000 bps for our given system parameters. These models have yet to be verified experimentally but do provide a good theoretical basis for approximating the System Throughput for our mission.

Using the analytical models for effective throughput of the AX.25 links in [36], the effective throughput of the halfduplex link established between the ODU CubeSat and ground station radios operating at 9600 bps is estimated to be around 5000 bps.

4.3 DIGITAL ENCODING, MODULATION AND GNU RADIO

GNU Radio is an open source software development toolkit that enables the user to design and implement software radios with processing blocks and processing runtime [37]. The users may use pre-configured blocks or write and implement their own blocks which can be written in C++ or Python [38]. The GNU Radio web page says: "[GNU Radio] is widely used in hobbyist, academic and commercial environments to support wireless communications research as well as to implement real-world radio systems" [37]. The ODU Space Systems Group uses GNU Radio, because it is an inexpensive solution which enables them to improve and modify the new ground station communication systems, utilizing off-the-shelf Software Defined Radios from Ettus Research.

GNU Radio Companion (GRC) is a graphical programming tool to design signal

processing flowgraphs. It automatically generates the dependent source code. For further information on how to launch and use GRC see the GNU Radio web site [38, 39]. Some of the used GRC blocks are excerpted from other projects and are not pre installed with GNU Radio.

4.4 DATA LINK BUDGET

In the design of any Wireless Communications Link, Engineers must understand the variations in signal strength due to propagation effects of the channel. In our model, Shadowing can generally be ignored as the Satellite is transmitting through space through the atmosphere to an antenna on top of the Engineering Hall.

The Free Space Pathloss Model for Aeternitas over the lifetime of the mission is given in Equation 8 where d = distance in m, f = frequency in Hz, c = Speed of Light, and G_T and G_R are respective antenna gains given in dB.

$$FSPL = 20 \log \left(\frac{\pi d}{\lambda} \right) + 32.44 + G_t + G_r \quad (40)$$

Figure 10 shows how the Pathloss for the Satellite increases as the distance between the satellite ground station increases. All values are taken from STK as distances measured from the Ground Station to the Satellite when access is possible. From the STK data, we know that the satellite will be 2025km away from the ground station at maximum and this corresponds to a Pathloss of 137.1dB. At minimum, the satellite will be accessible at a distance of 308km which corresponds to a Free Space Pathloss of 120.7dB.

The Signal To Noise Ratio (SNR) for Digital Communication Channels can be modeled by Equation 9 [40, 41].

$$\frac{E_b}{N_0} = \frac{P_t L_i G_t L_s L_a G_r}{k T_s R} \quad (41)$$

where P_t = Transmit Power, L_i = Feed Losses, G_t = Transmit Antenna Gain, G_r = Receive Antenna Gain, L_s = Free Space Path Loss, L_a = Miscellaneous Loss, k = Boltzman's Constant, T_s = System Noise Temperature, and R = System Data Rate.

It is also well known that Effective Isotropic Radiated Power can be found by Equation (36).

$$EIRP = P_t - L_c + G_a \quad (42)$$

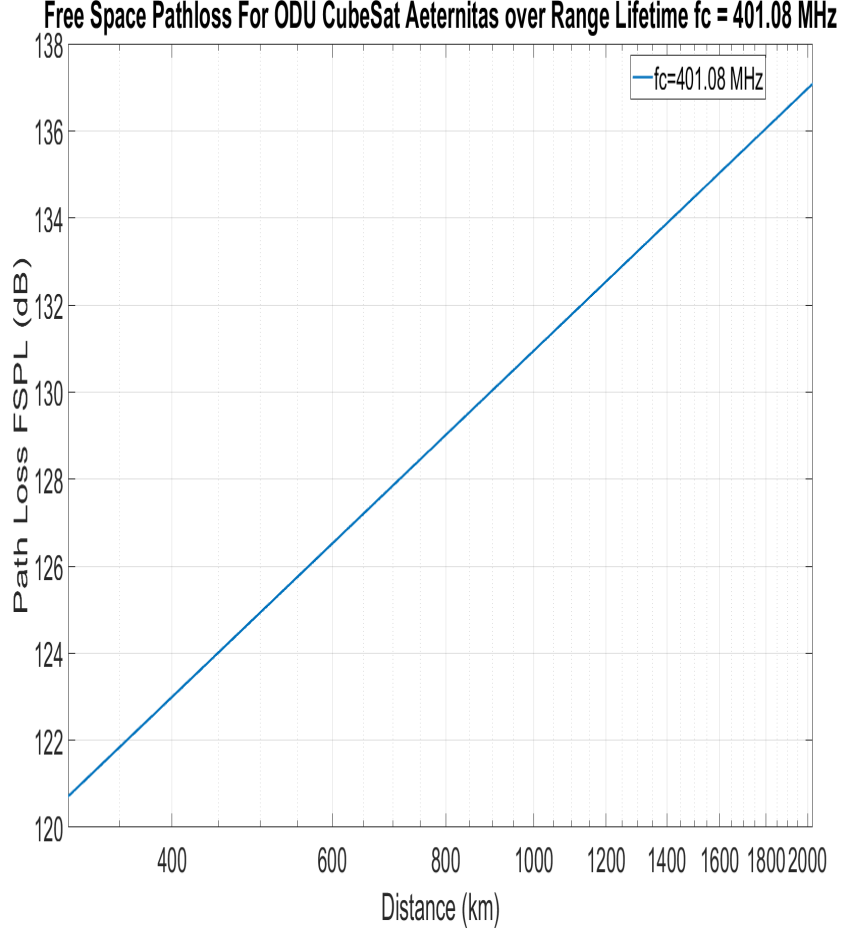


Fig. 34: Semilog Plot of Free Space Path Loss for Aeternitas across the satellite's range over the course of its lifetime.

Where P_t = Output Power losses in dBm, L_c = Cable losses in dB, and G_a = Antenna Gain in dBi.

With Equations 8-10, we are now prepared to compute the link budget margins.

$$M_{dB} = EIRP_{dBW} + G_r - E_b/N_0 - R_{dB} - kT_{dBW/Hz} - L_s - L_0 \quad (43)$$

From this analysis, a Plot in Fig. 48 is shown with best and worst case scenarios for Acceptable Link Margins given our system constraints vs the distance from CubeSat to Groundstation (and thus vs pathloss).

The budget for the CubeSat-to-ground station radio link determines the signal-to-noise ratio (SNR) at the receiver by considering the transmit power, the free space pathloss (FSPL) between the CubeSat and the ground station, the gains of the

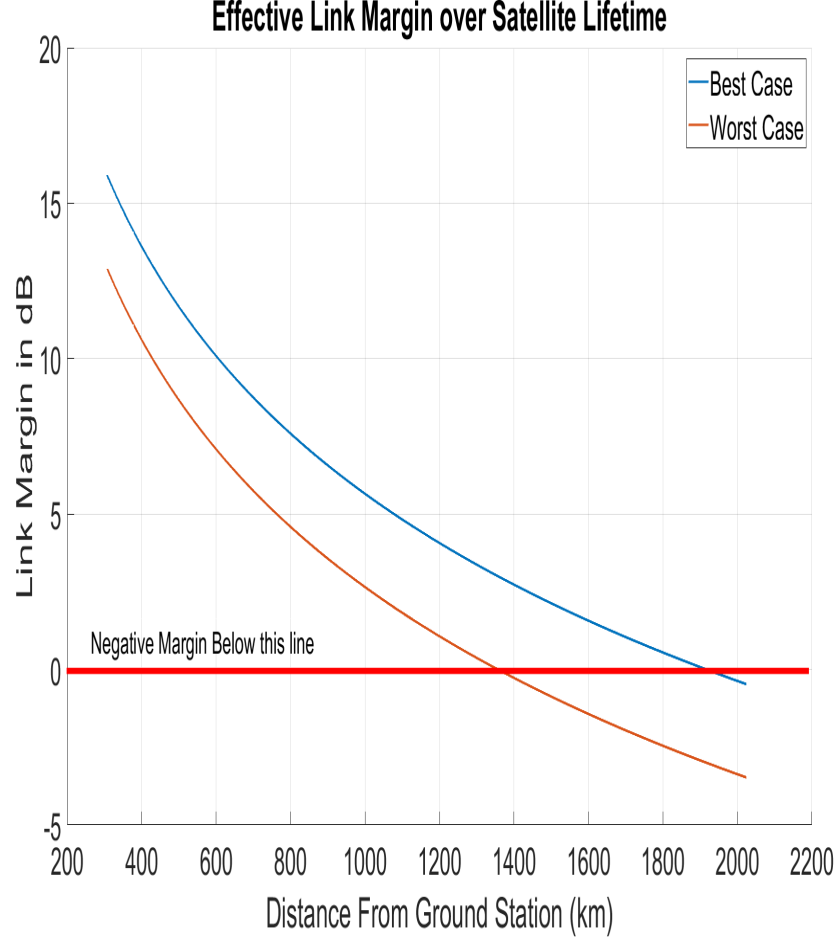


Fig. 35: Link Margin Worst and Best Case Scenarios for Satellite Access Distances Over the life of the Satellite.

CubeSat and ground station antennas, and the receiver noise [40]. The link budget calculations, which are summarized in Table XVI, use the numerical values outlined below.

$$FSPL = 20 \log \left(\frac{4\pi df}{c} \right) \quad (44)$$

Where $f = 401.08$ MHz is the frequency of the radio link, c is the speed of light, and d is the distance between CubeSat and ground station and can be determined by using the Systems Tool Kit (STK) software package. For the CubeSats in the VCC project, which will be deployed from the ISS at an altitude of 400 km with an orbital plane inclination of 52° , STK simulations show that for a ground station located in Norfolk, VA, the distance to the CubeSat varies from a maximum of about 2; 205 km

when the CubeSat is deployed to about 308 km, when the CubeSat is the upper edge of mesosphere at an altitude of 90 km and is expected to burn on re-entry. Thus, the corresponding values of the FSPL vary between the maximum value of 137.1 dB and minimum value of 120.7 dB, and for a worst-case scenario link budget the maximum value will be used. The CubeSat radio uses a custom designed dipole antenna with omnidirectional pattern and gain of 0 dBi, while the ground station uses a directional Yagi antenna with a beamwidth of about 40° and a gain of 11 dBi at 401 MHz.

The receiver noise spectral density is assumed uniform, and is expressed in terms of the system noise temperature as

$$N_0 = kTs \quad (45)$$

where k is Boltzmann's constant and T_s is the receiver noise temperature and is determined by adding antenna noise temperature T_{ant} , which includes noise sources that are external to the receiver (such as cosmic radiation, solar noise, man-made noise, etc.), and the receiver noise temperature T_r , which incorporates the noise contribution of the various circuit elements that connect the receive antenna to the digital demodulator (feed line, cabling, connectors, frontend band pass filter, low noise amplifier, etc.) [3]. For the CubeSat receiver, noise losses of approximately -1 dB and a receiver noise figure $F_c = 5$ dB are considered, which imply a receiver noise temperature of 855 K. For the ground station losses of about -3 dB and a receiver noise figure $F_c = 7$ dB are considered, which result in the corresponding noise temperature of 2,610 K for the ground station. The antenna noise temperature is taken to be 150 K for the CubeSat and 290 K for the ground station. We note from Table I that, for GMSK modulation with data rate of 9,600 bps and bit error rate (BER) of the order of 10^{-5} the link margin exceeds 20 dB, which means that a robust RF link is possible.

The table below summarizes this Link Budget given from the above discussion and that of previous chapters.

TABLE XVI: Aeternitas Link Budget with Full Analysis Performed with STK

	Uplink	Downlink
Frequency	401.08MHz	401.08MHz
Transmit Power P_t	43.98 dBm	33.01 dBm
Transmitter Loss	3 dB	0.5 dB
Transmit Antenna Gain G_t	11dBi	0 dBi
FSPL	137 dB	137 dB
Other Propagation Losses	4 dB	4 dB
Receive Antenna Gain G_r	0 dBi	11 dBi
Reciever Noise Temp $T - r$	2610 K	855 K
Antenna Noise Temp T_{ant}	290 K	150 K
System Noise Temp T_s	2900 K	1005 K
$10 \log T_s$	34.62 dBK	30.02 dBK
Boltzman Constant		
$10 \log k + 30$	-198 dBm/K/Hz	-198 dBm/K/Hz
Data Rate R	9600 bps	9600 bps
$10 \log 10R$	39.82 dBHz	39.82 dBHz
Received SNR	37.54 dB	30.67 dB
Required SNR for 10^{-5} BER	≥ 10 dB	≥ 10 dB
Link Margin	≤ 24.54 dB	≤ 20.67 dB

CHAPTER 5

EXPERIMENTAL RESULTS

First, a bell 202 modem was implemented in MATLAB as this 1200 AFSK scheme is the predecessor to the 9600 baud GMSK AX.25 modem that will be required for future development beyond this thesis. As a first step, this was implemented with two software defined radios and a combination of MATLAB and SDR Sharp.

5.1 RADIO LINK PERFORMANCE

Using MATLAB and GNU Radio with an ETTUS Research B200 an AFSK 1200 testbed was developed to begin proof-of-concept operation for the spacecraft and Ground Station. FSK, is the simplest form of frequency modulation and thus was chosen for the first testbed solution for proof-of-concept in our communications system design [30]. FSK is a scheme in which digital information is transmitted through discrete frequency changes of a carrier signal. For the purposes of the demonstration Audio FSK or AFSK was selected for ease of implementation and the two carriers chosen were two sinusoidal waveforms of 2KHz and 2.2KHz. The two tones are used to encode zeroes and ones in our digital bitstream "Hello World!" Using a pair of discrete frequencies to transmit binary (0s and 1s) information, we were able to implement an AFSK/BPSK scheme to transmit our "Hello World!" information along the two tones.

Difficulty arose when trying to synchronize the TX and RX signals. This was solved by using MATLAB to find the cross correlation of the power spectral densities of the two tones with the received signal. As a result, the peak correlation between signals was found by interacting with the MATLAB plot of the 'xcorr' function and determine the most correlated point on the plot. By doing this, we were able to find where the data begins and thus synchronize our output with a quick MATLAB script to start the data at point 137 of 160 and then proceed to wrap around to the end of the data. In doing so, we were able to take the 12 symbols for "Hello World!" and reproduce them on the output console.

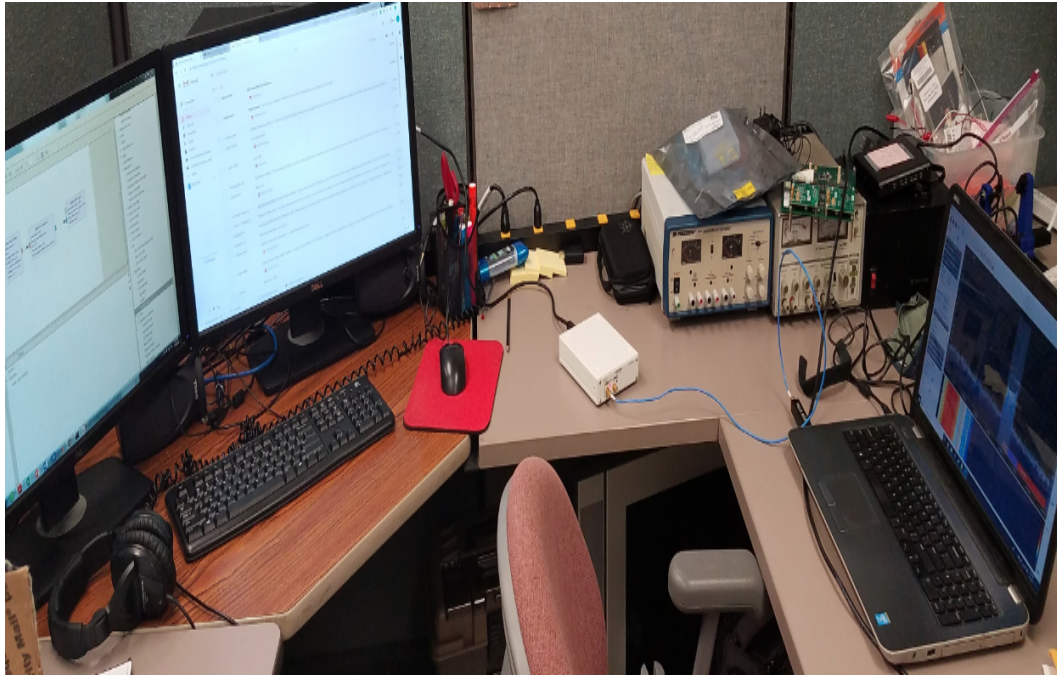


Fig. 36: Experimental Setup for AFSK 1200 and GMSK 9600.

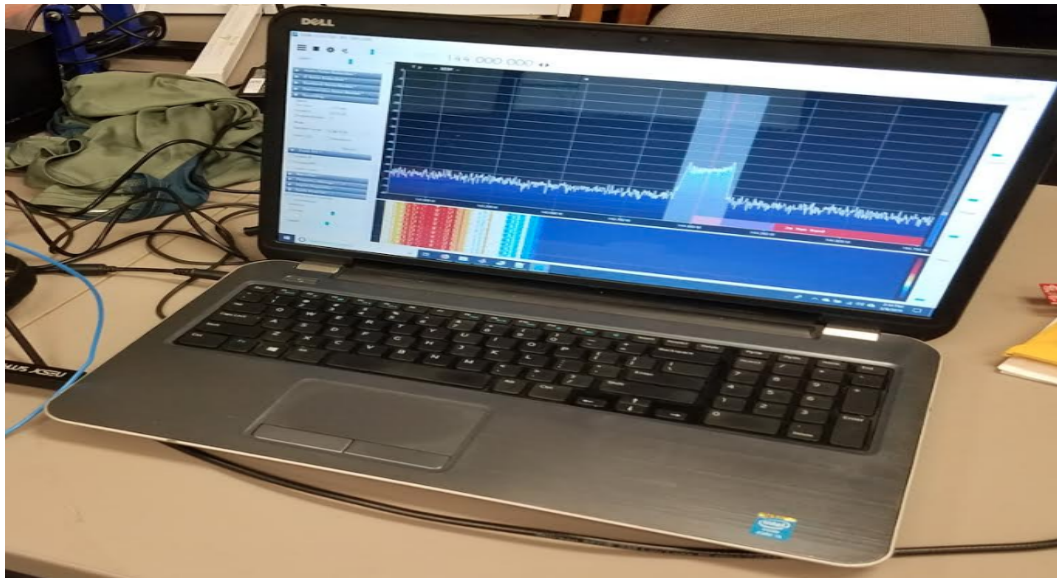


Fig. 37: RTL-SDR receiving "Hello World!" on 1200 AFSK

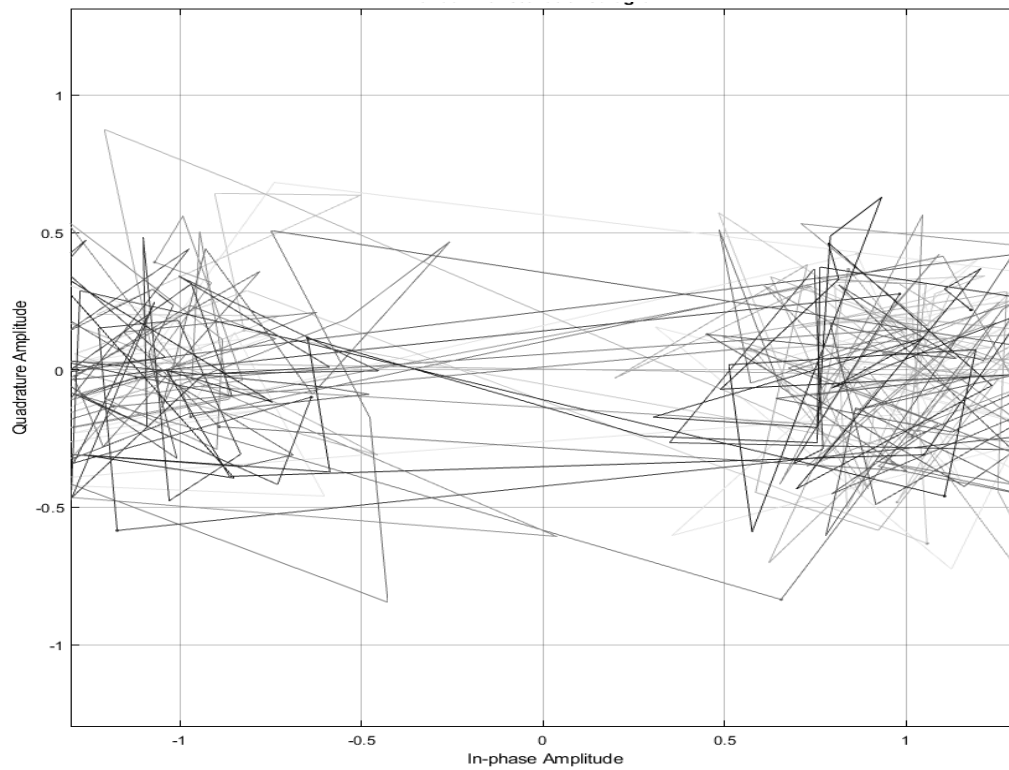


Fig. 38: Matlab Binary Decode Clarity at 7 dB SNR

5.1.1 MATLAB FEASIBILITY FOR MISSION CONSTRAINTS

Using Matlab Communications Systems and DSP toolbox, a simulated Wireless Channel was synthesized to measure bit error rates of the GMSK channel given the constraints of the CubeSat and Simulation results from STK.

By using this model, random payloads of 8 million bits were GMSK modulated and bit error rates were measured for several SNR values. The output results are shown in Figures 38 and 39 respectively for a GMSK modulated wireless channel with coherent detection in the worst and best case scenario.

5.1.2 GMSK IDEALIZED CHANNEL

Using a dummy packet of satellite payload information and the AX.25 Protocol to frame the data appropriately a GNU Radio Companion flow graph was used to model the communications channel the satellite and ground station will be operating over. Figures 38 and 39 show the experimental test bed configuration set up in GNU

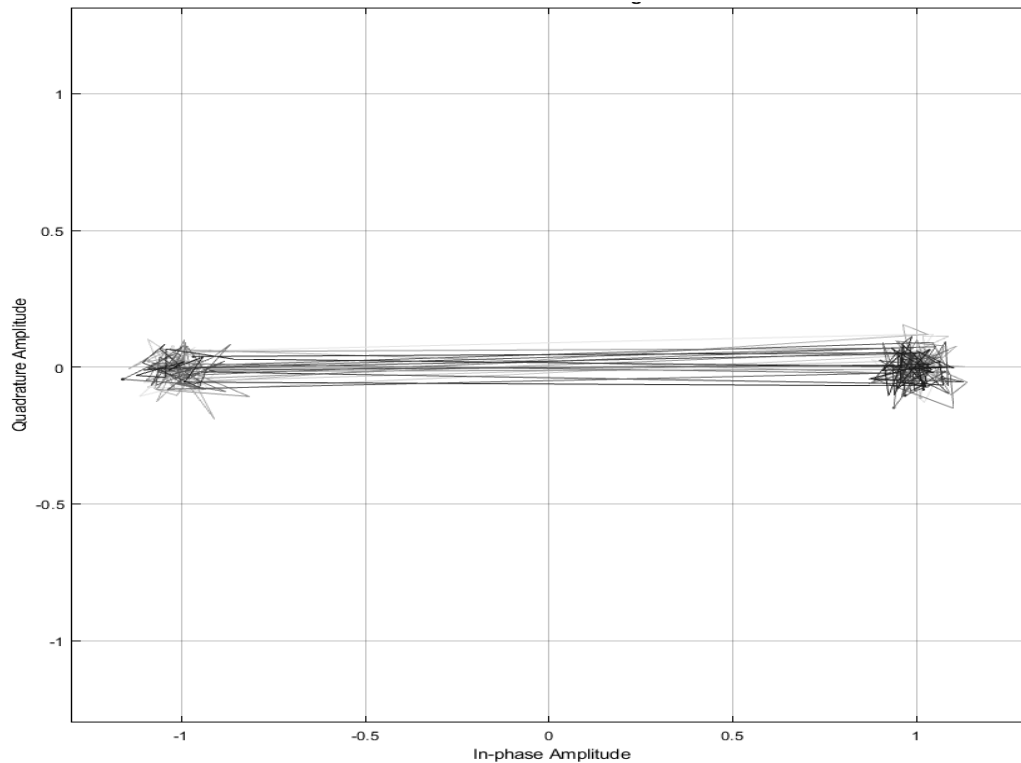


Fig. 39: Matlab Binary Decode Clarity at 22 dB SNR

Radio. Fig. 38 shows the transmit chain which models the Satellite and Fig. 39 shows the receive chain which serves as the model for the ground station.

The encoder block is used to frame the 256 byte text file used as the simulated payload data to fit the AX.25 Amateur Radio Protocol. In this block, the delimiting frames are book-ended onto the total packet and have a binary value of 01111110 or 7E.

Next, the encoder adds the address field which contains both the destination and source call signs. For ODU, WJ2XOH is the call sign for which the CubeSat transmissions are authorized and thus the source and destination is the same at a size of 6 bytes each. A bit of 0 is then appended to the address field for Secondary Station Identifier(SSID) because no layer 3 protocols are being implemented [21].

Because this is an information frame being sent, the Control and PID bytes are always 3F and F0 respectively [21].

After the payload sequence of the frame, the Frame Check Sequence is handled [21]. The FCS is a 16-bit number calculated by both the sender and the receiver of the

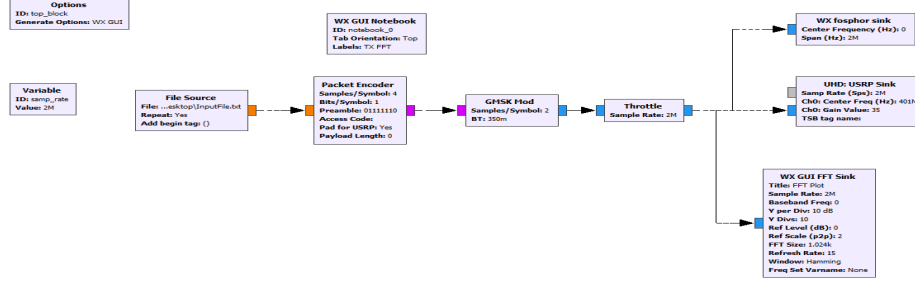


Fig. 40: Transmit Chain for Experiment

frame. Simply put, this ensures that the data was not corrupted during transmission and is calculated in accordance with ISO 3309 (HDLC)[21].

Using GNU radio, this flow graph was used to transmit not only simulated payload information in a text file fed in as a byte stream, but also other file formats such as .pdf and .wav files. This is because in the model, the information is broken down into its native form of a simple bit stream and fed through the encoder to be framed.

After the digital encoding has been handled, the digital information is then GMSK modulated by a GNU radio block called GMSK Mod the time bandwidth product for this modulator is the default value of .350 which is a good compromise between the GSM cellular standard and the classical GMSK time bandwidth product of 0.5. In accordance with the theory presented in the previous chapter, this information is shaped by a Gaussian filter with excellent rolloff characteristics and spectral efficiency.

5.1.3 RESULTS

By adjusting the gain on the TX and RX SDRs, we are able to not only transmit data, but get a qualitative measure of the radio link performance by comparing the same image of the three Virginia CubeSat Constellation SpaceCraft transmitted with a receive SNR of 7 dB and 22 dB respectively. This shows the minimum and

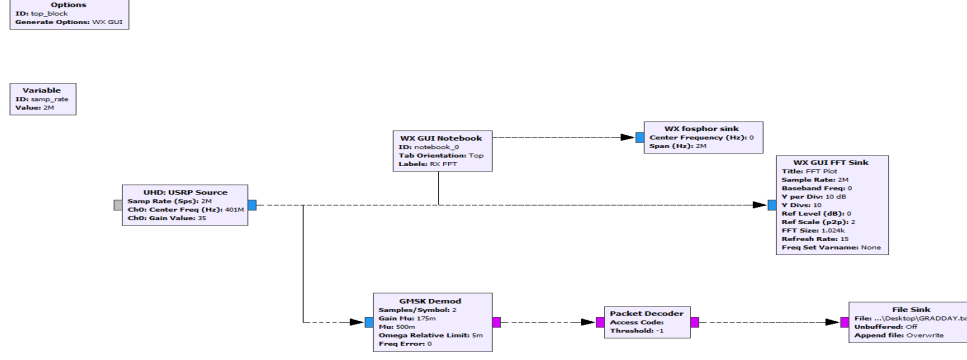


Fig. 41: Receive Chain for Experiment

maximum quality of system performance in Figures 42 and 43. Observe that the picture is still very recognizable in the 7 dB SNR, however, the clarity of the picture in the 22 dB SNR channel is drastically more clear. The simulated results and modeled GNU radio channel both show that within the mission constraints (Free Space Path Loss due to Orbit Geometry), an acceptable BER can be achieved.

TABLE XVII: Matlab Simulated SNR to BER

SNR	BER	Errors
7	9.80E-05	784
10	3.40E-05	272
13	1.20E-05	94
16	1.00E-09	2
19	1.00E-09	0
22	OVER RUN	0

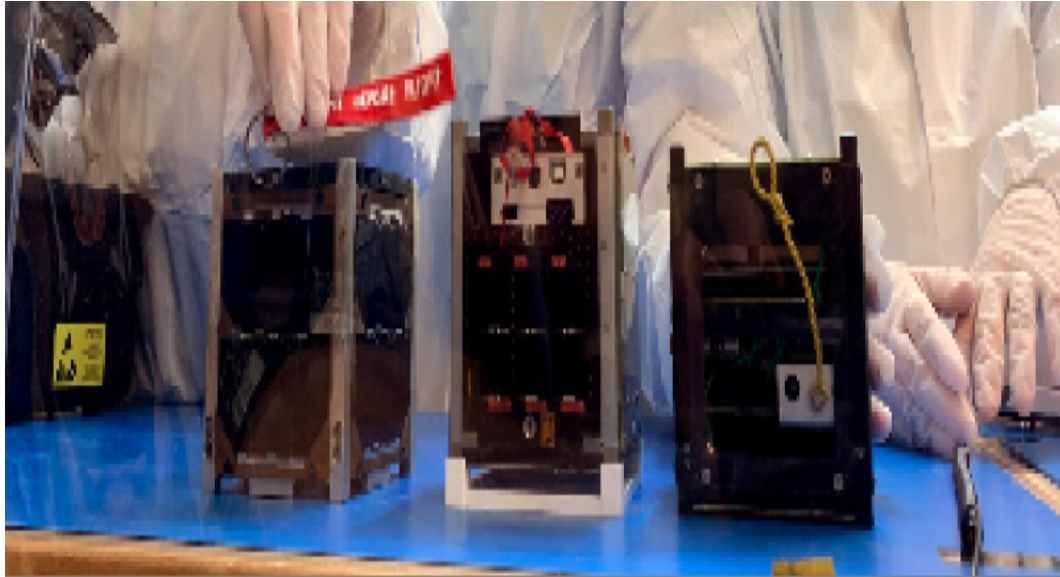


Fig. 42: Received Image Payload at 7 dB SNR

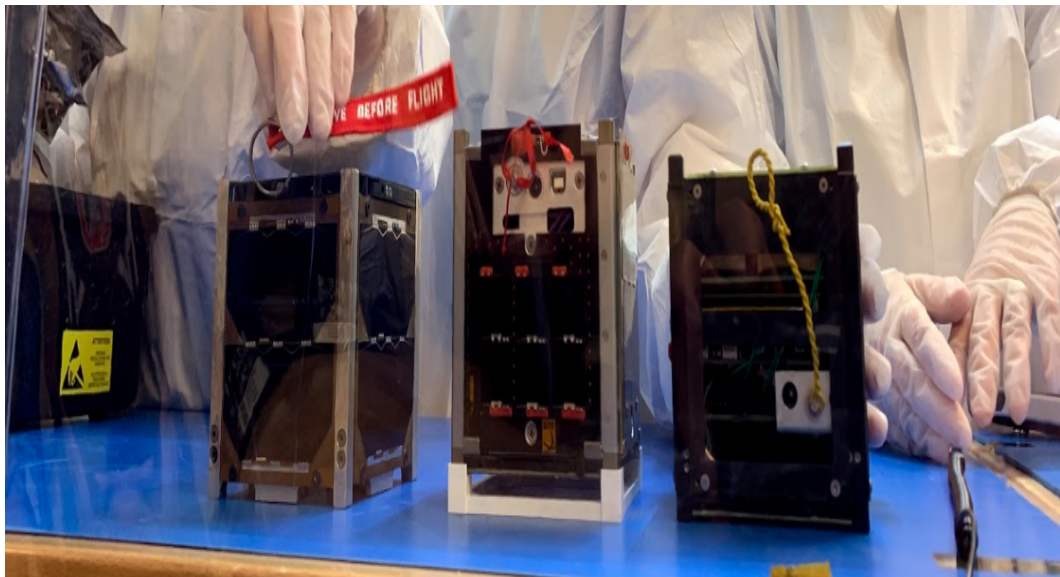


Fig. 43: Received Image Payload at 22 dB SNR

CHAPTER 6

CONCLUSION

In this thesis, a heuristic model for a University CubeSat Electrical System Architecture Design was presented. The thesis began by introducing the orbital mechanics necessary to formally specify the design work required for rapid implementation of the complete system while also highlighting the foundational importance of a power and link budget analysis. It was found that given the mission constraints and the selected commercial off the shelf parts, a power surplus estimate of over 1kWh and a link margin of up to 17dB for the mission is achieved. The thesis then presents the analysis required for proper dipole antenna design and the salient printed circuit board design methods required for impedance matching and interfacing the commercial off the shelf radio with the designed antenna. A discussion of the motherboard design completed to interface all telemetry and sensing equipment on board the satellite was presented. Salient design aspects of the motherboard design were also discussed while to the design constraints from a systems engineering level were discussed. An analysis of the communication link and wireless channel was presented. The modulation scheme and digital encoding and decoding rates were presented within the context of implementing the AX.25 Amateur Radio Protocol. The thesis concluded by presenting theoretical simulations and analysis which were leveraged in software to verify the wireless channel capacity and integrity. Using a test bed with two software defined radios, the satellite communication system was modeled and was shown to demonstrate for the expected SNR that quality bit error rates and information transmission is feasible, thus showing for the mission constraints that the communication link is closed and robust.

6.1 FUTURE WORK

The thesis and the resulting spacecraft from which it is born demonstrates that a student designed University CubeSat electrical system architecture can be more rapidly developed than is suggested in literature. Balancing custom designed hardware and software with carefully selecting commercial off the shelf parts requires

careful and deliberate analysis prior to design and future projects should be appropriately scaled to fit the time and budget constraints.

Work is currently in process to automate the ground station to synchronize with the satellite based on its two-line-element information, and automate the process of querying for the telemetry and sensing data acquired during the mission.

Several iterations of RF switching hardware have been made to duplex a single antenna to accommodate this mission and are currently being tested. In addition to the switching hardware, an RF amplifier will be used to maximize the transmit power of the software defined radios at Old Dominion University and will be switched on and off based on whether the ground station is in receive mode or transmit mode.

In addition to the hardware development, software is currently being developed to not only automate the telemetry querying process, but also to implement a fully functional AX.25 Modem which integrates with the RF switching hardware and the Old Dominion University Ground Station software defined radio.

REFERENCES

- [1] S. Waydo, D. Henry, and M. Campbell, “CubeSat Design for LEO-Based Earth Science Missions,” *Proceedings 2002 IEEE Aerospace Conference*, vol. 1, pp. 435–445, March 2002.
- [2] “Cubesat design specification.” <http://www.cubesat.org/images/developers/cdsrev13nal.pdf>. Accessed: 2018-9-28.
- [3] O. Popescu, “Power Budgets for CubeSat Radios to Support Ground Communications and Inter-Satellite Links,” *IEEE Access*, vol. 5, pp. 12618–12625, July 2017.
- [4] P. Fortescue, G. Swinerd, and J. Stark, *Spacecraft Systems Engineering*. The Atrium, Southern Gate, Chichester, West Sussex, PO19 8SQ, United Kingdom: Wiley, fourth ed., 2011.
- [5] “Virginia CubeSat Constellation Mission.” <http://www.vsgc.odu.edu/virginiacubesatconstellation/>. Accessed: Mar. 5, 2019.
- [6] J. S. Harris, “Analysis and implementation of communications systems for small satellite missions,” Master’s thesis, Old Dominion University, 2014.
- [7] Anonymous, *ICOM 910H Instruction Manual*. ICOM Inc., 1-1-32 Kamiminami, Hirano-ku, Osaka 547-0003 Japan, 1st ed., January 2000.
- [8] J. Oehrig, A. Schea, and A. e. a. Bennett, “TU Sat 1An Innovative Low-Cost Communications Satellite,” *15th Annual USU AIAA Conference on Small Satellites*, August 2002.
- [9] D. Kaslow, L. Anderson, and S. e. a. Asundi, “Developing a CubeSat Model-Based System Engineering (MBSE) Reference Model - interim status,” *2015 IEEE Aerospace Conference*, pp. 1–16, March 2015.
- [10] S. Palo, “High Rate Communications Systems for CubeSats,” *IEEE MTT-S International Microwave Symposium*, pp. 1–4, May 2015.
- [11] F. E. Tubbal, R. Raad, and K. W. Chin, “A Survey and Study of Planar Antennas for Pico-Satellites,” *IEEE Access*, vol. 3, pp. 2590–2612, December 2015.

- [12] B. S. Rani, E. Logashanmugam, S. Rajarajan, M. Sugadev, G. Jegan, N. J. Kumar, and N. J. Kumar, "On board communication subsystem for Sathyabama University nano-satellite," *Recent Advances in Space Technology Services and Climate Change 2010 RSTS and CC-2010*, pp. 143–145, 2010.
- [13] T. Sato, R. Mitsuhashi, and S. Satori, "Attitude estimation of nano-satellite "HIT-SAT" using received power fluctuation by radiation pattern," *2009 IEEE Antennas and Propagation Society International Symposium*, September 2009.
- [14] R. Zitouni and L. George, "Output Power Analysis of a Software Defined Radio Device," in *Proceedings 2016 IEEE Radio and Antenna Days of the Indian Ocean (RADIO)*, (Saint Gilles Les Bains, Réunion Island), October 2016.
- [15] G. Hunyadi, D. Klumpar, S. Jepsen, B. Larsen, and M. Obland, "A commercial off the shelf (COTS) packet communications subsystem for the Montana EaRth-Orbiting Pico-Explorer (MEROPE) CubeSat," *Proceedings, IEEE Aerospace Conference*, pp. 1–1, September 2002.
- [16] E. Tools, "Analytical graphics inc." <https://www.agi.com/products/engineering-tools>, month = March, year = 2019,.
- [17] J. Sellers, W. Larson, W. Astore, and D. Gay, *Understanding Space*. New York, NY: McGraw Hill, first ed., 1993.
- [18] K. Brown, *Lithium II Data Sheet*. Astronautical Development, LLC, 5588 Lakeshore Dr Ann Arbor, MI 48108 United States, 1st ed., January 2017.
- [19] K. Woellert, P. Ehrenfreund, A. Ricco, and H. Hertzfeld, "CubeSats: Cost-Effective Science and Technology Platforms for Emerging and Developing Nations," *Advanced Space Res.*, vol. 47, no. 4, pp. 663–684, 2011.
- [20] P. Bugryniec, "Cubesat: The Need for More Power To Realise Telecommunications," June 2016.
- [21] W. Beech, D. Nielsen, and J. Taylor, *AX.25: Link Access Protocol for Amateur Packet Radio*. Tucson Amateur Packet Radio Corporation, PO BOX 852754 Richardson, TX 75085-2754, 2.2 ed., July 1998.
- [22] T. Milligan, *Modern Antenna Design*. Hoboken, NJ: Wiley-Interscience IEEE Press, second ed., 2005.

- [23] Association Connecting Electronics Industries, 3000 Lakeside Drive, 105 N, Bannockburn, IL 60015, *IPC-2141 - Controlled Impedance Circuit Boards and High-Speed Logic Design*, April 1996.
- [24] B. Wadell, *Transmission Line Handbook*. Artech House, first ed., 1991.
- [25] Nelco, *Nelco N4000-6 High-TG Epoxy Laminate and Prepreg*. Park Electrochemical Corp., 48 S Service Rd 300, Melville, NY 11747, June 2006.
- [26] B. Parker, “A Wideband Balun for HF, VHF, and UHF Applications,” *IEEE Microwave Magazine*, vol. 15, pp. 86–91, January 2014.
- [27] H. Ott, *Noise Reduction Techniques in Electronic Systems*. New York, NY: Wiley-Interscience IEEE Press, second ed., 1989.
- [28] H. Ott, *Electromagnetic Compatibility Engineering*. Hoboken, NJ: Wiley-Interscience IEEE Press, second ed., 2009.
- [29] A. Kleinschrodt, A. Freimann, S. Christall, M. Lankl, and K. Schilling, “Advances in Modulation and Communication Protocols for Small Satellite Ground Stations,” *68th International Astronautical Congress*, September 2017.
- [30] J. G. Proakis and M. Salehi, *Communication Systems Engineering*. Upper Saddle River, NJ: Prentice Hall, second ed., 2002.
- [31] S. Seiichi, *Applications of digital Wireless Technologies to Global Wireless Communications*. Feher/Prentice Hall, first ed., 1997.
- [32] T. Pratt, C. Bostian, and J. Allnutt, *Satellite Communications*. Hoboken, NJ: John Wiley and Sons, second ed., 2003.
- [33] R. Ziermer and C. Ryan, “Minimum Shift Keyed modem implementations for high data rates,” *IEEE Communications Magazine*, pp. 28–37, October 1983.
- [34] M. Mammela and R. Broderon, “Constant Envelope Multicarrier Modulation: Performance Evaluation in AWGN and Fading Channels,” *MILCOM2005*, pp. 807–813, October 2005.
- [35] K. Murota, “GMSK Modulation for Digital Radio Telephony,” *IEEE Transactions on Communications*, pp. 1044–1050, May 1978.

- [36] M. Z. Bartlomiej, “EFFECTIVE TRANSMISSION SPEED IN AX.25 PROTOCOL,” *IEEE Eurocon 2009*, May 2009.
- [37] “About GNU Radio.” <http://www.gnuradio.org/about/>. Accessed: Mar. 5, 2019.
- [38] “Coding Guide.” https://wiki.gnuradio.org/index.php/Coding_guide_impl. Accessed: Mar. 5, 2019.
- [39] “GNU Radio Guided Tutorial.” https://wiki.gnuradio.org/index.php/Tutorials#Guided_Tutorials. Accessed: Mar. 5, 2019.
- [40] O. Popescu, “Power Budgets for CubeSat Radios to Support Ground Communications and Inter-Satellite Links,” *IEEE Access*, vol. 5, pp. 12618–12625, July 2017.
- [41] E. B. Z. Adnane A., Abdelhak K., “Design of a Telecommand and Telemetry System for use on Board a Nanosatellite,” *IEEE International Conference on Electronics, Circuits and Systems*, vol. 14, pp. 455–458, December 2007.

APPENDIX A

MATLAB

GMSK CODE

```

1 % Create a GMSK modulator, an AWGN channel, and a GMSK
  demodulator. Use a phase offset of pi/4.
2   hMod = comm.GMSKModulator('BitInput', true, '
      InitialPhaseOffset', pi/4);
3   hAWGN = comm.AWGNChannel('NoiseMethod', ...
4       'Signal to noise ratio (SNR)', 'SNR', .5);
5   hDemod = comm.GMSKDemodulator('BitOutput', true, ...
6       'InitialPhaseOffset', pi/4);
7 % Create an error rate calculator, account for the delay
  caused by the Viterbi algorithm
8   hError = comm.ErrorRate('ReceiveDelay', hDemod.
      TracebackDepth);
9   for counter = 1:1000
10      % Transmit 100 3-bit words
11      data = randi([0 1], 8000, 1);
12      modSignal = step(hMod, data);
13      noisySignal = step(hAWGN, modSignal);
14      receivedData = step(hDemod, noisySignal);
15      errorStats = step(hError, data, receivedData);
16   end
17   fprintf('Error rate = %f\nNumber of errors = %d\n', ...
18       errorStats(1), errorStats(2))

```

GMSK CONFIG CODE

```

1  %
   %%%%%%%%%%%%%%%%%%%%%%%%%%%%%%%%%%%%%%%%%%%%%%%%%%%%%%%%%%%%%%%%%%%%%%%%%
2  % Simulation Modell GMSK compared to MSK Type B and Type A
3  % 2009 by P. Fetzler, Konrad Benedict
4  %
   %%%%%%%%%%%%%%%%%%%%%%%%%%%%%%%%%%%%%%%%%%%%%%%%%%%%%%%%%%%%%%%%%%%%%%%%%

5
6  clear all;
7  clc;
8  %Go up three at a time SNR
9  %
   %%%%%%%%%%%%%%%%%%%%%%%%%%%%%%%%%%%%%%%%%%%%%%%%%%%%%%%%%%%%%%%%%%%%%%%%%

10 % ——— Config GMSK
11 SNR = 7; % SNR / dB
12 lengthOfSymbol = 8;
13 simulationTime = 2000;
14 sampleTime = 1;
15 simin.time = [0:sampleTime:simulationTime];
16
17 %
   %%%%%%%%%%%%%%%%%%%%%%%%%%%%%%%%%%%%%%%%%%%%%%%%%%%%%%%%%%%%%%%%%%%%%%%%%

18 % ——— create Inputdata (choose one of the Data sets)
19
20 simin.signals.values = randi([-0 1],length(simin.time),1);
21 % random Bitstream
22 % simin.signals.values = ones(length(simin.time), 1);
23 % Bitstream consisting of ones
24 % simin.signals.values = zeros(length(simin.time), 1);

```

```

25 % Bitstream consisting of zeros
26 % simin.signals.values = ((square(2*pi*simin.time/1.9999999,
    50)+1)/2)';
27 % Bitstream constantly switching between zero and one
28
29 %
    %%%%%%%%%%%%%%%%%%%%%%%%%%%%%%%%%%%%%%%%%%%%%%%%%%%%%%%%%%%%%%%%%%%%%%%%%
30 % ——— Simulation Simulink model
31
32     sim('GMSK_MSK.mdl');
33
34 %
    %%%%%%%%%%%%%%%%%%%%%%%%%%%%%%%%%%%%%%%%%%%%%%%%%%%%%%%%%%%%%%%%%%%%%%%%%
35 % ——— FFT-Analysis
36
37 L = length(simoutGmsk.signals.values);
38 Ts = simoutTime.signals.values(2)-simoutTime.signals.values
    (1);
39 Fs = 1/Ts;
40 window = blackman(L);
41
42 NFFT = 2^nextpow2(L);
43 f = Fs/2*linspace(-1,1,NFFT);
44
45 % GMSK-Signal
46 Y_Gmsk = fft(simoutGmsk.signals.values.*window,NFFT)/L;
47 Y_Gmsk = Y_Gmsk/max(abs(Y_Gmsk)); % Norm
48 Y_Gmsk_dB = 10*log10(abs([Y_Gmsk(end/2:end);Y_Gmsk(1:end/2-1)
    ]).^2);
49
50 % MSK-Typ B-Signal
51 Y_MskB = fft(simoutMskB.signals.values.*window,NFFT)/L;

```

```

52 Y_MskB = Y_MskB/max(abs(Y_MskB)); % Norm
53 Y_MskB_dB = 10*log10(abs([Y_MskB(end/2:end);Y_MskB(1:end/2-1)
    ]).^2);
54
55 % MSK-Typ A-Signal
56 Y_MskA = fft(simoutMskA.signals.values.*window,NFFT)/L;
57 Y_MskA = Y_MskA/max(abs(Y_MskA)); % Norm
58 Y_MskA_dB = 10*log10(abs([Y_MskA(end/2:end);Y_MskA(1:end/2-1)
    ]).^2);
59
60
61 % plot two-side spectrum
62 f1 = figure(1);
63 set(f1, 'Name', 'Power Density Spectrum ');
64 plot(f,Y_MskA_dB, 'g') ;
65 hold on;
66 plot(f,Y_MskB_dB, 'r') ;
67 plot(f,Y_Gmsk_dB, 'b')
68 hold off;
69 legend('MSK Type A', 'MSK Type B', 'GMSK');
70 title('Power Density Spectrum');
71 xlabel('Frequency / Hz');
72 ylabel('|Y(f)|^2 normed / dB');
73 ylim([-70;1]);
74 xlim([-3/sampleTime),(3/sampleTime)]);
75
76 %
    %%%%%%%%%%%%%%%%%%%%%%%%%%%%%%%%%%%%%%%%%%%%%%%%%%%%%%%%%%%
77 % ——— Plot Delay over time
78 f2 = figure(2);
79 set(f2, 'Name', 'Delay over time');
80
81 % MSK Typ A

```

```

82 subplot(3,1,1);
83 plot(simoutTime.signals.values,angle(simoutMskA.signals.
    values).*(180/pi));
84 set(gca, 'YTick', [-200 -100 0 100 200], 'YTickLabel', [-180
    -90 0 90 180]);
85 title('MSK Type A');
86 xlabel('time / s');
87 ylabel('Delay / Degree');
88
89 % MSK Typ B
90 subplot(3,1,2);
91 plot(simoutTime.signals.values,angle(simoutMskB.signals.
    values).*(180/pi));
92 set(gca, 'YTick', [-200 -100 0 100 200], 'YTickLabel', [-180
    -90 0 90 180]);
93 title(' MSK Type B');
94 xlabel('Zeit / s');
95 ylabel('Phase / Grad');
96
97 % GMSK
98 subplot(3,1,3);
99 plot(simoutTime.signals.values,angle(simoutGmsk.signals.
    values).*(180/pi));
100 set(gca, 'YTick', [-200 -100 0 100 200], 'YTickLabel', [-180
    -90 0 90 180]);
101 title('GMSK');
102 xlabel('Zeit / s');
103 ylabel('Phase / Grad');

```

APPENDIX B

COPYRIGHTS

The following copyright permission were obtained for legal reproduction or adaptation of previously published figures for use in this work:

The graphic for Figure 5 comes from a publication by Sellers [156].


The graphic for Figure 6 comes from a publication by Sellers [156].

The graphic for Figure 8 comes from a publication by Sellers [158].

The graphic for Figure 9 comes from a publication by Sellers [171].

The graphic for Figure 10 comes from a publication by Sellers [170].

The permission receipt is included on the following page.




Welcome, Anthony
Not you?

[Log out](#) |
 [Cart \(0\)](#) |
 [Manage Account](#) |
 [Feedback](#) |
 [Help](#) |
 [Live Help](#)

Get Permission / Find Title
 Go
[Advanced Search Options](#)

[Back to view orders](#)

[Copy order](#)


[Print this page](#)
[Print terms & conditions](#)
[Print citation information](#)
[\(What's this?\)](#)

Confirmation Number: 11802636
Order Date: 03/28/2019

Customer Information
Customer: Anthony Cappiello
Account Number: 3001427713
Organization: Anthony Cappiello
Email: acapp008@odu.edu
Phone: +1 (757) 793-6591


Search order details by: **Go**

This is not an invoice

Order Details

Understanding Space : An Introduction to Astronautics

Billing Status:
N/A

Order detail ID:	71862849	Permission Status:	 Granted
ISBN:	9780070570276	Permission type:	Republish or display content
Publication Type:	Book	Type of use:	Republish in a thesis/dissertation
Publisher:	McGraw Hill Education	Order License Id:	4557610707362
Author/Editor:	Sellers, Jerry Jon		

[View details](#)

Note: This item was invoiced separately through our **RightsLink service**. [More info](#)

Discount: -\$750.00
Discounted Price: \$ 0.00

Total order items: 1

Order Total: \$0.00

APPENDIX C

PIN MAPPING

CubeSat Pin Map		
Net Name	Microcontroller Pin	Arduino Equivalent
MPU_Switch	PD9	PIN 32
EPS_I2C_CLK	PD8	PWM12 (SDCLK CAPABLE)
EPS_I2C_DAT	PD7	PWM11 (SDAT CAPABLE)
COMMON_IN/OUT_MUX	PD6	PIN 29
S3	PD3	PIN 28
S2	PD2	PIN 27
S1	PD1	PIN 26
S0	PD0	PIN 25
MT1_REV	PC26	SS1/PWM4
MT1_FWD	PC25	PWM 5
MT2_REV	PC24	PWM 6
MT2_FWD	PC23	PWM 7
MT3_REV	PC22	PWM 8
MT3_FWD	PC21	PWM 9
DAT0	PC19	PIN 44
DAT1	PC18	PIN 45
DAT2	PC17	PIN 46
DAT3	PC16	PIN 47
DAT4	PC15	PIN 48
DAT5	PC14	PIN 49
DAT6	PC13	PIN 50
DAT7	PC12	PIN 51
BW_2	PC9	PIN 41
BW_1	PC8	PIN 40
CMD	PC7	PIN 39
SENSE1A	PC6	PIN 38
SENSE1B	PC5	PIN 37
SENSE2A	PC4	PIN 36
SENSE2B	PC3	PIN 35
SENSE3A	PC2	PIN 34
SENSE3B	PC1	PIN 33
JTAG_TCK	PB28	JTAG_TCK
JTAG_TDI	PB29	JTAG_TDI
JTAG_TDO	PB30	JTAG_TDO
JTAG_TMS	PB31	JTAG_TMS
LITHIUM_TX	PA8	RX

LITHIUM_RX	PA9	TX
AVR_RX	PA13	TXD1
AVR_TX	PA14	RXD1
MPU_DATA	PA17	SDA1
MPU_CLK	PA18	SCL1
TEMP_MISO	PA25	MISO
TEMP_MOSI	PA26	MOSI
TEMP_SCLK	PA27	SPCK
XOUT	XOUT	XOUT
XIN	XIN	XIN
GND	JTAGSEL	JTAGSEL
VDDANA	VDDANA	VDDANA
VDDOUTMI	VDDOUTMI	VDDOUTMI

VITA

Anthony G. Cappiello
 Department of Electrical and Computer Engineering
 Old Dominion University
 Norfolk, VA 23529

EDUCATION

Bachelor of Science Electrical Engineering
 Old Dominion University Summer 2018
 Norfolk, VA

Graduate Research Assistant NASAs Virginia Space Grant Consortium 2018-2019

Graduate Teaching Assistant ODU Department of Electrical and Computer Engineering 2018-2019

PUBLICATIONS

33rd Annual AIAA/USU Conference on Small Satellites A Systems Approach to Implementing a 1U Cubed Satellite within a Multi-University Science Mission

MILITARY EXPERIENCE

United States Navy Chief Petty Officer 2006-2015